UNIVERSITAT
POLITÈCNICA
DE VALÈNCIA

MULTI-SCALE REMOTE SENSING FOR TREE AND FOREST SPECIES IDENTIFICATION IN ECUADORIAN ANDES USING MACHINE LEARNING AND DEEP LEARNING METHODS

Diego Pacheco-Prado

2025

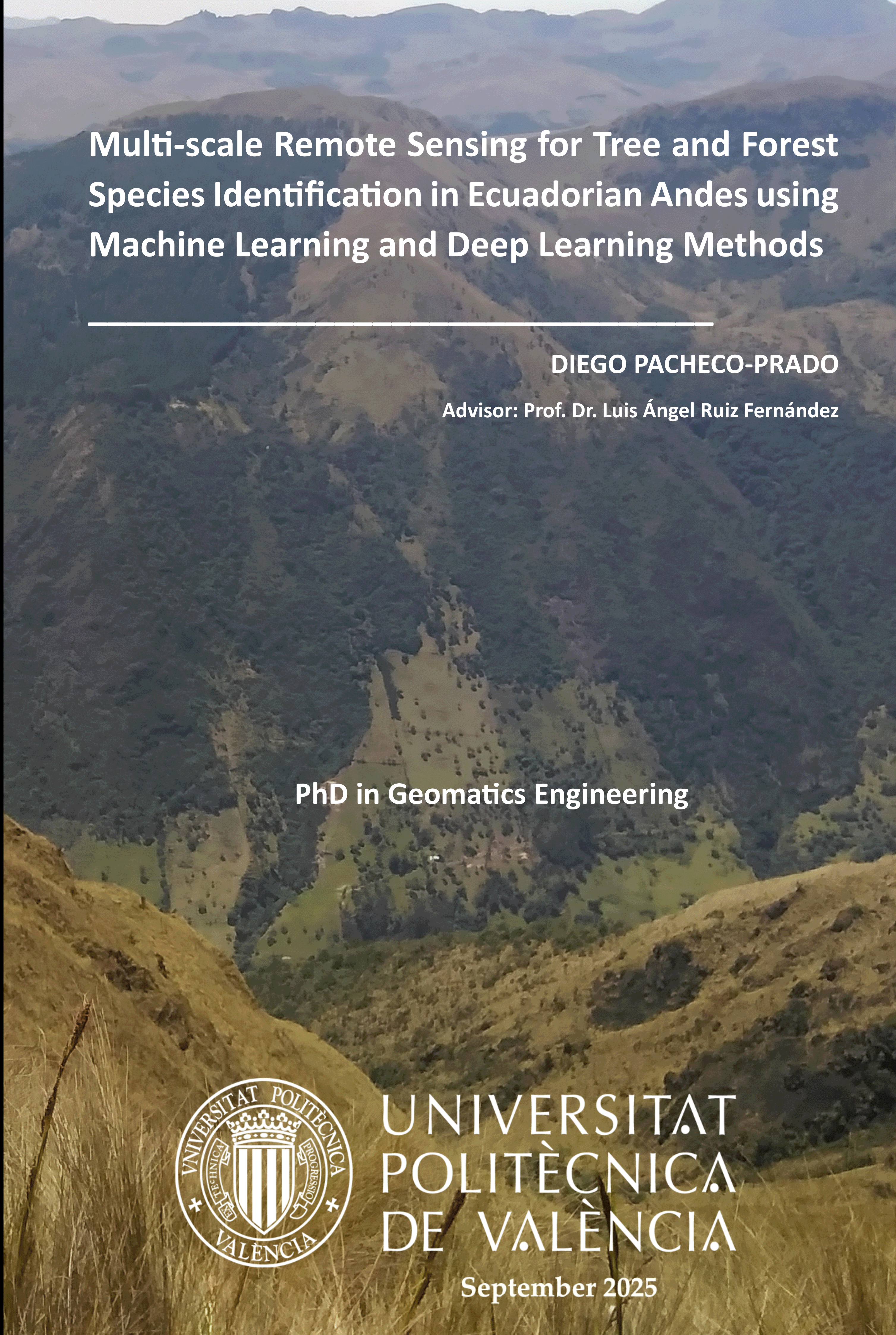

Multi-scale Remote Sensing for Tree and Forest Species Identification in Ecuadorian Andes using Machine Learning and Deep Learning Methods

DIEGO PACHECO-PRADO

Advisor: Prof. Dr. Luis Ángel Ruiz Fernández

PhD in Geomatics Engineering

UNIVERSITAT
POLITÈCNICA
DE VALÈNCIA

September 2025

Multi-scale Remote Sensing for Tree and Forest Species Identification in Ecuadorian Andes using Machine Learning and Deep Learning Methods

Diego Pacheco Prado

Advisor: Prof. Dr. Luis Ángel Ruiz Fernández

Geo-Environmental Cartography and Remote Sensing Group (CGAT)
Department of Cartographic Engineering, Geodesy and Photogrammetry
Universitat Politècnica de València (UPV), Spain

PhD in Geomatics Engineering

València, September 2025

DEPARTMENT OF CARTOGRAPHIC ENGINEERING, GEODESY AND PHOTOGRAMMETRY, UNIVERSITAT POLITECNICA DE VALENCIA

Multi-scale Remote Sensing for Tree and Forest Species Identification in Ecuadorian Andes using Machine Learning and Deep Learning Methods.

PhD thesis presented by Diego Pacheco Prado and directed by Dr. Luis Á. Ruiz, Professor at the Department of Cartographic Engineering, Geodesy and Photogrammetry (UPV). The thesis was developed within the GeoEnvironmental Cartography and Remote Sensing research group (CGAT) in collaboration with Instituto de Estudios de Régimen Seccional del Ecuador (IERSE) of University of Azuay (Ecuador), to obtain the title of Doctor in Geomatics Engineering. It has been conducted within the interuniversity program between Universidad Politécnica de Madrid and Universitat Politècnica de València.

The author of this PhD Thesis is thankful for the financial support provided by the University of Azuay (Ecuador).

This PhD Thesis was developed as a compendium of the following scientific papers:

1. **Pacheco-Prado, D.**, Bravo-López, E., Martínez, E., & Ruiz, L. Á. (2025). Urban Tree Species Identification Based on Crown RGB Point Clouds Using Random Forest and PointNet. Remote Sensing, 17(11), 1863. https://doi.org/10.3390/rs17111863
2. **Pacheco-Prado, D**., Bravo-López, E., & Ruiz, L. Á. (2024). Mapping *Polylepis* Forest Using Sentinel, PlanetScope Images, and Topographical Features with Machine Learning. Remote Sensing, 16(22), 4271. https://doi.org/10.3390/rs16224271
3. **Pacheco-Prado, D.,** Bravo-López, E., & Ruiz, L. Á. (2023). Tree Species Identification in Urban Environments Using TensorFlow Lite and a Transfer Learning Approach. Forests, 14(5), 1050. https://doi.org/10.3390/f14051050

Regarding the author rights for scholarly purposes, the published scientific papers (1), (2) and (3) are re-used by the author of portions or excerpts in other works (i.e., the present PhD thesis), with full acknowledgement of the original publications of the scientific papers.

In addition, this PhD Thesis was completed with the following scientific papers or conference presentations:

1. **Pacheco-Prado, D.,** Bravo-López, E., Martínez-Urgilés, E. (2025). Tree Species Identification Using UAV RGB and Multispectral Cloud Points. In: Olmedo Cifuentes, G.F., Arcos Avilés, D.G., Lara Padilla, H.V. (eds) Emerging Research in Intelligent Systems. CIT 2024. Lecture Notes in Networks and Systems, vol 1347. Springer, Cham. https://doi.org/10.1007/978-3-031-87704-9_5
2. **Pacheco, D.;** Bravo, P. Ruiz, L.Á., 2023. Mapping *Polylepis* Forests with Google Earth Engine. III Congreso Nacional de Geografía. Expandiendo horizontes disciplinares desde el pensamiento espacial. 1-2 June. Quito, Ecuador.
3. **Pacheco, D.**; Bravo, P. Ruiz, L.Á., 2023. Identificación de árboles en zonas urbanas por transferencia de aprendizaje. Actas de la XVIII CONFIBSIG 2023. Cáceres, 16-19 de mayo de 2023. ISBN: 978-84-9127-185-7. 16-19. Modalidad virtual. https://dialnet.unirioja.es/servlet/libro?codigo=971265

4. **Pacheco-Prado, D.** 2022**.** V Conferencia RIGTIG. Conocimiento en acción para la gestión territorial. Reflexiones y actuaciones sobre el territorio. Modalidad Virtual. https://youtu.be/fZKYL4bPz5c?t=5150
5. **Pacheco, D**; Ruiz, L.,2020. Identificación de bosques nativos en el Parque Nacional Cajas con Machine Learning y sensores remotos. Proceedings of the II Congreso Nacional de Geografía del Ecuador. 11-13 November, Cuenca, Ecuador. ISBN 978-9942-847-34-8. E-ISBN 978-9942-847-22-5. https://doi.org/10.33324/ceuazuay.194
6. **Pacheco, D**. 2019. Análisis multiespectral de coberturas naturales del Parque Nacional Cajas a través de drones e imágenes satelitales (Ecuador). XVII Conferencia Iberoamericana de Sistemas de Información Geográfica. 15-17 May. Buenos Aires, Argentina.
7. **Prado, D.P.;** Ruiz, L.Á., 2019. Comparative of Machine Learning Algorithms and Datasets to Classify Natural Coverage in the Cajas National Park (Ecuador) Based on GEOBIA Approach. Proceedings of the II Geomatics Engineering Conference, 19, 6. 26-27 June, Madrid, Spain. https://doi.org/10.3390/proceedings2019019020

Acknowledgments

Luego de varios años de esfuerzo en el desarrollo de esta tesis, una mezcla de pensamientos y sentimientos se encuentran al escribir estas palabras. Este trabajo se lo dedico con mucho amor a mis hijos Sofía y Juan Francisco. Sofía a su corta edad me dio ese impulso inicial para emprender este camino, aunque para ello tuvo que en varias ocasiones verme partir y no poder acompañarla en momentos importantes. Ahora que la veo convertida en una señorita, de quien me siento muy orgulloso, espero pueda comprender que el esfuerzo realizado también fue pensando en ella, para conseguir un mejor futuro para todos. Juan Francisco, el bebito de la casa, talvez no recuerde nada de esto en el futuro, pero en mi vivirá ese sentimiento de aliento y paz que recibía de su sonrisa y su ser. El a su corta edad se ha convertido en mi compañero de día, es lo primero que veo al despertar y lo último al acabar el día. Sin duda, el tenerlo en mi vida ha sido una de las mayores bendiciones que he recibido.

Mis padres, Juan y Yolanda; mis hermanos Juan y Priscila, mi cuñada Irma y mi cuñado Vladimir; y mis sobrinas Romina y Amelia; me brindaron ese apoyo incondicional y necesario durante estos años. Este trabajo también es fruto de toda su ayuda.

En los últimos años de tesis pude compartir este sueño con una maravillosa mujer, Jenny, y sus hijos David y Carlitos, quienes a veces sin saberlo, supieron darme ese apoyo necesario para continuar, algo preciso cuando las fuerzas faltan y el sueño abunda, ellos estuvieron a mi lado.

Hacer un doctorado, creo que nace en la academia, y tuve la fortuna que, en el Instituto de Estudios de Régimen Seccional del Ecuador (IERSE), de la Universidad del Azuay (Ecuador), encontré a esas personas que sembraron en mi esa chispa investigadora. En muchas ocasiones Chester, Omar, Julita, Andrea, Jheymi, Daniela, Andrés, Fersita, Paul, Emanuel y mis amigos del IERSE han colaborado enormemente para aclarar ese camino, encontrar las ideas y palabras adecuadas para enrumbar el trabajo investigativo, que en ciertas ocasiones se vuelve oscuro y sin salida.

Adicionalmente debo reconocer a la Universidad del Azuay, la que ha sido mi casa durante varios años, en primer lugar, por darme la formación y conocimientos necesarios para enfrentar al mundo, tanto a nivel de pregrado como en el posgrado. Posteriormente, tuve la fortuna de sumarme a su planta docente, donde cada día y trabajo realizado fueron con la meta de engrandecer el prestigio de esta noble institución. Finalmente, un enorme agradecimiento a su rector, profesor Francisco Salgado Arteaga, quien depositó en mí su confianza y brindó el apoyo a través de la institución para cursar mis estudios de doctorado y realizar el proceso investigativo que ello conlleva.

El hecho de ir a un país extraño, sin saber que esperar, genera un miedo natural. Tuve la fortuna de llegar a un grupo de investigación muy prestigioso y con una calidad humana excepcional como el Grupo de Cartografía

GeoAmbiental y Teledeteccion (CGAT), quienes hicieron que mis estadías en España sean muy confortables. Entre ellos recuerdo con mucho cariño a Pabi, Juan Pedro, Jesús, Jesús Palomar, Jaime, Carlos, Javier, Marina, Roberto, Elena, Marta, Alfonso, entre otros. No puedo dejar de mencionar a las amistades que se cultivaron fuera del campus universitario, entre ellas Aurora y Arturo, quienes durante mis estancias doctorales se convirtieron en mi familia adoptiva.

Finalmente, mi gratitud a mi director de tesis, Dr. Luis Ángel Ruíz Fernández, quien durante estos años ha sido un guía y un apoyo fundamental en el desarrollo de los distintos artículos e investigaciones. Una vez escuche decir que hacer un doctorado consiste en "cultivar un nuevo conjunto de destrezas investigativas", y estoy seguro de que gracias a la guía de Luis he podido conseguir ello.

Gracias a todos, y a aquellos que he olvidado mencionar, porque han sido muchas personas que han pasado en esta etapa de mi vida, y cada una de ellas contribuyo de una u otra forma.

List of abbreviations

Abbreviation	Explanation
CNN	Convolutional Neural Network
CNP	Cajas National Park
DL	Deep Learning
ESA	European Spatial Agency
GBIF	Global Biodiversity Information Facility
GEE	Google Earth Engine
GLCM	Gray-Level Co-occurrence Matrix
LidAR	Light Detection And Ranging
LULC	Land Use Land Cover
MAE	Ministerio de Ambiente de Ecuador
ML	Machine Learning
MSI	Multispectral Instrument
MODIS	Moderate-Resolution Imaging Spectroradiometer
NDVI	Normalized Difference Vegetation Index
NGBDI	Normalized Green-Blue Difference Index
NGRDI	Normalized Green-Red Difference Index
NRBDI	Normalized Red-Blue Difference Index
NIR	Near infrared channel
RF	Random Forest
RFE	Recursive Feature Elimination
RGB	Red, Green, and Blue channels
SAR	Synthetic Aperture Radar
SRF	Smile Random Forest implementation in GEE
S2, S1	Sentinel-2 and Sentinel-1 imagery
TIC	Tree Inventory of Cuenca
UAV	Unnamed Aerial Vehicle
UTI	Urban Tree Inventory

Table of contents

List of figures

CHAPTER 4

List of tables

Abstract

The Andes mountain range that runs through Ecuador contributes to the presence of a wide variety of microclimates, which, along with factors such as altitude and soil moisture, strongly influence the distribution and growth of various forest species, making the country one of the most megadiverse in the world. In Cuenca canton (the study area), located in the central-southern region of the Ecuador, ecosystems such as paramos, montane forests, wetlands, lagoons, and inter-Andean valleys can be found. Among these, Andean montane forests are of high conservation priority due to their functions in water flow regulation, carbon sequestration, soil regeneration, and the retention of nutrients and sediments.

However, deforestation and agricultural expansion pose ongoing threats to these ecosystems. This issue is also evident in urban areas, where city expansion and the maintenance of public green spaces have displaced native species. Therefore, forest species identification becomes a key task for the conservation and sustainable management of native ecosystems.

In this context, forest/tree species identification was addressed at three spatial scales, defined according to the spatial extent and the type of sensor used for data acquisition. The first scale, referred to as regional, evaluated satellite data in Cuenca canton (Ecuador). The second, or local scale, assessed drone-based photogrammetric data at the tree level. Finally, close-range scale involved evaluating photographs taken with a smartphone at the tree level. The last two scales were evaluated within the urban area of the canton.

At the regional scale (satellite), stands of the *Polylepis* genus were identified with a global accuracy of 0.91 and a Kappa coefficient of 0.80. This was achieved using topographic variables (elevation, slope, and aspect), along with spectral variables (bands and indices) obtained from Sentinel-2. Processing was carried out on the Google Earth Engine platform using the Random Forest algorithm. It is worth noting that in several official maps, these stands were generalized as native forests or absorbed by the dominant surrounding class, which is paramo.

At the local scale (UAV), *Populus alba L.* and *Melaleuca armillaris (Sol. ex Gaertn.) Sm. were* identified with a global accuracy of 0.70 and a Kappa of 0.65, among eight species evaluated. This identification used RGB data from drone-derived photogrammetric point clouds, complemented by vertical tree characterization based on the normalized Z coordinate of the point cloud, using maximum Z values and the 10th, 50th, and 90th percentiles, as well as the point cloud density per tree.

Finally, at the close-range scale (smartphone), *Yucca gigantea Lem., Salix humboldtiana,* and *Melaleuca armillaris (Sol. ex Gaertn.) Sm.* achieved a high identification rate among 14 species evaluated. This scale yielded a global accuracy of 0.80 and a Kappa of 0.79.

For the regional and local scales, the selection of the most relevant features was carried out by evaluating multiple variables obtained from a literature review. Among these, the Recursive Feature Elimination (RFE) technique using Random Forest was applied to eliminate less important variables. This approach aimed to minimize the number of variables used in identification while maintaining model accuracy. In contrast, at the close-range scale, a Deep Learning model was used, in which the relevant features are treated as a "black box," making it impossible to directly determine which variables were used for identification. Instead, activation maps were employed to identify which regions of the image were most relevant to species classification.

Each scale presented its own challenges, particularly regarding access to field data, which was essential for training the Machine Learning and Deep Learning models, which will be analyzed in this document.

Resumen

La cordillera de los Andes que atraviesa Ecuador contribuye a la presencia de una enorme variedad de microclimas, que junto a factores como altitud y humedad del suelo influyen fuertemente en la distribución y crecimiento de distintas especies forestales, haciendo del país uno de los más megadiversos del mundo. En el cantón Cuenca (área de estudio), ubicado en la zona centro/sur del Ecuador, se pueden encontrar ecosistemas como páramos, bosques montanos, humedales, lagunas, valles interandinos. De estos, los bosques montanos andinos tienen una alta prioridad de conservación dadas sus funciones de regulación del flujo de agua, secuestro de carbono, regeneración de suelos y retención de nutrientes y sedimentos.

Sin embargo, la deforestación y la expansión agrícola son una amenaza latente para estos ecosistemas. Esta problemática también se manifiesta dentro del área urbana, donde la expansión urbana y el mantenimiento de las áreas verdes públicas han desplazado a las especies nativas de la región. Por ello, la identificación forestal se convierte en una tarea clave para la conservación y el manejo sostenible de los ecosistemas nativos.

En este contexto, la identificación de especies forestales se abordó en tres escalas, definidas según la extensión espacial y el sensor usado para la toma de datos. La primera escala, denominada regional, evaluó los datos satelitales en el cantón Cuenca (Ecuador). La segunda escala denominada local, evaluó los datos fotogramétricos obtenidos con dron a nivel de árbol. En la última escala denominada a corta distancia, se evaluaron fotografías tomadas con smartphone a nivel de árbol. Las dos últimas escalas fueron evaluadas dentro del área urbana del cantón.

En la escala regional (satelital), se consiguió la identificación de rodales del género *Polylepis*, con una fiabilidad global de 0,91 y un coeficiente Kappa de 0,80. Para ello se utilizaron las variables topográficas (elevación, pendiente y orientación), junto con variables espectrales (bandas e índices) obtenidas de Sentinel-2. Esto se realizó en la plataforma Google Earth Engine con el algoritmo Random Forest. Cabe destacar que, en varios mapas oficiales, estos mapas se encontraban generalizados como bosques nativos o eran absorbidos por la clase mayoritaria que rodeaba a estos rodales que es el Páramo.

En la escala local (dron) se identificaron con una fiabilidad global de 0,70 y Kappa de 0,65 las especies *Populus alba L.*, y *Melaleuca armillaris (Sol. ex Gaertn.) Sm*, entre ocho especies evaluadas. Para ello se utilizó la información RGB de las nubes de puntos fotogramétricas de dron, complementadas con la caracterización vertical del árbol basada en la coordenada Z (normalizada) de la nube de puntos, a través de los valores de Z máximo y los percentiles 10, 50 y 90; además de la densidad de la nube de puntos por árbol.

Finalmente, en la escala a corta distancia (smartphone), las especies *Yucca gigantea Lem.*, *Salix humboldtiana* y *Melaleuca armillaris (Sol. ex Gaertn.) Sm.* tuvieron una alta tasa de acierto entre 14 especies evaluadas. En esta escala se registró una fiabilidad global de 0,80 y kappa de 0,79.

Para la identificación, en la escala regional y local la selección de las características más relevantes se realizó evaluando múltiples variables obtenidas de una revisión bibliográfica. De todas estas se usó la técnica *Recursive Feature Elimination* (RFE) a través de *Random Forest*, para eliminar las variables de menor importancia. Con ello se buscó reducir al mínimo la cantidad de variables a usar en la identificación, y a su vez mantener el nivel de fiabilidad. Finalmente, en la escala a corta distancia, al usar un modelo de *Deep Learning*, donde las características se presentan como una "caja negra", no se pudieron determinar las variables usadas para la identificación. En su lugar se utilizaron los mapas de activación para determinar qué regiones de la fotografía fueron las más relevantes en la asignación de la especie forestal.

Cada nivel evaluado tuvo su complejidad, principalmente en acceso a datos en campo, necesarios para el entrenamiento de los modelos de *Machine* y *Deep Learning*, los cuales serán analizados en este documento.

Resum

La serralada dels Andes que travessa l'Equador contribueix a la presència d'una enorme varietat de microclimes, que, juntament amb factors com l'altitud i la humitat del sòl, influeixen fortament en la distribució i el creixement de distintes espècies forestals, fent del país un dels més megadiversos del món. Al cantó Cuenca (àrea d'estudi), situat a la zona centre/sud del Ecuador, es poden trobar ecosistemes com els páramos, boscos montans, aiguamolls, llacunes i valls interandines. D'aquests, els boscos montans andins tenen una alta prioritat de conservació per les seues funcions de regulació del flux hídric, segrest de carboni, regeneració del sòl i retenció de nutrients i sediments.

Tanmateix, la desforestació i l'expansió agrícola són una amenaça latent per a aquests ecosistemes. Aquesta problemàtica també es manifesta dins de l'àrea urbana, on l'expansió urbana i el manteniment de les zones verdes públiques han desplaçat les espècies natives de la regió. Per això, la identificació forestal es converteix en una tasca clau per a la conservació i la gestió sostenible dels ecosistemes natius.

En aquest context, la identificació d'espècies forestals es va abordar en tres escales, definides segons l'extensió espacial i el sensor utilitzat per a la presa de dades. La primera escala, denominada regional, va avaluar dades satellitals al cantó Cuenca (Equador).La segona escala, denominada local, va avaluar dades fotogramètriques obtingudes amb dron a nivell d'arbre. L'última escala, denominada a curta distància, va analitzar fotografies preses amb telèfon intel·ligent a nivell d'arbre. Les dues últimes escales van ser avaluades dins de l'àrea urbana del cantó.

A l'escala regional (satellit), es va aconseguir identificar rodals del gènere *Polylepis* amb una precisió global de 0,91 i un coeficient Kappa de 0,80. Per a això s'utilitzaren variables topogràfiques (elevació, pendent i orientació), juntament amb variables espectrals (bandes i índexs) obtingudes del Sentinel-2. El processament es va dur a terme en la plataforma Google Earth Engine mitjançant l'algorisme Random Forest. Cal destacar que en diversos mapes oficials, aquests rodals apareixien generalitzats com a boscos natius o eren absorbits per la classe majoritària que els envolta, el páramo.

A l'escala local (dron), es van identificar amb una precisió global de 0,70 i un Kappa de 0,65 les espècies *Populus alba L. i Melaleuca armillaris (Sol. ex Gaertn.) Sm.*, entre vuit espècies avaluades. Per a això, s'utilitzà la informació RGB de núvols de punts fotogramètrics del dron, complementada amb la caracterització vertical de l'arbre basada en la coordenada Z (normalitzada) del núvol de punts, mitjançant els valors de Z màxim i els percentils 10, 50 i 90; a més de la densitat del núvol de punts per arbre.

Finalment, a l'escala a curta distància (telèfon intel·ligent), les espècies *Yucca gigantea Lem.*, *Salix humboldtiana* i *Melaleuca armillaris (Sol. ex Gaertn.) Sm.*

mostraren una alta taxa d'encert entre 14 espècies avaluades. En aquesta escala es registrà una precisió global de 0,80 i un Kappa de 0,79.

Per a la identificació, a les escales regional i local, la selecció de les característiques més rellevants es va realitzar avaluant múltiples variables obtingudes d'una revisió bibliogràfica. De totes aquestes, s'utilitzà la tècnica Recursive Feature Elimination (RFE) mitjançant Random Forest, per eliminar les variables de menor importància. Amb això es buscava reduir al mínim la quantitat de variables utilitzades en la identificació, mantenint alhora el nivell de fiabilitat. Finalment, a l'escala a curta distància, en utilitzar un model de Deep Learning, on les característiques es presenten com una "caixa negra", no es pogueren determinar les variables utilitzades per a la identificació. En el seu lloc, es van emprar mapes d'activació per determinar quines regions de la imatge van ser les més rellevants en l'assignació de l'espècie forestal.

Cada nivell avaluat va presentar la seua pròpia complexitat, principalment en l'accés a dades de camp, necessàries per a l'entrenament dels models de Machine Learning i Deep Learning, els quals seran analitzats en aquest document.

Chapter 1

Introduction

1. INTRODUCTION

1.1. Importance and issues of Ecuadorian Andean forests

Ecuador is recognized as one of the most biodiverse countries in the world (Aguirre et al., 2024; Jadán et al., 2021; MAE & FAO, 2015), with a high number of species per unit area (Sierra et al., 2002). The favorable climate of Ecuador's highland valleys allows a wide range of species from other regions and continents to thrive (Guzmán-Salinas et al., 2023). Additionally, the presence of the Andes Mountains in the country allows for a wide variety of microclimates (Vallejo et al., 2007), along with factors such as altitude and soil moisture strongly influencing species distribution and growth (Blundo et al., 2012). The Montane forests of the region are characterized by the presence of epiphytes and mosses that grow on trees. Most epiphyte species belong to the *Orchidaceae* family, with over 4000 species recorded in Ecuador. Other abundant families include *Araceae* (*anthuriums*) and *Bromeliaceae* (*huicundos*), which serve as habitats for a variety of amphibians, reptiles, and other insects such as beetles and arachnids (MAE & FAO, 2015).

High-altitude forests in the Andes region have a high conservation priority given their functions of water flow regulation, soil regeneration, retention of nutrient and sediments (Tejedor Garavito et al., 2012), and carbon sequestration, with a capacity per unit equal or even greater than that reported for Amazonian forests (Duque et al., 2021). The southern highlands of Ecuador, especially within the Andean region, are home to unique and highly diverse native forest ecosystems. Notably, the area supports species from the genus *Polylepis* and *Gynoxys* (Minga-Ochoa et al., 2019).

On the other hand, in urban areas, the trees, shrubs, and gardens create a rich mosaic of native and introduced species (Guzmán-Salinas et al., 2023). In this context, urban trees provide numerous benefits for both people and cities (Uçar et al., 2020), including improving their quality of life (Solomou et al., 2019), providing spaces for recreation and psychophysical well-being, improving air and water quality, reducing noise, improving biodiversity and soil protection (Pacheco & Ávila, 2017; Solomou et al., 2019; Uçar et al., 2020), and playing a key role in climate change mitigation (Naciones Unidas, 2018).

Understanding the distribution of trees and their associated species at all levels enables city administrators to make informed decisions regarding sustainable forest management (Salam, 2020; Solomou et al., 2019).

1.2. Background and research justification

Despite the importance of Andean forest, these ecosystems are altered daily in Ecuador by human impact (Noh et al., 2022), and faces multiple threats, including deforestation, land use, and land cover change, agriculture, mining, and others (Astudillo et al., 2015; Balthazar et al., 2015; Kleemann et al., 2022; Tejedor Garavito et al., 2012, 2015). These factors are driving significant alterations in the structure and composition of Andean habitats (Herzog et al., 2012).

In the context of deforestation, historical data reveal that Ecuador is one of the countries with the highest forest loss rate in South America. Between 1990 and 2018, the country lost approximately 21,263 km^2 of forest. According to the Ministry of Environment of Ecuador, the country's annual net deforestation was 92,742 ha/year between 1990-2000, 77,748 ha/year between 2000-2008, 47,497 ha/year between 2008-2014 (Calva et al., 2020), and 61,112 ha/year between 2014-2016 (MAE, 2017), with the period 1990-2000 of highest incidence. Areas of high deforestation density are located along the northern coastal region, in the northern basin of the Amazon region, and along the slopes of the Andes throughout the country (Kleemann et al., 2022). This led to a significant reduction in forest connectivity and increased fragmentation, especially in the coastal region (Rivas et al., 2024). The most common cause of deforestation in Ecuador and the Andean region is the change from native forests to agricultural land (Castillo Vizuete et al., 2023); livestock farming, and demographic pressure (Armenteras et al., 2011; Navarro et al., 2005); even within protected areas (Astudillo et al., 2015; Buxton et al., 2000).

On the other hand, remote sensing for forest applications has gained relevance in recent years. At a national or regional scale, satellite data allows the generation of global forest cover maps, forest-change assessments, national and regional forest inventories, quantification of forest extent, and production of disturbance-related datasets covering large areas (Fassnacht et al., 2024; Waser et al., 2021). However, this technology presents several limitations, including its dependence on ground reference data for model training (Fassnacht et al., 2024), challenges in areas with fragmented forest cover and complex topography (mountainous terrain) (Curatola Fernández et al., 2015; Fassnacht et al., 2024; Waser et al., 2021), and difficulties in obtaining tree canopy structure and species information using traditional methods (R. Pu, 2021). These traditional methods, such as field measurement and aerial photograph interpretation, are often time-consuming, costly, and require specialized human expertise (Diez et al., 2021; Pacheco-Prado et al., 2023), especially when applied to the creation or updating of forest and tree inventories over extensive areas (Branson et al., 2018; Das et al., 2022; R. Pu, 2021).

Emerging technologies such as Unnamed Aerial Vehicle (UAV), Aerial Laser Scanning (ALS), Terrestrial Laser Scanning (TLS), and smart devices are facilitating the creation of inventories and enabling the identification of forest species at the individual tree level (Pacheco & Ávila, 2017). For instance, smartphones foster the development of new applications and innovative approaches suitable for assessing a diverse range of forest attributes in the field (Fassnacht et al., 2024).

Identifying tree and forest species remains a significant challenge in forestry, ecology, and environmental management due to the forest’s inherent complexity and variability (Clark et al., 2005). In the Andean mountains, the challenging terrain and limited accessibility often render ground-based data collection for forest species unfeasible. Furthermore, in the context of remote sensors, the following should be considered several limitations include spatial/spectral resolutions, temporal resolution or seasonal effect, forest environmental setting/background, shadow, shaded effect, an appropriate image segmentation, spectral variation of tree crowns in the image, and different tree species overlapping effects (R. Pu, 2014). In urban zones, the individual tree species identification adds additional challenges, such as complex vertical structures and complex composition of tree species (Man et al., 2025), bearing in mind that trees located in public areas are often pruned to control their size or avoid damage to infrastructure (modify the tree natural structure).

Given these factors, it is necessary to study forest/tree species identification at multiple scales, particularly in the Andean region, where the forest's high structural and spectral diversity, complex topography, and frequent cloud cover pose significant challenges to remote sensing. Comprehending the distribution of forest species at multiple scales, from regional ecosystems to microhabitats or individual trees, facilitates target conservation strategies for mountain forests in the Ecuadorian Andes.

1.3. Study zone

Cuenca is located in the south-central region of Ecuador (Figure 1.1), in the Andes Mountain range. It occupies an area of 366,532.96 hectares (3,665.32 km^2). Its territory extends between the western mountain range and the inter-Andean valley of the Andes, between an altitude of 20 to 4560 meters above sea level (m.a.s.l). The predominant slopes range from 30 to 50 %. The canton is crossed from north to south by the Andes Mountain range, whose summit line divides the hydrographic network into two oceanic slopes: Pacific and Atlantic. The predominant climate types are equatorial mesothermal semi-humid (between 18 and 22 °C), which occupies 52 % of the surface of the canton's territory, and high mountain equatorial (fluctuates around 8 °C), which covers 34.4 %. According to the Development and Land Use Plan, natural areas (including forests, shrublands, and paramo with native vegetation) account for 60 % of the territory (Cuenca, 2016).

Meanwhile, intervened areas, such as agricultural and forestry zones combined with residential structures, occupy 36.67% of the land. Urban areas and rural parish centers comprise the remaining 2.45% of the cantonal area. It includes ecosystems such as paramo, montane forests, wetlands, lagoons, and inter-Andean valleys, all supporting unique flora and fauna (Cuenca, 2016).

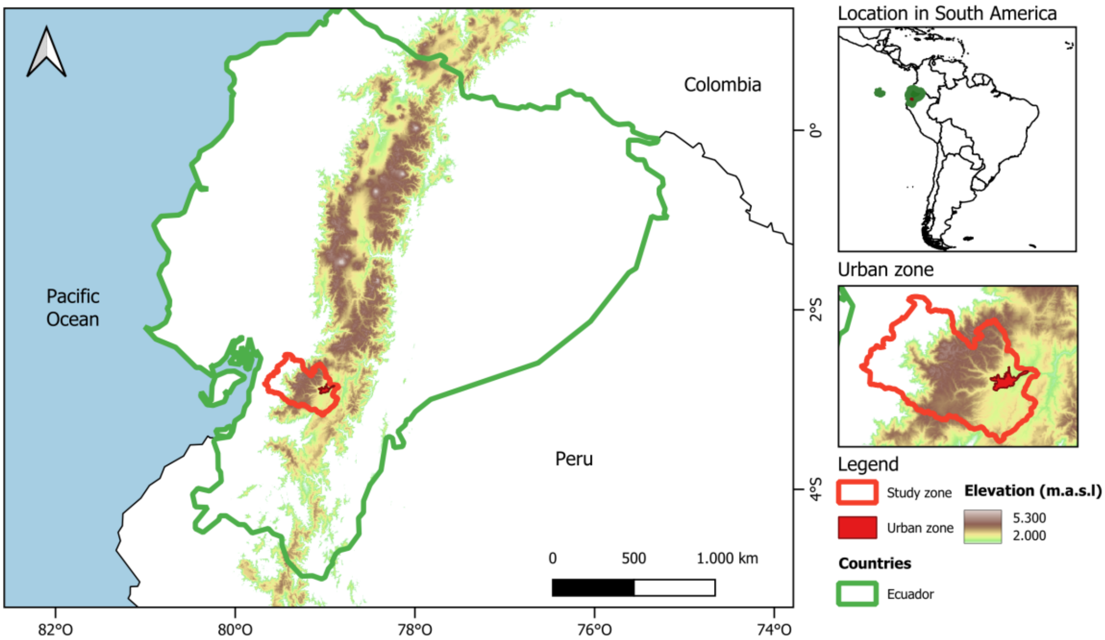

Figure 1.1. Location of study zone.

This Andean region presents high levels of endemism and biological diversity (Castillo et al., 2017; Gobierno Provincial del Azuay, 2015). In the inter-Andean valley between Cuenca and Azogues, at elevations between 2500 and 3000 m.a.s.l., *Eucalyptus* plantations dominate, featuring an understory composed of native and introduced shrubs. Above 3000 m.a.s.l., in paramo zones critical for water recharge, *Pinus Patula* plantations are found.

Native forests include formations dominated by *Hesperomeles ferruginea*, and between 3400 and 4000 m.a.s.l., *Polylepis reticulata* and/or *Polylepis incana* forests occur, often accompanied by *Gynoxys cuicochensis*. On the western slopes, *Polylepis* forests are composed of species such as *P. lanuginosa*, *P. weberbaueri*, *P. incana, and Gynoxys sp.*, along with shrubs like *Chuquiraga jussieui*, *Valeriana hirtella*, and *Brachyotum jamesonii*. In cloud forest areas, grasslands are interspersed with trees such as motilón (*Hyeronima duquei*), jiguas (*Ocotea spp.*), and capulí (*Freziera sp.*). Finally, at elevations below 1800 m.a.s.l., piedmont evergreen forests (occasionally disturbed) are characterized by high floristic richness and the presence of trees reaching up to 30 meters in height, with dominant species including *Iriartea deltoidea*, *Cecropia sp.*, *Ficus sp.*, *Ocotea cernua*, *Brosimum alicastrum*, *Cousapoa villosa, and Sapindus Saponaria* (Cuenca, 2015, 2016).

In the urban area of Cuenca, one can find trees, shrubs, and flowering gardens that form an interesting mix of native and introduced species. Several introduced species, such as *Jacaranda mimosifolia D. Don, Fraxinus excelsior L, Melaleuca armillaris (Sol. ex Gaertn.) Sm.*, *Cinnamomum camphora (L.) J. Presl* and *Eucalyptus globulus*, have found favorable climatic conditions and water availability for their adaptation. At the same time, some native species, such as *Tecoma stans (L.) Juss. ex Kunth, Prunus serotina Ehrh, Alnus acuminata Kunth,* and *Salix humboldtiana Willd.*, have adapted to urban conditions and stand out for the color of their flowers and the majesty of their crowns (Guzmán-Salinas et al., 2023). However, the vegetation of the Tomebamba and Yanuncay rivers as they enter the urban area suffers a gradual deterioration (Carrasco Espinoza et al., 2010), despite their importance for the river ecosystems (Dufour et al., 2013). A contributing factor to this is the replacement of native vegetation with species such as *Eucalyptus globulus Labill* (Carrasco Espinoza et al., 2010; Minga & Verdugo, 2016), which can retain more CO_2, but may also affect ecosystem processes in the area. Moreover, urban expansion and demographic development play an important role in deforestation (Kleemann et al., 2022).

1.4. Multi-scale approaches

The concept of multi-scale remote sensing has been used in several forestry-related fields. For instance, Strasser et al. (2014) employed this approach in the monitoring of forest habitats, using high-resolution (HR) satellite data to analyze broad-scale disturbances (extensive areas), and very high-resolution (VHR) data to assess complex habitats and their quality at finer scales, such as specific sites. Xu et al. (2019) and Lou et al. (2021) define a multi-scale approach based on spatial, spectral, and temporal satellite image characteristics applied to land-cover classification and the estimation of canopy chlorophyll, respectively. Wang et al. (2020) highlight the potential of integrating multi-scale satellite observations (from individual tree canopies to the ecosystem level) to extend fine-scale monitoring of leaf phenology in evergreen tropical forests. Huang et al. (2021) use a multi-scale approach at the regional scale with multiple spatial resolution images (Google Earth images, Landsat 8 OLI, MODIS), multi-sensor, and multitemporal data to estimate forest canopy characteristics. In this work, high-resolution imagery was used to obtain accurate measurements at the local scale, and the scale transition is achieved through extrapolation methods based on the Normalized Difference Vegetation Index (NDVI). Y. Hong et al. (2023) applied this approach to monitor forest biomass, with the scale determined by the object of monitoring, such as a single tree, stand, management unit (considered small to medium scale), or an entire region. LiDAR technology serves as a key tool for data collection on these scales. Finally, J. Chen et al. (2024) express that species identification at multiple spatial scales (from individual trees to entire landscapes) improves the accuracy of forest condition assessments and, thus, the understanding of forest ecosystem functions, services, and processes.

Forest species identification in this thesis has been conducted using a multi-scale approach at three distinct levels, defined according to a criterion such as spatial extent, spectral resolution, type of sensor used for data acquisition, and the object of identification (individual tree or forest stand). This methodology permits species identification at broad-scale and close-range levels, enabling a comprehensive understanding of multi-scale analysis's diverse characteristics and techniques. The first scale, the regional scale, involved the analysis of satellite data in the Cuenca canton (Ecuador) and was applied at the forest or stand level. The second scale, known as the local scale, utilized UAV-based photogrammetric data and enabled the identification of tree species at both the stand and individual tree levels. Finally, the close-range scale involved the evaluation of photographs captured with a smartphone, focusing on individual trees. In this context, while satellite data are primarily suited for broader stand-level analysis, UAV and smartphone data provide finer details suitable for tree-level identification.

Each scale offers certain advantages and is adapted to specific applications, depending on the level of detail required and the area of interest. For example, one of the most widely used techniques in detecting and monitoring forest ecosystems is remote sensing with satellite data (Lechner et al., 2020). However, studies in which these techniques have been applied to Andean Mountain forests are scarce (Vega Isuhuaylas et al., 2018). Among other reasons, these studies are limited due to the high complexity of mountain topography, variation in surface illumination, shadows, and illuminated areas (Hościło & Lewandowska, 2019), and the availability of cloud-free images in the study area.

1.5. Tree and forest species identification using remote sensing

Remote sensing technologies have become essential for identifying vegetation at different spatial scales, from individual trees to forest stands and entire forest landscapes. This section presents a bibliometric analysis of recent scientific literature to explore how satellite, UAV, and ground-based (close-range scale) data have been combined with Machine Learning (ML) and Deep Learning (DL) techniques for identifying tree, stand, and forest species. The analysis aims to highlight prevailing trends, frequently used sensors and algorithms, and the evolution of methodological approaches in this rapidly advancing field.

Satellite data have played a central role in regional-scale assessments, where the detection and monitoring of forest ecosystems are carried out through remote sensing (Lechner et al., 2020), and the presence of clouds can impede the development of monitoring and control tasks. At this scale, vegetation indices and other indicators allow large areas to be monitored to detect changes in forest cover. Based on the Scopus database, the equation “**remote AND sensing AND forest AND species AND satellite AND (identification OR classification)”** returns 457 documents exploring tree/forest identification using satellite imagery between 2019 and June 2025. The word cloud of Figure 1.2 highlights "remote sensing" as the most important term, reflecting its significant role in the study and application of geospatial technologies. Keywords such as "random forest", ”support vector machine”, "machine learning", and "deep learning" highlight the increasing dependence on these computational methods for analyzing and classifying satellite data. The presence of mission satellite names such as “Sentinel-2” and “Landsat” underlines the importance of satellite data in species identification. Terms such as “forest inventory”, ”tree species”, “tree species classification”, “invasive species”, “biodiversity”, and “species classification” represent a focused approach to species classification-related studies. At the same time, “Google Earth Engine” highlights the use of cloud-based platforms for broad-scale analysis. Other frequently occurring terms, such as “vegetation indices", "lidar", "hyperspectral", "mangrove", and "time series", reflect the commonly used data types and applications within this context.

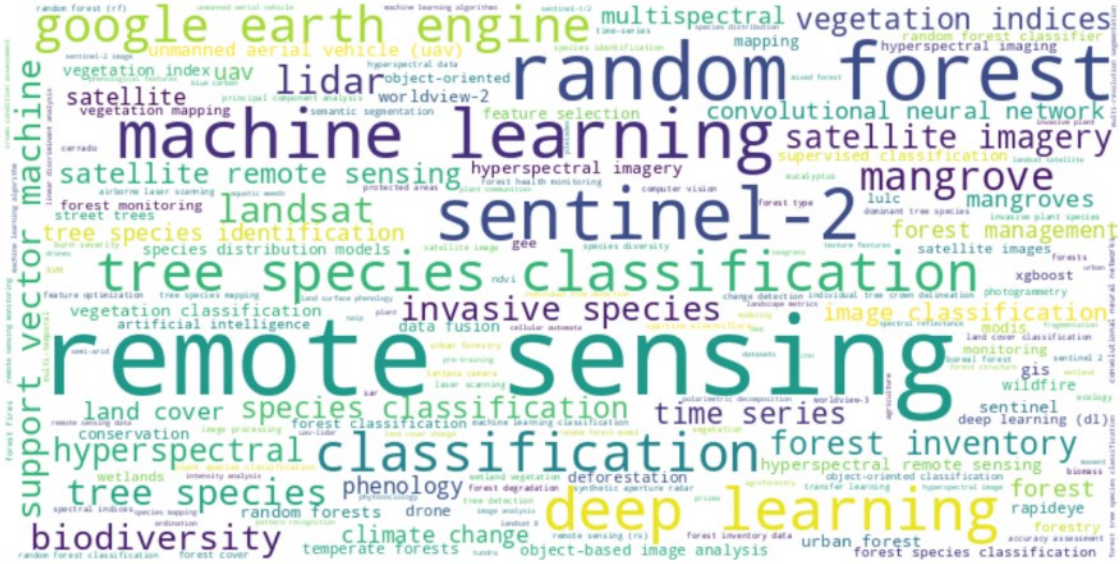

Figure 1.2. Cloud words of forests or tree identification using satellite data.

Unmanned Aerial Vehicles (UAVs) provide high spatial and temporal resolution imagery that is especially beneficial for accurate tree species identification and health status monitoring. UAVs are an effective alternative for geomatics applications in small areas due to the low cost of information production, high temporality, and spatial resolution of the data (Uysal, Toprak, & Polat, 2015). Operating at low altitudes makes UAVs especially suitable for forest monitoring, as favorable weather conditions facilitate flight operations. UAV-derived data support various applications, including forest monitoring (Paneque-Gálvez et al., 2014), species detection based on pixels or point clouds (Puliti et al., 2017; Sothe et al., 2019), and cost-effective management of urban green spaces (Roca & Arellano, 2021).

Some of the main applications of UAVs in forestry include the assessment of forest regeneration or degradation, obtaining forest-related parameters such as tree height, diameter crown area, diameter at breast height, volume, among others (Guimarães et al., 2020), the construction of forest cover maps (Pizarro et al., 2022), estimates of forest parameters such as structure (Nevalainen et al., 2017), density, and biomass (Nandy et al., 2021), forest health (Dash et al., 2018), among others. There are studies for the identification of tree and shrub species (Carbonell-Rivera et al., 2022), some of them based on the extraction of tree crown data (Feng & Li, 2019), as support in the construction of forest inventories (Pacheco, 2017).

Tree species identification from UAVs is a growing in remote sensing and forestry management field. This process involves capturing high-resolution imagery using UAVs equipped with RGB, multispectral or hyperspectral sensors. A Scopus search using the query **"forest AND uav AND tree AND (identification OR classification)"** returns 715 elements. A bibliometric analysis of this data presents a word cloud of Figure 1.3 that reflects a focused research area on applying UAVs and advanced “machine learning” and “deep learning” techniques. Notable algorithms include “random forest”, “support vector machine”, and “convolutional neural network”. Key topics include “remote sensing”, “tree species classification”, ”classification”, “precision agriculture”, “forest inventory”, highlighting the use of UAVs for high-resolution imaging, integrating “lidar”, “hyperspectral”, and “multispectral” data types in the tree species identification.

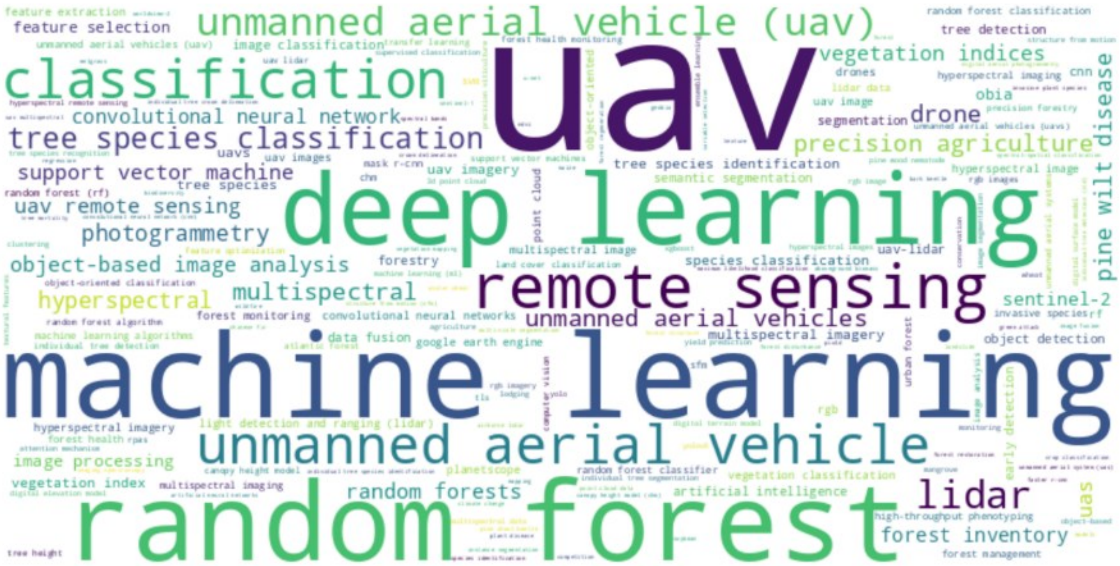

Figure 1.3. Cloud words of forests or tree identification using UAV data.

By conducting a close-range identification of individual trees, the Scopus search using the query "**neural AND network AND tree AND species AND (trunk OR leaf) AND (identification OR classification)**" returns 112 documents, highlighting a significant research focus on the application of artificial intelligence, particularly neural networks (NNs) and deep learning, for “tree species identification” (Figure 1.4). The main topics identified include "deep learning" and "convolutional neural network", with applications such as "tree species identification" and "leaf recognition", employing advanced techniques like "image classification", "computer vision", "feature extraction", and "artificial neural networks". Among these, transfer learning emerges as one of the most widely used methods to enhance the reliability of neural network-based models.

Furthermore, terrestrial photogrammetry captures complex details at the trunk and leaf level, facilitating species identification and complementing larger-scale UAV analyses. The integration of these technologies significantly enhances our capacity to map, classify, and effectively protect threatened forest species.

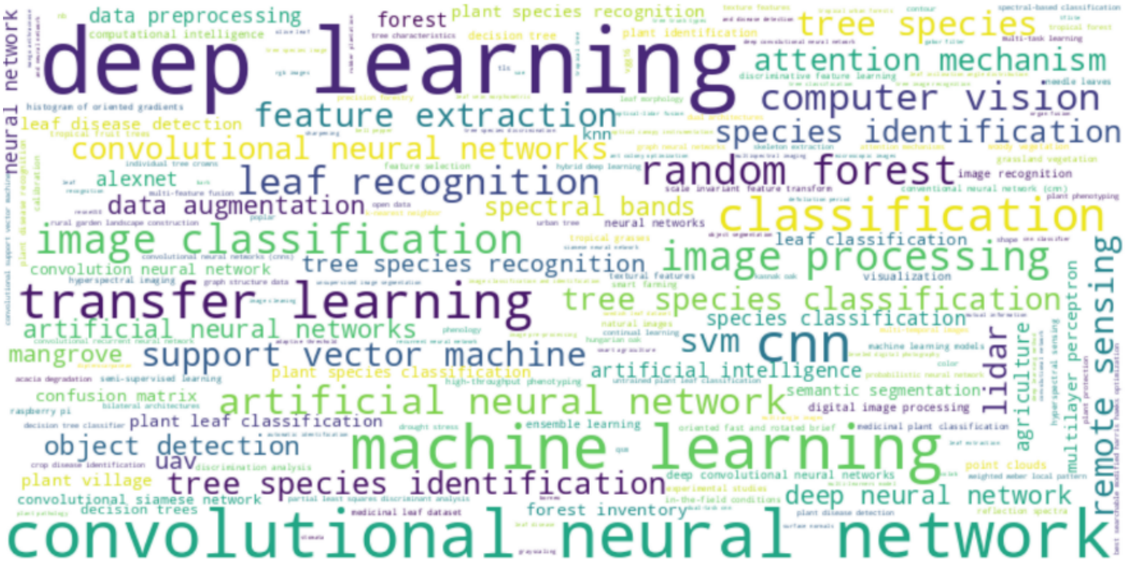

Figure 1.4. Cloud words of forests or tree identification using terrestrial data.

1.6. Machine and Deep Learning in tree/stand species identification

At all three spatial scales and sensor types, Machine Learning (ML) and Deep Learning (DL) are the key tools for forest species identification. These methods are applied across different platforms, including satellite imagery (Hościło & Lewandowska, 2019; Pacheco-Prado et al., 2024; Persson et al., 2018; Pizarro et al., 2022), unmanned aerial vehicles (UAVs) for local-scale and individual tree identification, such as (Pacheco-Prado et al., 2023), and close-range sensing for individual classification, such as (Balipa & Castalino, 2022; Wäldchen & Mäder, 2018; R. Zhang et al., 2022).

ML and DL are essential elements of artificial intelligence (AI) that have revolutionized how data is processed and analyzed, increasing interest in applications (Michałowska & Rapiński, 2021). The main difference between ML and DL is human expertise in the subject matter; in ML, it is required to extract meaningful input features from the data. Traditional ML methods are often based on mathematical relationships or clear rules that allow humans to understand how decisions are made (J. Chen et al., 2024; L. Pu et al., 2021).

Among the most widely used ML algorithms are Decision Tree (DT), Random Forests (RF), and Support Vector Machines (SVM). DT is usually used for classification and regression problems, offering simplicity and interpretability by segmenting data into hierarchical structures to generate decision rules. RF extends the functionality of DT by enhancing accuracy and reducing overfitting. SVM, in turn, determines optimal hyperplanes to divide the data into different classes (Gerón, 2019).

In urban forestry, ML methods are applied in various areas such as tree detection and classification, biomass and carbon sequestration, spatial analysis and planning, data-driven decision making, and health and ecosystem services evaluation; using supervised learning (labeled data) or unsupervised learning (absence of labeled data) (Zeybek, 2025).

In the context of species identification, Carbonell-Rivera et al. (2020) evaluated RGB point clouds to extract geometric and spectral metrics for classifying vegetation and ground cover of five classes, using ML algorithms Decision Trees (DT), Extra Trees (ET), Multilayer Perceptron (MLP), K-Nearest Neighbors (KNN), Random Forest (RF), and Ridge regression (RR). Hartling et al. (2021) assessed 96 individual trees across seven species using a pixel-based approach and UAV-derived datasets, including multispectral, hyperspectral, LiDAR, and thermal infrared imagery, finding that the RF algorithm consistently outperformed SVM in terms of overall accuracy and the kappa index across all sensor-feature combinations. Carbonell-Rivera et al. (2022) evaluated geometrical, spectral, and neighbour-based features obtained from the multispectral point cloud using ML algorithms such as DT, ET, Gradient Boosting (GB), RF, and MLP. According to the review by J. Chen et al. (2024), ML feature extraction is crucial for tree species recognition, requiring domain knowledge, expertise, and experience. Their review also compiles studies using UAV image-based point clouds and images with algorithms such as RF, KNN, SVM, MLP, Naive Bayes (NB), linear discriminant analysis (LDA), and DT. The review of Zeybek (2025) concluded that RF, SVM, and DL enable automated tree species classification in urban areas. Finally, Man et al. (2025) using RF in terms of pixel-based classification over 15 dominant tree species, indicate that LiDAR outperformed Digital Aerial Photogrammetry (DAP), achieved higher pixel-level classification accuracy due to spectral-textural features.

On the other hand, DL operate as "black boxes" due to their high complexity and the large number of parameters (J. Chen et al., 2024; L. Pu et al., 2021). Unlike ML, DL automatically learns the features from the raw data (Tufail et al., 2023). In forestry, DL algorithms show strong potential for remote sensing image classification (Hou et al., 2023). The most frequently used neural network models include Convolutional Neural Networks (CNN), Recurrent Neural Networks (RNN), and Feedforward Neural Networks (FNN). CNNs, in particular, have achieved high accuracy in image recognition using convolutional layers (Tufail et al., 2023).

DL proposes new solutions for tree species identification problem, such as using RGB mosaics, photogrammetric point clouds, which in the past could only be solved using LiDAR and multi-or hyperspectral images (Diez et al., 2021), or identifying tree species based on a photograph, although the main challenges include acquiring sufficient labeled training data, selecting appropriate architectures and hyperparameters, and avoiding overfitting to ensure generalizability (Hamedianfar et al., 2022). For instance, Briechle et al. (2020) performed the classification of multiple tree species (pine, birch, alder) and standing dead trees with crowns using the 3D deep neural network (DNN) PointNet++ along with UAV-based lidar data and multispectral (MS) imagery. Diez et al. (2021) identify two main approaches to tree species classification in DL: (1) individual tree detection, which involves capturing treetops and pixel information from aerial imagery using models such as ResNet, VGG, or

DenseNet; and (2) semantic segmentation, in which each pixel is assigned a category (class) based on classifications made by forestry experts. Onishi & Ise (2021) constructed a machine vision system for tree identification and mapping using Red–Green–Blue (RGB) images taken by an unmanned aerial vehicle (UAV) and a convolutional neural network (CNN). Hamedianfar et al. (2022) declare that a significant challenge in training CNNs for species classification is the time-consuming task of labeling training samples. B. Liu, Huang, et al. (2022) classified and identified the individual tree point clouds of eight tree species using deep learning models, including pointwise multi-layer perceptron (MLP) (PointNet, PointNet++, PointMLP), convolution-based (PointConv), graph-based (DGCNN), and attention-based (PCT). Hou et al. (2023) propose a remote sensing image forest tree species classification method based on the Multi-Scale Convolution and Multi-Level Fusion Network (MCMFN) architecture, replacing the original 7 × 7 convolution at the first layer of ResNet-50. Z. Ma et al. (2023) use the spatial and shape features of the point cloud to study accurately segmented four types of vertical structure features in the forest sample with the Forest-PointNet Deep Learning model (adapted based on the PointNet).

ML and DL helped researchers to analyze datasets more efficiently, improve vegetation classification accuracy, and monitor forest disturbances over time (Diez et al., 2021). In the future, with growth in computing power and data availability, ML and DL are expected to play an increasingly important role in forestry.

1.7. Thesis objectives

Based on the characteristics of the study area and the background on the identification of forest species using ML and DL techniques, we have proposed the following hypothesis and objectives for this work:

Hypothesis 1 (Satellite-based): The spectral, spatial, and topographic characteristics derived from satellite imagery at regional scales enable the identification of forest species within the Andean Forest of Ecuador.

Hypothesis 2 (UAV-based): The high-resolution spatial and geometric features captured by UAV imagery at local scales enable the identification of tree species in urban areas of the Ecuadorian Andes.

Hypothesis 3 (Smartphone-based): The photographs obtained from close-range smartphone imagery allow the identification of individual tree species within urban areas of the Ecuadorian Andes.

General Objective: Identify forest and tree species in the Andean forests of Ecuador using a multi-scale approach, remote sensing data, and machine learning and deep learning methods.

Objective 1: Compare classification scenarios using different spatial resolutions and evaluate how the spatial resolution of the input data affects the efficiency of *Polylepis* stand detection.

Objective 2: Identify the optimal combination of optical, radar, and topographic variables for the identification of *Polylepis* stands using a pixel-based approach.

Objective 3: Assess the potential of spectral and geometric features derived from UAV-based photogrammetric point clouds for the identification of urban tree species.

Objective 4: Compare machine learning and deep learning classification algorithms to identify the most effective features and models for tree species identification based on tree crown UAV photogrammetric point clouds.

Objective 5: Evaluate the identification of individual tree species in urban environments using smartphone imagery and deep learning methods.

Objective 6: Explore the use of transfer learning and data augmentation techniques to enhance the efficiency of tree species identification in urban environments.

1.8. Thesis outline

Figure 1.5 illustrates a comprehensive framework for multi-scale forest and tree species identification, integrating remote sensing technologies across three scales: regional, local, and close-range, within a chronological timeline from 2023 to 2025. At the center, a forest represents the focal point of analysis, despite being the same object, the characteristics to be obtained vary according to the sensor and the scale used.

In the regional scale (2024), shown on the left with satellite imagery and a spacecraft, provides broad-scale forest monitoring, enabling the identification of dominant forest types and broad-scale vegetation patterns. In this scale analyzed in this thesis (Chapter 2) focus on the mapping of *Polylepis* forest (high importance in the Andean region of Ecuador), using Sentinel and PlanetScope satellite imagery (two spatial resolutions) together with topographic features and Machine Learning. This work includes spectral analysis, variable importance and the generation of multiple scenarios based in the combination of data type and spatial resolution.

The local scale (2025), illustrated at the top with drone-based imagery and classification outputs, offers high-resolution data for detailed analysis of individual tree crowns and forest structure. In this scale (Chapter 3) focuses on tree species identification by analyzing point clouds of tree crowns obtained with UAV-mounted RGB sensors to identify tree individual species using ML and DL in urban environments. These techniques leverage platforms such as UAVs and ground-based devices to generate models that analyze structural features of the forest, such as the tree canopy, with greater accuracy.

Finally, the close-range scale (2023), depicted on the right with a smartphone capturing in situ forest imagery, emphasizes ground-level data collection for validating and training classification models. In this scale (Chapter 4) discusses deep learning techniques, based on edge and relevant feature detection, for tree species identification from a terrestrial perspective. In this section, we evaluate the use of deep learning techniques in urban environments, employing TensorFlow Lite and a Transfer Learning approach. This method leverages a pre-trained neural network (both its architecture and weights) to train a new model.

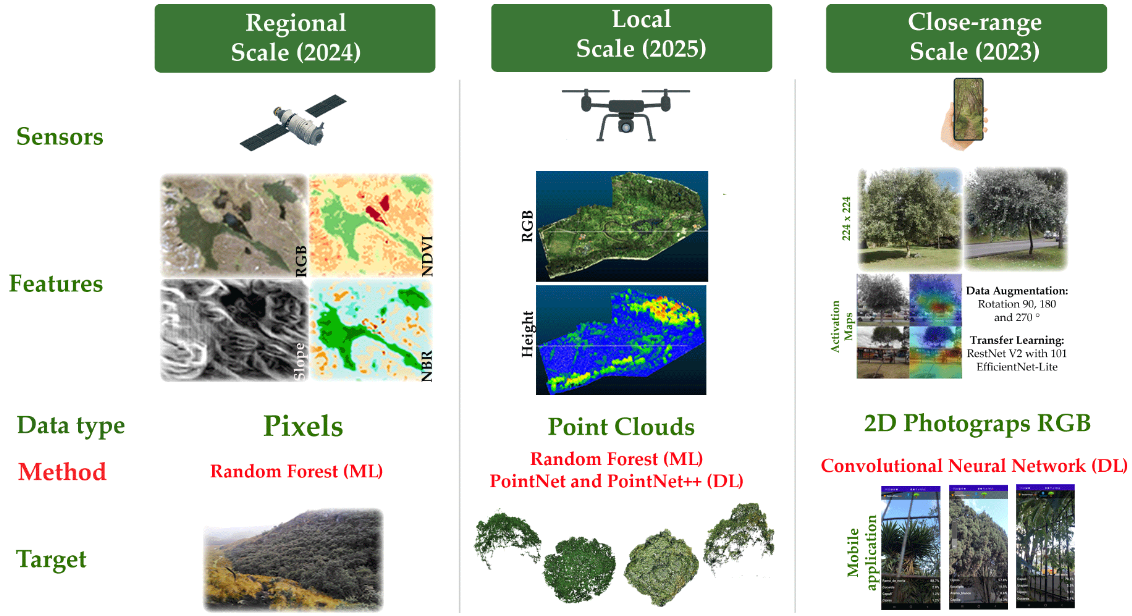

Figure 1.5. Diagram of multiple scales in forest and tree species identification.

In summary, the integration of different types of data such as spectral and spatial, together with the advancement of automatic machine and deep learning methods, allowed addressing complex problems in forest identification at different scales, where the identification of stands is analyzed regionally, then at a local scale for the identification of forest species from a zenithal view, and the identification of a single tree through smartphones (terrestrial). The projects presented reflect the evolution and potential of these techniques, highlighting their application both in natural ecosystems in the high Andes and in urban environments.

Table 1.1 summarizes the main aspects of each scientific paper, such as scale and classification method. At a regional scale, the classes evaluated include Native Forest (NFO), *Polylepis* (POL), Pine (PIN), Shrub vegetation (SVE), Other Land Use and Lan Cover classes (OCL), which are used to distinguish the land use and forestry categories. At local and close-range levels, the tree species evaluated are *Acacia dealbata Link* (ADE), *Callistemon lanceolatus (Sm.) Sweet* (CLA), *Cupressus macrocarpa Hartw. ex Gordon* (CMA), *Melaleuca armillaris (Sol. ex Gaertn.) Sm.* (CPI), *Delostoma integrifolium D. Don* (DIN), *Eucalyptus globulus Labill.* (EGL), *Fraxinus excelsior L.* (FEX), *Hibiscus rosa-sinensis L.* (HRO), *Jacaranda mimosifolia D. Don* (JMI), *Populus alba L.* (PAL), *Prunus serotina Ehrh.* (PSE), *Podocarpus sprucei Parl.* (PSP), *Pittosporum undulatum Vent.* (PUN), *Salix humboldtiana Willd.* (SHU), *Sambucus canadensis L.* (SME), *Schinus molle L.* (SMO), *Tecoma stans (L.) Juss. ex Kunth* (TST), and *Yucca gigantea Lem.* (YGU).

Table 1.1. Summary of papers by method, scales, sensors, data, reliability and classes used.

Paper title/DOI	Method	Unit	Scale	Forest	Sensor	Data	Classes number	Species evaluated	Accuracy	Kappa	Features number
Mapping *Polylepis* Forest Using Sentinel, PlanetScope Images, and Topographical Features with Machine Learning https://doi.org/10.3390/rs16224271	ML	Pixel	Regional	Stand	Satellite	Sentinel-2 Topography	5	NFO, POL, PIN,SVE, OCL	0.91	0.80	11
Urban Tree Species Identification Based on Crown RGB Point Clouds Using Random Forest and PointNet https://doi.org/10.3390/rs17111863	ML-DL	Object	Local	Tree	UAV	Point Clouds	8	ADE, CPI, FEX, JMI, PAL, SHU, SMO, TST	0.70	0.65	11
Tree Species Identification in Urban Environments Using TensorFlow Lite and a Transfer Learning Approach https://doi.org/10.3390/f14051050	DL	Object	Close-range	Tree	Smartphone	Photography	14	CLA, CPI, CMA, DIN, EGL, FEX, HRO, PAL, PSE, PSP, PUN, SHU, SME, YUG	0.80	0.79	N/A

Chapter 2

Identification of Forests at a Regional Scale using Satellite Imagery

Edited version of:

Pacheco-Prado, D.; Bravo-López, E.; Ruiz, L.Á. Mapping *Polylepis* Forest Using Sentinel, PlanetScope Images, and Topographical Features with Machine Learning. Remote Sens. 2024, 16, 4271. https://doi.org/10.3390/rs16224271

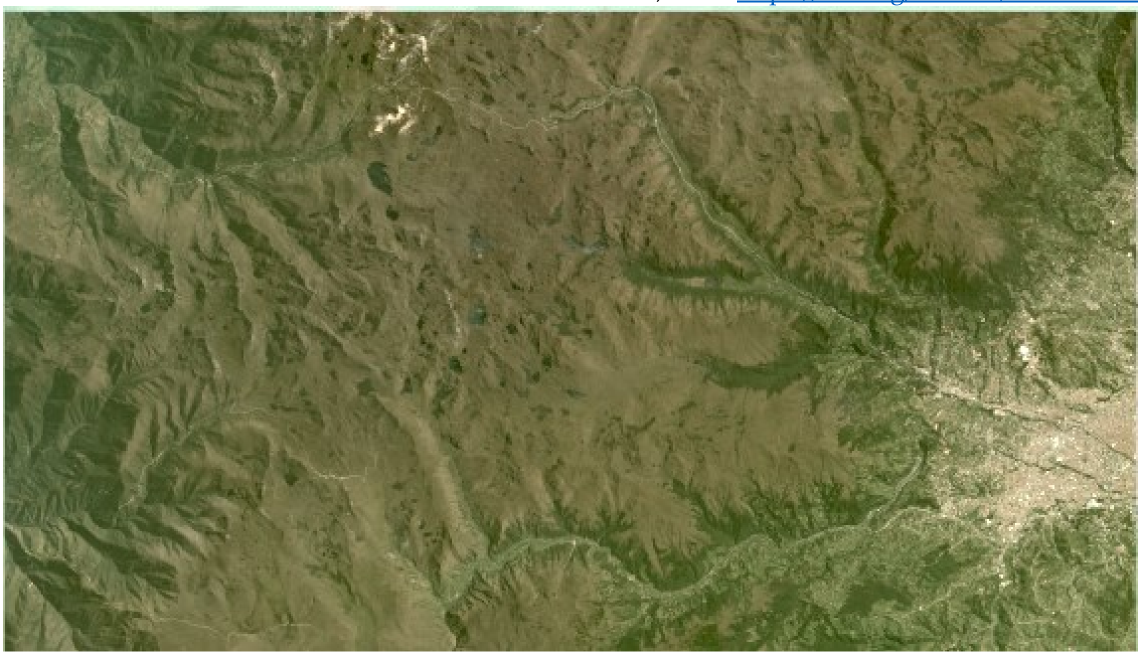

Planet Scope 2020-06_2020-08_mosaic (4.77 m)

Sentinel-2A 2020-08-24 image mosaic covering tiles 17MPS, 17MPT, 17MQS, and 17MQT (10 m)

2. IDENTIFICATION OF FORESTS AT A REGIONAL SCALE USING SATELLITE IMAGERY

In this chapter, the use of satellite imagery and the fusion of diverse data types such as multispectral, topographical, and radar data obtained from Google Earth Engine is explored. These data are used to train a machine learning model using Random Forest in Google Collaboratory, aiming to identify the locations of *Polylepis* stands at a regional scale. The Random Forest algorithm is employed for both variables' selection and pixel classification.

2.1. Introduction

In the South American Andes, the *Polylepis* forests hold significant conservation importance due to their roles in regulating water flow, facilitating soil regeneration, and retaining essential nutrients and sediments (Castillo et al., 2017; Cuyckens & Renison, 2018; Tejedor Garavito et al., 2012, 2015); however, it is one of the most threatened ecosystems (Armenteras et al., 2011) mainly due to anthropogenic activities such as deforestation (Tejedor Garavito et al., 2012, 2015), agriculture (Balthazar et al., 2015; Kleemann et al., 2022), broad-scale cattle ranching and demographic pressure (Armenteras et al., 2011; Navarro et al., 2005). Therefore, detecting the location of *Polylepis* stands is crucial for maintaining these ecosystems, particularly in Ecuador, which experiences high deforestation rates and significant forest loss along the Andean slopes (Kleemann et al., 2022). For instance, the remnants of native forests have been reduced from approximately 68% to 56% between 1990 and 2018 (Sierra et al., 2021).

Polylepis is generally found in protected areas (near lagoons, in rocky areas, canyons, and stream banks) of the Andes Mountains (Contreras, 2019; López et al., 2022) in Venezuela, Colombia, Ecuador, Peru, Bolivia, Chile, and Argentina, in altitudinal ranges from 1800 to 5200 meters above sea level (m.a.s.l.) (Romoleroux et al., 2016), in isolated stands with limited surface area and difficult accessibility (Contreras, 2019). However, certain factors that influence the distribution of *Polylepis* trees are still not known in depth (Caballero-Villalobos et al., 2021).

On the other hand, remote sensing techniques have been used to identify, characterize, and assess forest species in biodiversity conservation and ecosystem management. For example, the review by Kivinen et al. (2020) *of Populus tremula L.*, an ecologically important species in boreal forests, identified the importance of integrating ecological knowledge with remotely sensed information to understand the biodiversity patterns of this species, as well as its suitability for mapping (Kivinen et al., 2020). In other studies, Schwager & Berg (2021) used remote sensing to improve Species Distribution Models (SDM) to determine the distribution of alpine plant species (Schwager & Berg, 2021). Similarly, but in the Qilian Mountains (China), M. Ma et al. (2021) classified four tree species: *Sabina przewalskii, Picea crassifolia, Betula,* and *Populus* using satellite imagery (specifically Sentinel-2 imagery). Remote sensing has also made it possible to assess spatiotemporal changes in forest cover, biomass, plant species composition, and health, thus improving the ability to estimate biomass at the level of individual trees (D. Xu et al., 2021); classify forests into species groups (Bjerreskov et al., 2021); assessing the health status of urban forests (Georgieva et al., 2022); understanding succession patterns in tropical forests to monitor their biodiversity (Chraibi et al., 2021) or analyzing forest recovery under diverse climatic conditions (Luber et al., 2023).

Using specific satellite images also makes identifying and characterizing species possible, as evidenced in the works cited above. Another important aspect refers to the Sentinel mission images. Sentinel is a satellite constellation part of the Copernicus program of the European Space Agency (ESA), providing free and medium-resolution satellite imagery. In this context, two of the missions are Sentinel-1 (S1) and Sentinel-2 (S2). The first (S1) has a Synthetic Aperture Radar (SAR) sensor that generates its energy wave and measures backscattered radiation from the ground (Vali et al., 2020) and can penetrate cloud cover and obtain data in different atmospheric conditions (Vega Isuhuaylas et al., 2018). In addition, S1 mission data are used in the construction of forest masks (Dostálová et al., 2016), in the assessment of physical characteristics and properties such as roughness, water content (moisture), and structural geometry of forest species (Mngadi et al., 2021), in the detection of forest degradation and regeneration (W. Ma et al., 2019). However, it can have substantial distortions due to the effect of topography (Dostálová et al., 2016). S2 optical images are used in the detection and monitoring of land cover and other applications through the MultiSpectral Instrument (MSI). Thanks to the operation of two similar satellites, S2A and S2B, the image acquisition of the same area is achieved every five days. Its usefulness is reflected in the different applications of these images for the detection of invasive species (Phiri et al., 2020), the identification and classification of tree species (Xi et al., 2021), or the use of multitemporal data for the characterization of regenerating forest stands (Akbari et al., 2021). To enhance the discrimination of forest species, various studies have demonstrated the effectiveness of combining S1 and S2 data (Mngadi et al., 2021; Vali et al., 2020), as well as their integration with topographic information (Liu et al., 2018), in Cloud Computing platforms such as Google Earth Engine (GEE) (Gorelick et al., 2017; Pizarro et al., 2022; Svoboda et al., 2022). On the other hand, there is currently spectral information with better spatial resolution available through the PlanetScope platform, acquiring images with 3 m/pixel spatial resolution, and captures data in the red (R), green (G), blue (B), and near-infrared (NIR) channels. However, the open-access data provided by Norway's International Climate & Forests Initiative program (NICFI), in collaboration with Planet Labs of the PlanetScope data, are available in semiannual or monthly mosaics with a resolution of 4.77 m per pixel. Some studies, such as the one from Vizzari (2022), use these data in GEE environment to compare ten land use and land cover (LULC) classification approaches, highlighting the advantages of adopting an object-based (OB) approach with PlanetScope (PS) data and integrating PS with Sentinel-2 and

Sentinel-1 data. These studies incorporate Gray Level Co-occurrence Matrix texture variables to aid classification.

Although remote sensing is widely applied in identifying, monitoring, and characterizing forest species, its implementation presents important challenges in the study of the genus *Polylepis*. Some studies are focused on this species, such as the one conducted by López et al. (2022), who evaluated the distribution and cover of a *Polylepis* species (*P. tarapacana*) and its relationship with topographic, environmental, and climatic factors in the Andean zone of northern Argentina, identifying that elevation and slope are significant factors in the distribution of this species within the study sector. Caballero-Villalobos et al. (2021) evaluated the possible distribution of *Polylepis quadrijuga* in the Colombian Andes due to its ecological importance, using different future temporal scenarios, demonstrating that climate change could generate a considerable loss of suitable habitat for this species. Rojas et al. (2022) evaluated the unique climatic habitat conditions of *Polylepis Tarapacana* in the Chilean Andes. They highlighted the urgent need to develop studies that analyze adaptive strategies for this species to withstand climate changes at high altitudes. It is worth noting that studies employing pixel and object classification methods (Hościło & Lewandowska, 2019; Tassi & Vizzari, 2020) within the mountainous forests of the Andean region have major limitations (Vega Isuhuaylas et al., 2018), mainly due to the topographic complexity, shadows, and illuminated areas (Hościło & Lewandowska, 2019), the limited availability of cloud-free satellite images (Ai et al., 2020; Navarro et al., 2005), and the challenge of finding completely homogeneous pixels (Vega Isuhuaylas et al., 2018). However, there are approximations through the detection of native forests with the combination of optical and radar features (Prado & Ruiz, 2019).

Combining remote sensing data with image processing and classification methods is useful to analyze and identify forest entities (Haq et al., 2021). Several works present the feasibility of the evaluation of forest ecosystems through Machine Learning (ML) algorithms such as Random Forests (RF) (Bolyn et al., 2018; Contreras, 2019; Hościło & Lewandowska, 2019; Ligono & Okolie, 2022; Prado & Ruiz, 2019; Ruiz et al., 2016; Svoboda et al., 2022; Tassi & Vizzari, 2020; Vega Isuhuaylas et al., 2018), Support Vector Machines (De Luca et al., 2019; Hościło & Lewandowska, 2019; Tassi & Vizzari, 2020; Vega Isuhuaylas et al., 2018), Gradient Boosting (Georganos et al., 2018), Naive Bayes (Balha et al., 2021), being RF one of the most used, especially in the discrimination and identification of mountain forests and shrublands (Vega Isuhuaylas et al., 2018). Additionally, some researchers used hyperspectral images obtained from Unmanned Aerial Vehicles (UAV) for the identification of *Polylepis* and other forest species (Castillo et al., 2018; Li et al., 2023; Zhou et al., 2023).

Despite this progress, several challenges remain in identifying *Polylepis* using remote sensing. These challenges include: 1) The small size of *Polylepis* stands limits their detection with freely available satellite data. 2) Accessibility to these forests is complicated, making it challenging to obtain field validation data. 3)

The spectral signature of *Polylepis* is like those of other shrub vegetation in the study zone.

Given this background, the objective of this chapter is to: (a) Compare classification scenarios at spatial resolutions of 5 and 10 m and evaluate if there is any difference in the efficiency of *Polylepis* detection based on the spatial resolution of the input data; (b) evaluate the combination of optical, radar and topographic data for *Polylepis* stands identification; and (c) identify the minimum variables needed to classify *Polylepis* stands using a pixel-based approach.

2.2. Materials and Methods

2.2.1. Study zone

The study area is in the Andes Mountains in southern Ecuador (Figure 2.1), with an approximate area of 137,211 ha. It has an altitude range from 918 to 4534 m.a.s.l. The predominant land cover is paramo, an ecosystem where *Polylepis* species are present (Minga-Ochoa et al., 2019), occupying approximately 45% of the area. Vegetation classes such as native forests, *Polylepis* stands, forest plantations, and shrublands (chaparro) account for approximately 24% of the area, with *Polylepis* being one of the least represented, covering less than 1%. *Polylepis* stands are believed to be "possible remnants of vegetation that once covered larger areas" (Ulloa et al., 2008). The remaining area corresponds to other classes, such as water bodies and bare soil.

Although a significant portion of the study area falls within the protected boundaries of Cajas National Park (CNP), it remains vulnerable to deforestation and associated threats (Kleemann et al., 2022).

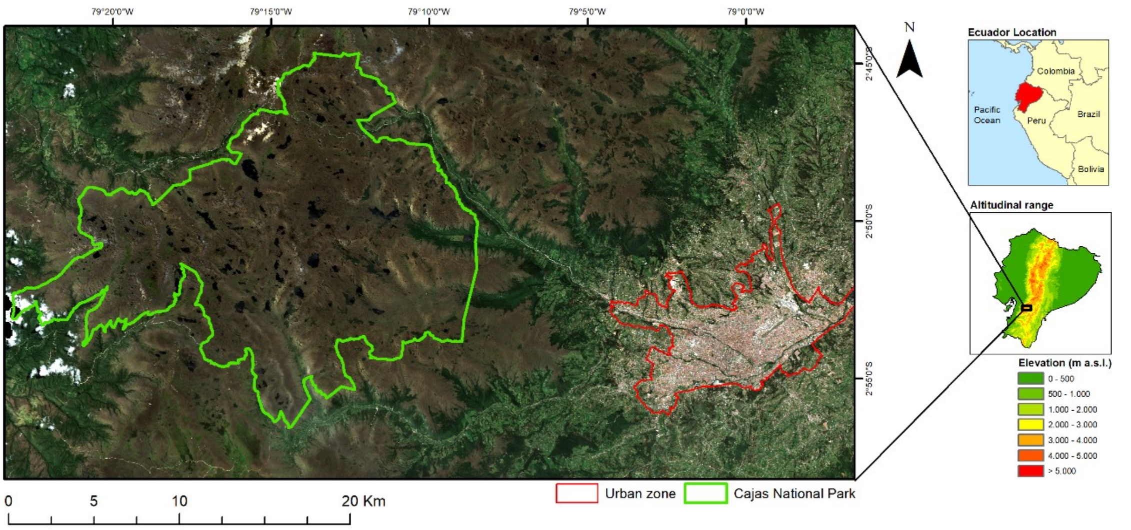

Figure 2.1. Sentinel Sentinel-2A image mosaic covering tiles 17MPS, 17MPT, 17MQS, and 17MQT (August 24, 2020) of the study area and location of *Polylepis* stands.

2.2.2. *Polylepis* stands

Polylepis stands are distributed along the western and eastern sierras (Minga-Ochoa et al., 2019), and in Ecuador, according to the Global Biodiversity Information Facility (GBIF) database https://www.gbif.org/es/ (accessed on 25 July 2022), these stands can be found above 1067 m.a.s.l. Their height ranges from 8 to 10 m, with twisted branches covered with moss (Minga-Ochoa et al., 2019). Ecuador is the eighth country with the greatest variety of tree species in the world (FAO & UNEP, 2020). Of the genus *Polylepis* (identification target), seven native species can be found: *P. incana, P. lanuginosa*, *P. microphylla*, *P. pauta*, *P. reticulata*, *P. sericea* and *P. weberbaueri*. In the study area (southern Ecuador), four of these species are found: P. *reticulata* (Figure 2.2), *P. lanuginosa, P. weberbaueri and P. incana* (Minga-Ochoa et al., 2019).

(a) (b)

Figure 2.2. *Polylepis* reticulata trees (a) and stand (b) in Luzpa lagoon zone.

2.2.3. Workflow description

With the vector and satellite data available, a methodology was proposed that can be explained in four stages (Figure 2.3). The first stage consisted of searching for information on the location of *Polylepis* stands in the study area and integrating it with a Land Use Land Cover (LULC) map, which generated a base map from which the target classes of the classification model were determined (green section). In the second stage, satellite data were selected and prepared through the GEE platform, including S2 and PlanetScope spectral data (bands and indices) and textures of the NIR band of PlanetScope image, S1 radar data, and the Digital Elevation Model (DEM) obtained from the Sigtierras project (*SigTierras – Ministerio de Agricultura, Ganadería, Acuacultura y Pesca*, n.d.) (yellow section). In the third stage, the scenarios to be evaluated were defined, considering the spatial resolution and the combination of different types of variables (orange section). The final stage consisted of comparing different scenarios and variables to determine the combination that produces the highest reliability in detecting *Polylepis* stands. Metrics from each scenario were evaluated, and the best-performing scenario was selected. Using this scenario, a *Polylepis* map was generated and validated by forestry specialists in the region (blue section).

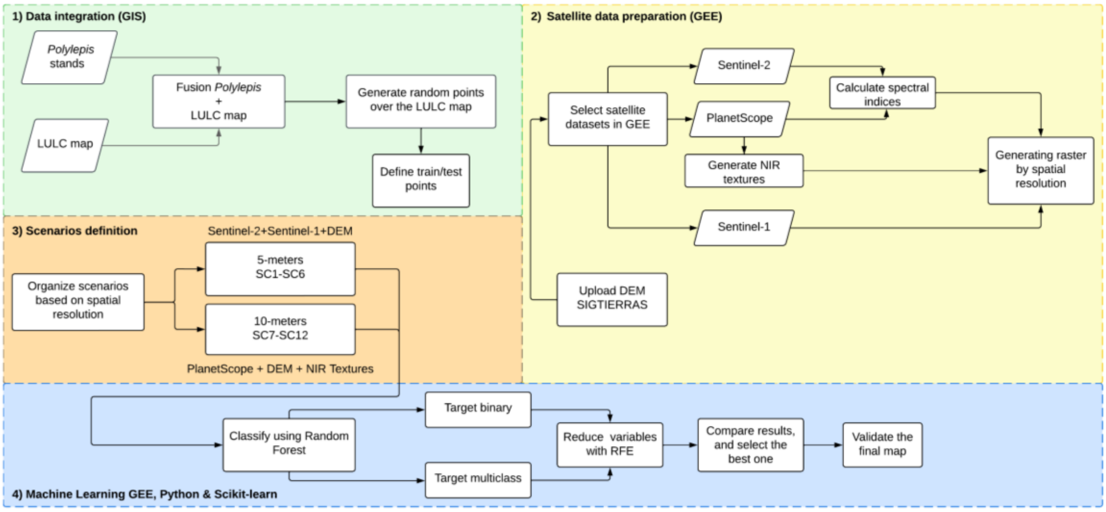

Figure 2.3. Workflow diagram.

2.2.3.1. Data integration

The LULC map of the study area was obtained from the Azuay province at a scale of 1:5,000 (Tenesaca et al., 2017), which was constructed from the aerial orthophotography of the SIGTIERRAS project of Ecuador (SIGTIERRAS, 2017). The *Polylepis* occurrence data for the study area were sourced from georeferenced records available in online repositories, including the Global Biodiversity Information Facility (GBIF) and Herbario Azuay, collected in 2016. These initial records were validated through field verification conducted between July 2016 and October 2017. The final dataset comprises 244 stands records of the *Polylepis* genus distributed as follows: 55 records for *P. incana*, 86 for *P. lanuginosa*, 50 for *P. reticulata*, and 53 for *P. weberbaueri*. Of the total dataset, 73% represent field-verified observations, while the remaining 27% corresponds to botanical collection data or herbarium records.

Based on this LULC map generating random points in two targets, multiclass and binary, for the classification processes (Table 2.1). In the binary target, the No *Polylepis* class groups classes such as native forests, pine, shrub vegetation, and non-forest classes. Finally, seventy percent of the points were allocated for training, while the remaining thirty percent were reserved for validation.

Table 2.1. Forest classes and points (pixels) number for training and validation in multiclass and binary targets.

	Multiclass target					Binary target			
Class name	**Code**	**Train**	**Validation**	**Total**	**Class Name**	**Code**	**Train**	**Validation**	**Total**
Polylepis	1	2,362	974	3,336	*Polylepis*	1	2,362	974	3,336
Native forest	2	303	150	453	No *Polylepis*	2	11,732	5,113	16,845
Pine	3	93	35	128					
Shrub vegetation	4	1,674	700	2,374					
Other classes	5	9,662	4,228	13,890					

2.2.3.2. Satellite data preparation

Satellite data acquisition (Table 2.2) and the generation of satellite information indices (Table 2.3) were conducted using the GEE tool. This Cloud Computing approach enabled multiple tasks to be performed on a high volume of data (L. Kumar & Mutanga, 2018), facilitating the workflow. The data used were as follows:

a) Sentinel-2 optical data (level 2A), radiometrically corrected to ground reflectance level, were used. This data corresponds to the mosaic of tiles 17MPS, 17MPT, 17MQS, and 17MQT from 24 August 2020 to compose an image with the minimum presence of clouds. In GEE, the COPERNICUS/S2_SR_HARMONIZED repository was used in which the values of the scenes were harmonized so that the most recent data (after 25 January 2020) are in the same range as the oldest scenes (*Sentinel-2 MSI: MultiSpectral Instrument, Level-2A*, n.d.).

b) Synthetic Aperture Radar (SAR) data in Interferometric Wide (IW) mode and processed in Ground Range Detected (GRD) format were obtained from the Sentinel-1 sensor. This sensor offers two polarities: VV (vertical transmit/vertical receive) and VH (vertical transmit/horizontal receive).

c) Norway's International Climate & Forests Initiative (NICFI) provides free access to high-resolution PlanetScope imagery in GEE. This dataset includes the red, green, blue, and near-infrared (NIR) bands, available as a mosaic spanning from June 2020 to August 2020, and resampled from 4.77 m to 5 m of pixel size. The textural features obtained from the NIR band were extracted via gray-level co-occurrence (GLCM). The features generated include Max Corr. Coefficient (N_maxcorr), Angular Second Moment (N_asm), Entropy (N_ent), Cluster prominence (N_prom), Difference entropy (N_dent), Sum Entropy (N_sent), Variance (N_var), Inertia (N_inertia), Information Measure of Corr. 1 (N_imcorr1), Information Measure of Corr. 2 (N_imcorr2), Contrast (N_contrast), Difference variance (N_dvar), Sum Variance (N_svar), Correlation (N_corr), Dissimilarity (N_diss), Shade (N_shade), and Inverse Difference Moment (N_idm).

d) Topography data was obtained from the Ecuador Sigtierras project, which provides data distributed with a pixel size of 3 m. This dataset was used to determine the terrain topography and derive slope and orientation, resampled to a pixel size of 5 and 10 m using bilinear interpolation. Due to the varying spatial resolutions of the satellite data, the data were grouped into categories of 5 m and 10 m resolutions.

Table 2.2. Multispectral, SAR, and topographic datasets were used in the study.

Dataset	Temporality	Spatial resolution/bands	Reference
Sentinel-2A MSI	Mean value August 24, 2020	10 m (TCI_R, TCI_G, TCI_B, B2, B3, B4, B8) 20 m (B5, B6, B7, B8A, B11, B12) 60 m (B1, B9)	(*Sentinel-2 MSI: MultiSpectral Instrument, Level-2A*, n.d.)

Sentinel-1 SAR GRD	Mean value August, 2020	10 m (VH, VV)	(Nandy et al., 2021) (Dostálová et al., 2016)
PlanetScope normalized analytic	Mosaic 2020-06 - 2020-08	4.77 m (R, G, B, NIR)	(Vizzari, 2022)
Topographic data	Photogrammetric fly 2010	3 m (Elevation, Slope, Aspect)	(Jarvis et al., 2008)

Table 2.3. Vegetation indices and formulas used in this study.

Indices	Formula	Reference
EVI Enhanced Vegetation Index	$2.5 \times \frac{NIR - Red}{(NIR + 6Red - 7.5\ Blue) + 1}$	(Arekhi et al., 2019)
NDWI Normalized Difference Water Index	$\frac{Green - NIR}{Green + NIR}$	(Nandy et al., 2021)
MSI Simple Ratio 1600/820 Moisture Stress	$\frac{SWIR\ 1}{NIR}$	(Bolyn et al., 2018)
SIPI Structure Insensitive Pigment Index	$\frac{NIR - Aerosols}{NIR - Red}$	(*IDB - Index DataBase*, n.d.)
ARI Anthocyanin Reflectance Index	$\frac{1}{Green} - \frac{1}{Red\ Edge\ 1}$	
CCCI Canopy Chlorophyll Content Index	$\frac{\frac{NIR - Red\ Edge\ 1}{NIR + Red\ Edge\ 1}}{\frac{NIR - Red}{NIR + Red}}$	
MSR Modified Simple Ratio 670/800	$\frac{NIR - Blue}{Red + Blue}$	
NGRDI Normalized Green Red Difference Index	$\frac{Green - Red\ Edge\ 1}{Green + Red\ Edge\ 1}$	
GLI Green Leaf Index	$\frac{2Green - Red\ Edge\ 1 - Blue}{2Green + Red\ Edge\ 1 + Blue}$	
NDVI Normalized Difference Vegetation Index	$\frac{NIR - Red}{NIR + Red}$	(Bolyn et al., 2018) (Nandy et al., 2021) (Arekhi et al., 2019) (Vizzari, 2022)

2.2.3.3. Scenarios definition

After defining the datasets to be used, we evaluated different scenarios while maintaining spatial resolutions of 5 m (RF1-RF6) and 10 m (RF7-RF12). This analysis aimed to determine whether spatial resolution influenced the outcomes, as summarized in Table 2.4. The datasets are represented as follows: "TOPO" refers to digital elevation model data from Sigtierras, including slope and aspect derivatives. "PS" represents PlanetScope imagery and indexes, while "GLMC" denotes textures derived from the near-infrared band of PS. "S2" represents Sentinel-2 data and indexes, and "S1" represents Sentinel-1 data. In the proposed scenarios, the multiclass or binary target approach will also be evaluated to distinguish *Polylepis* from other shrub classes.

Table 2.4. Scenario definition based on dataset combination.

Scenario	Resolution	Dataset combination	Variables number
SC1	5m	TOPO	3
SC2		PS	7
SC3		GLCM NIR	18
SC4		TOPO + PS	10
SC5		TOPO + GLCM NIR	21
SC6		PS + TOPO + NIR GLCM	28
SC7	10m	S1	2
SC8		S2	24
SC9		S1+TOPO	5
SC10		S2+TOPO	27
SC11		S2+S1	26
SC12		S2+S1+TOPO	29

2.2.3.4. Variable reduction

GEE provides a variety of supervised classification algorithms suitable for satellite image classification. This study employed the Random Forest (RF) algorithm, implemented in GEE as smileRandomForest (SRF). RF is a nonparametric statistical method of decision tree assembly widely used in land cover classification from remote sensing data (Vali et al., 2020). Each tree is trained with different data so that by combining the results, some errors are compensated by others. This algorithm is used by several authors in forestry domains based on pixel classification of satellite images (Balha et al., 2021; Grabska et al., 2019; Mishra et al., 2021; Praticò et al., 2021; Vega Isuhuaylas et al., 2018) and with object approach as in (Ruiz et al., 2016; Tassi & Vizzari, 2020). For this study, the number of trees was set to 50, while other parameters were left at their default values to facilitate scenario reliability comparison.

From the former, the Recursive Feature Elimination (RFE) technique has been selected for its ability to eliminate noise and irrelevant features, using a Machine Learning algorithm to rank features by importance, discarding the least important features, and re-fit the model to improve the performance of the classification model (Pratama, 2023). In GEE, the SRF algorithm was employed to assess the importance of variables in each classification scenario. The variable reduction with RFE was performed by being the first iteration run with all variables, and, in the following runs, the features of lesser importance were removed. After eliminating the least significant variables, the classification process was run again, and the proposed metrics were evaluated.

2.2.3.5. Scenarios comparation

The classification results with all variables were evaluated in a general way, using the Global Accuracy, which refers to the ratio between correctly classified pixels and all verification pixels (the main diagonal of the confusion matrix), and the kappa coefficient to evaluate the classification performance compared to the expected random assignment (Gerón, 2019). Other metrics used focused on evaluating the classification performance of the *Polylepis* class, using for this purpose the User Accuracy (UA), which refers to the ratio between the total number of correctly classified samples for a particular class and the total number of reference samples classified in that same class; and the Producer Accuracy (PA) which shows the ratio between the accurately classified reference samples of a particular class and the total number of reference samples of that class (Gerón, 2019), this in GEE.

Finally, the F-score is a harmonic mean between Precision and Recall (Vizzari, 2022), which allows individual evaluation of class behavior. This process will be carried out on the most reliable scenarios using scikit-learn library version 1.5.2 and Python version 3.10.12.

2.3. Results

2.3.1. Variable reduction using RFE and comparison of classification metrics for different scenarios

The reliability values obtained from the various classification scenarios (GEE) are compared in Table 2.5. This table reports the total number of variables and the variables selected by the RFE process, considering their importance in the RF algorithm. The initial variable set (N column) is significantly reduced in most scenarios through the Recursive Feature Elimination (RFE) process, underscoring its effectiveness in filtering out less informative features. For example, in SC6, the original 28 variables are pared down to 11 post-RFE (Figure 2.4). Conversely, RFE retains a smaller subset of features in scenarios that start with fewer variables (e.g., SC1 and SC7), suggesting that these scenarios either have inherently simpler data structures or initially contain fewer irrelevant features.

Table 2.5. *Polylepis* classification scenarios: spatial resolution of input features, number of features produced and selected, Accuracy (Acc), and kappa coefficient after the RFE reduction process for binary and multiclass targets. UA and PA refer to the *Polylepis* class.

				Multiclass target					Binary target				
Name	**Resolution**	**Datasets**	**N***	**RFE**	**Acc**	**Kappa**	**UA**	**PA**	**RFE**	**Acc**	**Kappa**	**UA**	**PA**
SC1	5m	TOPO	3	3	0.73	0.37	0.46	0.30	3	0.83	0.26	0.45	0.29
SC2		PS	7	7	0.86	0.69	0.75	0.79	7	0.93	0.72	0.80	0.74
SC3		GLCM NIR	18	5	0.68	0.12	0.36	0.12	18	0.84	0.08	0.42	0.07
SC4		TOPO + PS	10	9	**0.90**	**0.78**	**0.87**	**0.89**	**9**	**0.96**	**0.86**	**0.89**	**0.87**
SC5		TOPO + GLCM NIR	21	7	0.76	0.41	0.64	0.25	6	0.85	0.29	0.59	0.25
SC6		PS + TOPO + NIR GLCM	28	11	0.90	0.78	0.88	0.88	7	0.96	0.86	0.90	0.87
SC7	10m	S1	2	2	0.68	0.24	0.29	0.20	2	0.82	0.09	0.31	0.12
SC8		S2	24	8	0.88	0.74	0.85	0.85	8	0.95	0.81	0.87	0.81
SC9		S1+TOPO	5	5	0.82	0.60	0.74	0.66	4	0.88	0.53	0.69	0.54
SC10		S2+TOPO	**27**	**11**	**0.91**	**0.80**	**0.90**	**0.89**	7	**0.97**	**0.87**	**0.90**	**0.88**
SC11		S2+S1	26	13	0.89	0.76	0.85	0.86	10	0.95	0.82	0.88	0.82
SC12		S2+S1+TOPO	29	7	0.91	0.80	0.89	0.90	9	0.96	0.86	0.90	0.87

The reports and confusion matrix of the best scenarios is available at https://gis.uazuay.edu.ec/papers/polylepis/ (accessed on 24 September 2024)

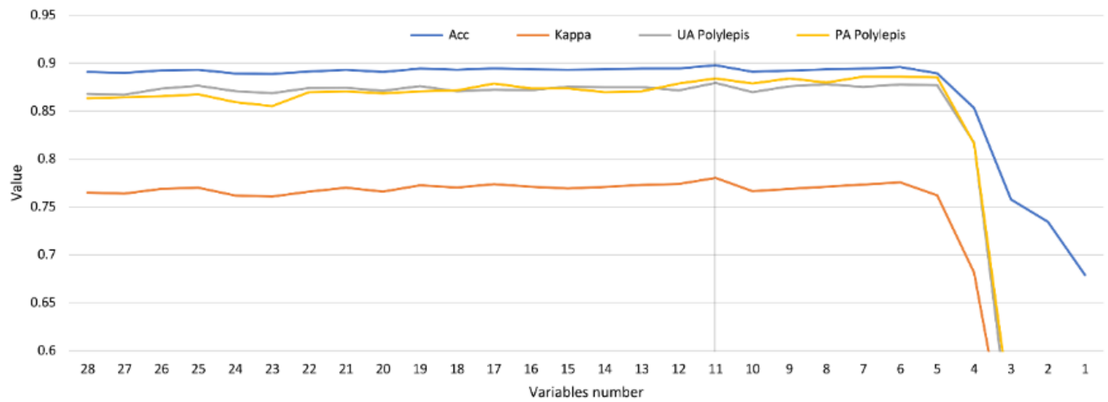

Figure 2.4. Behavior of Accuracy (blue line), Kappa (orange line), UA (gray line) and PA (yellow line) metrics during the RFE process in the SC6 scenario. Peak values are obtained with 11 variables.

The scenarios that produced the best accuracy and kappa values are SC4 (0.90 and 0.78) for the 5-meter datasets. In the 10-meter datasets for the multiclass approach, SC10 (0.91 and 0.80) and SC12 (0.91 and 0.80) were the best. For the binary target, SC6 (0.96 and 0.86) and SC10 (0.96 and 0.87) were the best. On the other hand, the scenarios that evaluated the datasets without multispectral information (SC1, SC3, SC7, SC9) had lower reliability compared to the other scenarios that included these types of variables.

In scenarios using 10-meter resolution data (SC7–SC12), the models exhibit strong predictive performance across both multiclass and binary classification tasks, with particularly notable gains when Sentinel-2 imagery is combined with topographic data (TOPO). Meanwhile, in scenarios employing 5 m resolution data, the integration of PlanetScope imagery with additional layers, such as topographic or texture-based features (e.g., SC4, SC5, and SC6), consistently improves classification accuracy. These findings imply that the combined use of high-resolution data and a diverse set of feature types can mitigate the constraints imposed by the coarser resolution of certain datasets, thereby enhancing overall model performance.

An examination of the F1-scores (Table 2.6) across various land cover classes in optimal scenarios (SC4, SC6, SC10, and SC12) reveals a consistent trend in the multiclass classification. For instance, the *Polylepis* class maintains high accuracy across all configurations, ranging from 0.88 to 0.90, whereas the Pine class exhibits substantial variability, with accuracy scores ranging from as low as 0.00 in SC6 to 0.48 in SC10. In the binary classification setting, which differentiates between *Polylepis* and No *Polylepis*, both classes achieve robust accuracies, with scores between 0.88 and 0.98. Lower performance is observed in classes with limited sample sizes, such as Pine and Native Forest, potentially due to restricted data representation or class overlap, which may challenge the model's discrimination capacity.

Table 2.6. F1-Score comparison by best scenarios.

Target	Class	Pixels number	SC4	SC6	SC10	SC12
Multiclass	*Polylepis*	974	0.88	0.88	**0.90**	**0.89**
	Native forest	150	0.49	0.45	0.37	0.25
	Pine	35	0.06	0.00	0.48	0.37
	Shrub vegetation	700	0.72	0.73	0.73	0.74
	Other classes	4,228	0.94	0.95	0.95	0.95
Binary	*Polylepis*	974	0.88	0.88	**0.89**	**0.89**
	No *Polylepis*	5,113	0.98	0.98	0.98	0.98

In the best scenarios, several variables are repeated multiple times, indicating their importance across different scenarios. This is particularly true for topographic variables such as elevation, slope, and aspect (Figure 2.5). In the multispectral domain, the indices PS_NDVI (5 m), CCCI, MSR, and MSI from S2 (10 m) appeared in various classification scenarios; these indices have in common the band 8 of S2 in the range of 835.1 nm.

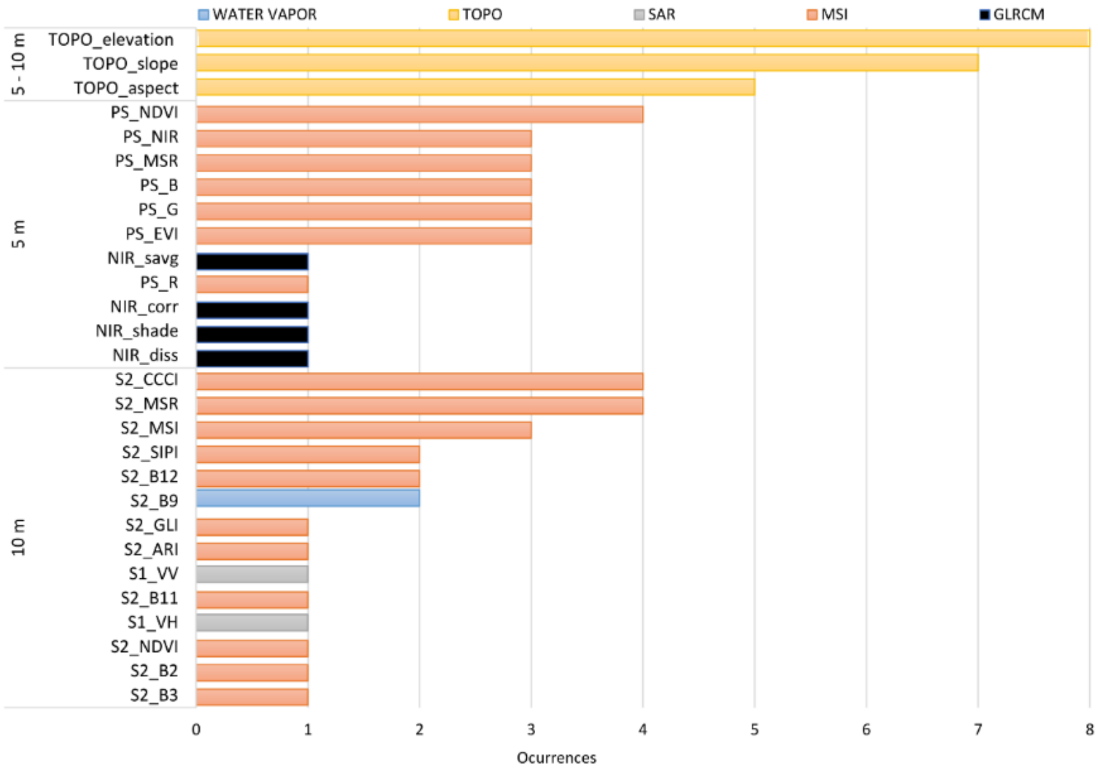

Figure 2.5. Variables that were repeated (occurrences) in the best eight scenarios. S2 (Sentinel-2), S1 (Sentinel-1), TOPO (Topography) and PS (PlanetScope).

2.3.2. Comparison of the maps of the best scenarios

Figure 2.6 presents a detailed example of the supervised classification results in a sub-area of the Toreadora Lagoon, which includes a variety of shrub classes. In this region, pixels classified as *Polylepis* are shown in green. The scenario SC4, with a multiclass target and a spatial resolution of 5 m, also performs well with a high accuracy of 0.90 and Kappa of 0.78, indicating that different resolutions can yield similar results depending on the dataset combination. However, the evaluation of known areas reveals high separability between *Polylepis* and other vegetation classes in the 10 m SC10 and SC12 multiclass scenarios. In the multiclass target, red polygons indicate a Pine plantation. Although the Accuracy and Kappa metrics favor the SC4 scenario in the binary classification, the UA and PA for *Polylepis*, when evaluated together, were better in the SC10 multiclass scenario. This is reflected in an improved distinction of the *Polylepis* class from other shrubs, as shown in Figure 2.6.

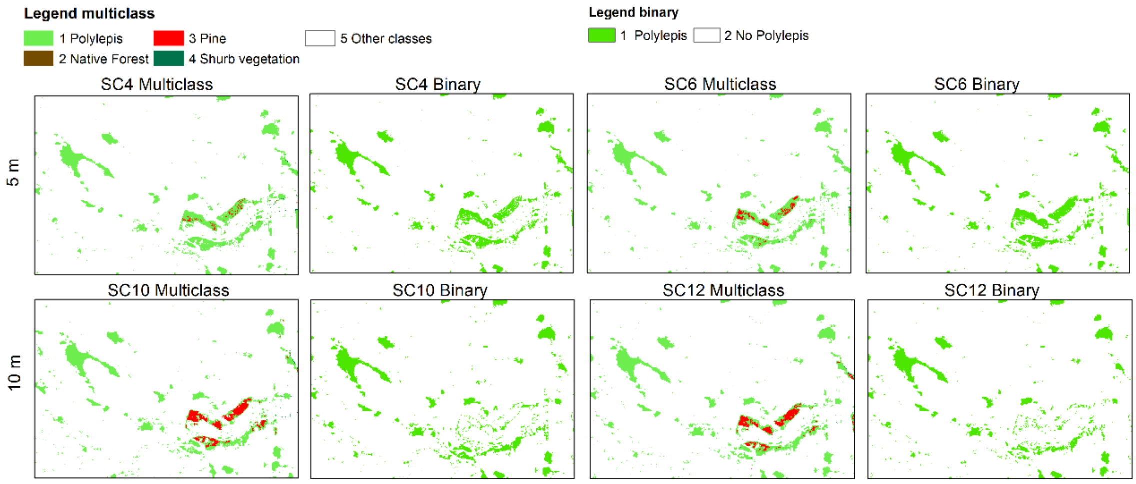

Figure 2.6. Detailed view of the eight best classification scenarios in the Toreadora Lagoon region.

The final scenario selected was SC10 with a multiclass target (Figure 2.7), showing *Polylepis* located in the paramo zone. This was achieved using variables MSI, B9, B2, MSR, CCCI, B12, ARI, and NDVI of S2 in conjunction with aspect, slope, and elevation. The variable importance (Figure 2.8) revealed that elevation and slope were the most significant factors, while the selected spectral indices and S2 bands made a similar contribution. In this map, another known area is Llaviuco Lagoon, where a clear distinction can be observed between *Polylepis* stands and shrub vegetation despite both classes presenting similar spectral characteristics.

The map in Figure 2.7 presents the spatial distribution of land cover classes in the study area, focusing on the classification of *Polylepis* stands, native forest, pine plantations, shrub vegetation, and other vegetation types. *Polylepis* stands are highlighted in light green, native forests in brown, pine plantations in red, shrub vegetation in dark green, and other classes in gray. The mapped area includes two highlighted zones outlined in red and magenta, labeled as “Llaviuco” and “Toreadora,” respectively, indicating specific regions of interest for *Polylepis* detection.

The spatial extent shows that *Polylepis* stands are dispersed in specific regions, mostly fragmented and interspersed with other vegetation classes. Native forest areas appear more contiguous, primarily concentrated in the lower central part of the map, while pine plantations are present in relatively small clusters, mostly located near the Llaviuco region. Shrub vegetation and other classes occupy larger contiguous areas, particularly along the central and southern regions of the map, suggesting a gradient of vegetation types influenced by altitude and possibly other topographic variables.

This map allows for a visual evaluation of classification accuracy and the spatial distribution of *Polylepis* stands within a diverse landscape matrix, providing insights into potential ecological factors affecting *Polylepis* distribution.

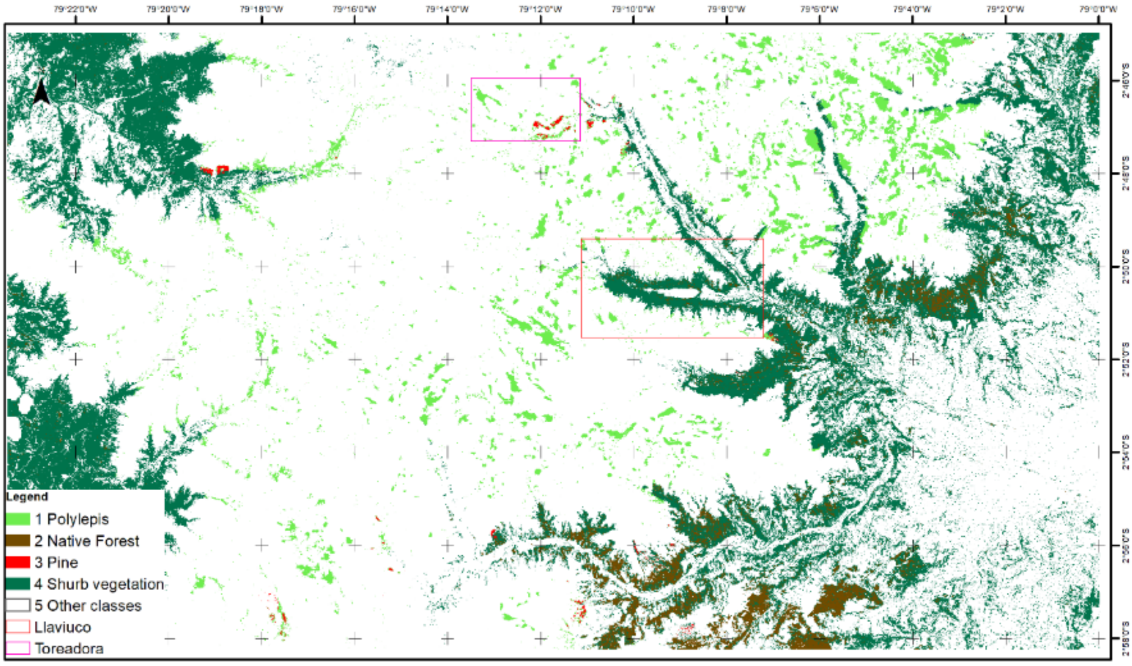

Figure 2.7. SC10 multiclass map was selected as the best scenario. Known regions such as Toreadora Lagoon (purple polygon) and Llaviuco Lagoon (red polygon) helped to visually interpret the quality of the classification models. Other land uses and coverages in the area are shown in white color.

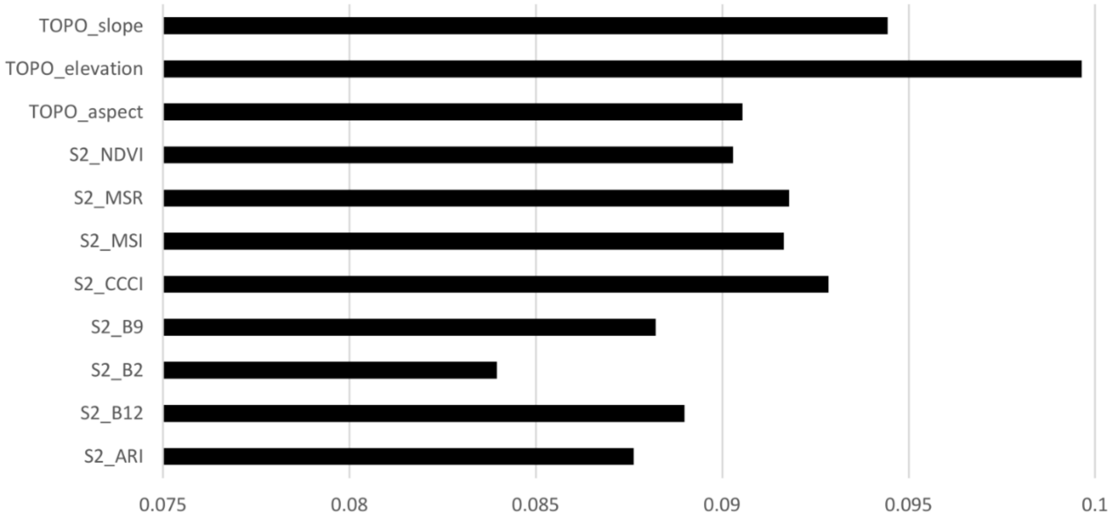

Figure 2.8. Feature importance of SC10 multiclass scenario

2.4. Discussion

In this work, we compared twelve scenarios resulting from combinations of Sentinel-2 (S2), Sentinel-1 (S1), PlanetScope (PS), texture GLCM for NIR PS band, and topographic data (elevation, slope, and aspect), using two target types (multiclass or binary) for the classification of *Polylepis* stands. Among all scenarios, four (SC4, SC6, SC10, and SC12) demonstrated the highest reliability in Accuracy and Kappa. Although in several scenarios, the metrics did not show significant differences, selecting known review areas allowed for a better detection of the best scenario by *Polylepis* discrimination, providing a qualitative assessment of each scenario's validity.

The combination of Sentinel-2 and topographic data (S2 and TOPO) provides the most effective scenario for achieving high classification accuracy in a multiclass context. Pizarro et al. (2022) obtained the highest reliability with this same combination of variables using Random Forest. However, their study focused on discriminating against land use and land cover in the Andes, while ours specifically targeted the identification of *Polylepis*.

Discrimination between *Polylepis* and pine was more effective in a 10 m scenario (SC10 and SC12) despite the fact that the metrics Accuracy and the Kappa of scenarios SC4 and SC6 do not have a significant difference. This makes us think that a greater range of radiometric spectra promotes the distinction of *Polylepis*. This finding challenges the assumption that higher spatial resolution automatically translates to better classification results.

The superior performance of the multiclass approach, as opposed to binary, suggests that capturing the variation within *Polylepis* stands, rather than simply the presence or absence, is crucial for accurate mapping. By distinguishing between multiple classes, the model can account for the ecological diversity within *Polylepis* habitats. This approach enables a more detailed understanding of *Polylepis* distribution, which is essential for effective conservation and management. The stands of these forests often exhibit substantial heterogeneity due to environmental gradients, such as altitude, slope, and soil type.

The reduction of variables using RFE in the best scenario (SC10); it was possible to reduce the number of variables from 27 to 11 (8 spectral and 3 topographic) without significantly affecting accuracy and Kappa. The selected variables were MSI, B9, B2, MSR, CCCI, B12, ARI, and NDVI of S2, in conjunction with aspect, slope, and elevation, characterized by the inclusion of elevation and slope as key variables , findings consistent with prior studies (Dostálová et al., 2016; Hościło & Lewandowska, 2019; López et al., 2022; Mngadi et al., 2021). Conversely, scenarios with the lowest reliability (SC1, SC3, and SC7) omitted topographic factors. This underscores the sensitivity of *Polylepis* to altitude (typically above 3000 m) and slope (favoring drainage and sunlight exposure), highlighting the critical role of these variables in its growth.

In classifying *Polylepis* stands, the moisture content of vegetation, indicated by various spectral indices, plays a crucial role in distinguishing these areas. The

Moisture Stress Index (MSI), alongside Sentinel-2 bands B9 and B12, is particularly sensitive to water content in the high canopy moisture. Band B2, while mainly used for detecting chlorophyll content, can also provide insight into vegetation health and indirectly reflect moisture levels.

Additionally, indices like the Modified Simple Ratio (MSR) and the Anthocyanin Reflectance Index (ARI) highlight specific vegetation properties, with ARI being useful for detecting stress in plants, which can signal varying moisture content. The Canopy Chlorophyll Content Index (CCCI) integrates red-edge bands, useful for capturing subtle changes in chlorophyll and moisture, which estimates chlorophyll content variations within the canopy, offering insights into plant health and vitality. Previous studies, such as (Kapari et al., 2024), compared ML algorithms to estimate water stress in maize crops, obtaining that CCCI was an important predictor variable. Finally, the Normalized Difference Vegetation Index (NDVI), while more general in application, supports overall vegetation classification and health monitoring. By combining these indices, a more accurate understanding of *Polylepis* conditions is achievable, aiding in reliable classification by isolating forest areas with specific moisture and health characteristics.

In RFE, we selected the iteration with the highest values of Accuracy and Kappa as the optimal number of variables, even if the differences from other variable sets were not statistically significant. This approach was chosen to maximize the inclusion of variables, allowing for a broader analysis of their relevance in identifying *Polylepis* stands. By prioritizing the highest value, we aimed to capture a comprehensive range of contributing variables, providing a more robust understanding of their relative importance in the classification model. This method enabled a more thorough interpretation of each variable's role, ultimately supporting a refined and potentially more effective identification of *Polylepis* ecosystems.

The ability to detect smaller *Polylepis* stands was constrained by the spatial resolution of S2, which impacts the result. While Sentinel-2 provides valuable data for broad-scale vegetation analysis due to its high spatial resolution and multispectral bands, its 10 to 20 m resolution poses challenges when it comes to identifying and accurately mapping smaller or fragmented *Polylepis* patches. These limitations can lead to an underestimation of the distribution and extent of these smaller stands.

Future endeavors will prioritize ongoing expert data validation to augment the dataset and acquire additional samples for broader coverage of the study area. Furthermore, there will be an exploration of advanced techniques like Neural Networks applied to high spatial resolution imagery such as PS, aiming to enhance classification reliability in remote sensing images.

.

2.5. Conclusions

This work demonstrates the effectiveness of combining Sentinel-2 imagery with topographic variables for the detection of *Polylepis* stands. The integration of Sentinel-2 spectral bands and topographic data outperforms the use of higher spatial resolution data from PlanetScope, texture-based variables derived from the NIR spectral band of PlanetScope, or SAR data from Sentinel-1. The importance of spectral and topographic features over spatial resolution in this specific classification task is notably.

Utilizing RFE with smileRandomForest within GEE proved to be effective, reducing the number of variables from 27 to 11 without compromising accuracy. The key variables selected include Sentinel-2 derived indices and bands (NDVI, MSR, MSI, B9, B2, CCCI, B12, and ARI) along with topographic features (elevation, aspect, and slope). The selected variables represent a balanced combination of spectral indices, specific Sentinel-2 bands, and topographic features, indicating that these features are essential for differentiating *Polylepis* stands from other land cover types.

The streamlined feature set includes critical indices sensitive to vegetation health, structure, and moisture content, such as NDVI, MSR, and CCCI, as well as elevation and slope, which are known to influence *Polylepis* distribution. By focusing on these key variables, the model achieves a high degree of accuracy in detecting *Polylepis* habitats, which are often found in challenging, high-altitude environments with unique topographic characteristics. The effectiveness of this variable reduction also underscores the value of the RFE process for refining remote sensing models, enabling a focus on the most informative features while reducing noise from less relevant data.

Moreover, the success of smileRandomForest within GEE highlights the utility of cloud-based platforms for broad-scale ecological classification tasks. GEE’s extensive data library and computational power facilitate the integration of multispectral, SAR, and topographic datasets, making it possible to replicate and scale this approach for other regions or similar ecological studies. This streamlined approach not only improves the efficiency of data processing and analysis but also makes it feasible to apply the model across large or multi-temporal datasets, supporting long-term monitoring efforts.

Random Forest (RF) has been demonstrated to be a powerful tool for managing imbalanced datasets, especially when distinguishing the *Polylepis* class. Additionally, RF is highly resilient to overfitting, making it particularly effective in complex classification tasks.

The results suggest that the identification of *Polylepis* stands was more effective when combining spectral (S2) and topographic variables, with spectral resolution playing a more critical role than spatial resolution.

Identifying *Polylepis* forests using satellite data is essential as a baseline for applying advanced remote sensing techniques in Land-Use Change monitoring in the Andean region. This approach enables tracking changes over time with diverse data sources, including radar and spectral imagery, to improve classification accuracy and support the establishment of remote monitoring mechanisms. Accurately mapping these unique, high-altitude ecosystems enhances the precision of Land Use, Land-Use Change and Forestry (LULUCF) inventories and identifies areas where *Polylepis* forests significantly contribute to carbon sequestration. Developing robust detection methodologies and validating the reliability of remote sensing data for these stands can greatly support national and international reporting requirements.

Chapter 3

Identification of Forests at a Local Scale using UAV Data

Edited version of:

Pacheco-Prado, D.; Bravo-López, E.; Martínez, E.; Ruiz, L.Á. Urban Tree Species Identification Based on Crown RGB Point Clouds Using Random Forest and PointNet. Remote Sens. 2025, 17, 1863. https://doi.org/10.3390/rs17111863

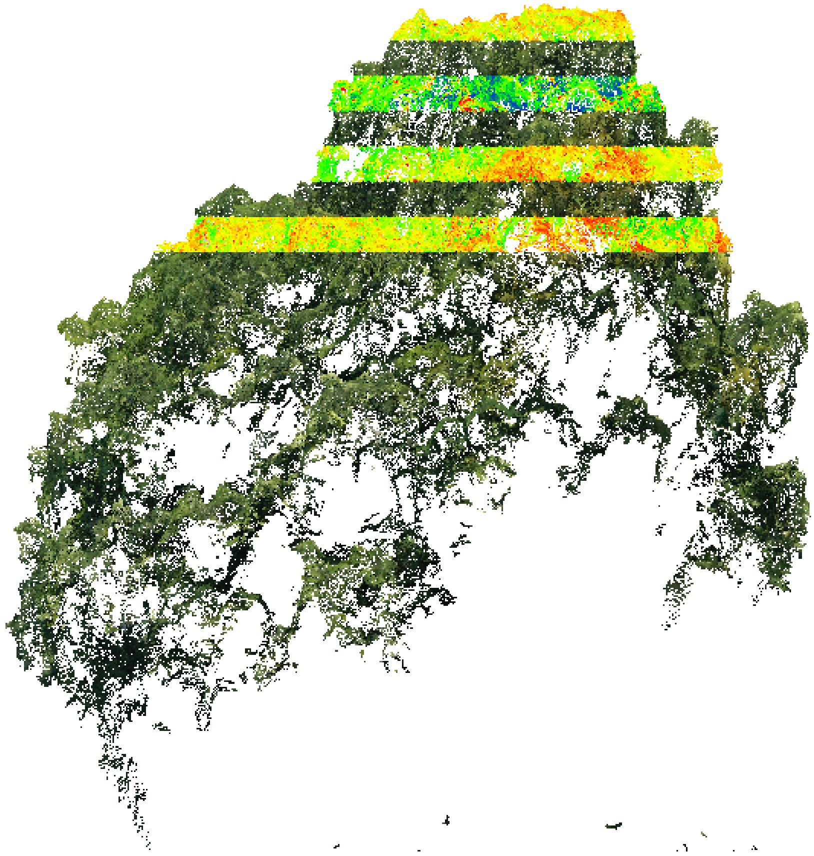

Acacia dealbata Link

3. IDENTIFICATION OF TREE SPECIES AT A LOCAL SCALE USING UAV DATA

This chapter describes the advantages and limitations of using UAV RGB derived point clouds, obtained from the Tree Inventory of Cuenca, to identify individual tree species based on their canopies. To achieve this, Machine Learning and Deep Learning models are trained to evaluate the identification of eight forest species.

3.1. Introduction

Tree species identification plays a fundamental role in forest management (J. Liu et al., 2019; R. Pu, 2021) as it contributes to the sustainable control and conservation of forest resources. This task is relevant and challenging (B. Liu, Chen, et al., 2022) due to Latin America's rich forest species variety (Rieckmann et al., 2011). Ecuador is recognized as one of the most biodiverse countries in the world (Aguirre et al., 2024; Jadán et al., 2021; MAE & FAO, 2015), housing approximately 12.75 million hectares of forest (Cuesta et al., 2017). The differentiation of species is fundamental not only for improving their conservation through the design of effective strategies but also for identifying them accurately to avoid confusion between species and contributing to the creation of appropriate forestry practices (FAO, 2020). Despite the relevance of these tasks, these studies are scarce in Latin American countries, and most of them have been conducted in countries such as China (J. Chen et al., 2021; Fan et al., 2023; Lian et al., 2022; B. Liu, Chen, et al., 2022; Z. Ma et al., 2020), and the United States (Hartling et al., 2019; Seidel et al., 2021); or regions such as Central Europe (Seidel et al., 2021; Shi et al., 2018), which have forest resources but is not as lush and biodiverse as in tropical regions.

Traditional single-tree species identification is often costly, time-consuming, and resource-intensive (Diez et al., 2021; Pacheco-Prado et al., 2023). However, recent advances in remote sensing technologies have revolutionized ecological and forestry research, providing high-resolution data to understand forest structure and composition (Atkins et al., 2023; Guimarães et al., 2020; Lines et al., 2022; Mouafik et al., 2024). One of these is based on Unmanned Aerial Vehicles (UAVs), which have introduced new approaches for tree species identification (Ecke et al., 2024; Li et al., 2023) using photogrammetric systems (Diez et al., 2021) in RGB (Onishi & Ise, 2021), multispectral (Briechle et al., 2020; Feng & Li, 2019; Z. Xu et al., 2020), hyperspectral (Nevalainen et al., 2017; Sothe et al., 2019), and Light Detection and Ranging (LiDAR) data (J. Chen et al., 2024; Kovanič et al., 2023; Pleşoianu et al., 2020).

In this context, one of the most relevant characteristics offered by UAVs is the very precise spatial resolutions at a low flight altitude (Nevalainen et al., 2017), which can be applied to object detection at distances ranging from a few meters to several hundred meters, using three-dimensional (3D) data (Cetin & Yastikli, 2022; Remondino et al., 2011) facilitating the detailed assessment of individual trees (Nevalainen et al., 2017), crown characterizations (Fassnacht et al., 2024;

Pleşoianu et al., 2020), tree height estimation (J. Chen et al., 2024; Mesas-Carrascosa et al., 2020), detection of tree species (R. Pu, 2021), and biomass estimation (Carbonell-Rivera, Ruiz, et al., 2024; Fassnacht et al., 2024). The most used are LiDAR sensors, whether aerial (ALS) or terrestrial (TLS). LiDAR data enables the estimation of stand attributes across extensive areas at a significantly lower cost compared to traditional field-based methods (Picos et al., 2020). For instance, Lindberg and Holmgren (2017) evaluated Individual Tree Crown (ITC) delineation from LiDAR data, achieving high accuracy in tree detection and the mapping of vegetation in urban environments, providing information on tree species at various spatial scales. Seidel et al. (2021) utilized Deep Learning (DL) algorithms to predict tree species in a temperate forest in Germany and Oregon (USA) from TLS data, achieving an accuracy of 86%. Key variables included tree height, crown width, and the 3D canopy structure. The predicted species included several hardwood species, such as oak and maple. Despite its advantages, LiDAR presents challenges for species classification (Fan et al., 2023) with some being the lack of accuracy in classifying forest structures due to their complexity (C. Xu et al., 2015); insufficient data resolution to distinguish structural details (Favorskaya et al., 2015); need for sophisticated computational resources due to the size of point clouds (Tao, 2014); or even omitting the classification of certain species (B. Liu, Huang, et al., 2022).

Another alternative is the use of UAV-based photogrammetry, which offers a cost-effective option and technical advantages, including integration with other technologies (Greco et al., 2023; Westoby et al., 2012). This approach facilitates the extraction of individual tree crowns (Ke & Quackenbush, 2011) or stands characteristics through methods such as the use of multispectral sensors and laser scanners (UAV -LS), spectral angle classification algorithms (SAM), and crown height model (CHM) segmentation techniques, among others (Lian et al., 2022), thereby improving classification accuracy (Burt et al., 2019). However, significant challenges remain in tree identification from a UAV zenithal view, such as the heterogeneity of tree structures, canopy overlaps, diverse species compositions, canopy architectures, tree densities, complex tree structures, and variations in foliage density, which can affect the accuracy of boundary detection (J. Chen et al., 2024; Fassnacht et al., 2024).

A low-cost photogrammetry technique that has been implemented in various studies is 'Structure-from-Motion' (SfM) photogrammetry (Eltner & Sofia, 2020; Iglhaut et al., 2019), which allows for the generation of dense point clouds from UAV imagery (Westoby et al., 2012). SfM enables the acquisition of 3D remote sensing data in forestry with low cost and technical expertise (Iglhaut et al., 2019); also, UAV-based SfM can be used to model forest type, tree density, and aboveground biomass in certain types of forests (Alonzo et al., 2018). These point clouds have been successfully used for tree identification (Carbonell-Rivera et al., 2022; Mesas-Carrascosa et al., 2020; Pacheco-Prado et al., 2025; Z. Xu et al., 2020; Zeybek, 2021) and integrated with various data types to improve species classification (Hartling et al., 2021). Several methods offer a promising way for the identification of individual trees, such as (Carbonell-Rivera et al., 2020; Nevalainen et al., 2017; Pleşoianu et al., 2020) exploiting the rich geometric and spectral information within 3D datasets. Other studies have demonstrated the effectiveness of point cloud-based methods for obtaining structural attributes such as tree height, crown diameter, and canopy volume (J. Chen et al., 2024; Fassnacht et al., 2024). Spectral information from multispectral or hyperspectral imagery improves species discrimination based on leaf chemistry and pigmentation (Sothe et al., 2019). Nevalainen et al. (2017) evaluated the effectiveness of UAV-based photogrammetry and hyperspectral imagery for detecting and classifying individual trees in boreal forests. The classification experiments, which employed Random Forest (RF) and Multilayer Perceptron (MLP) classifiers, achieved global accuracies of 95% and an F-score of 0.93. The accuracy of individual tree identification from photogrammetric point clouds varied between 40% and 95%, depending on area characteristics. Sothe et al. (2019) focused their work on classifying 12 major tree species in a subtropical forest in Southern Brazil using UAV-based photogrammetric point clouds, hyperspectral data, and an SVM algorithm, achieving a global accuracy of 72.4% and a Kappa index of 0.70. The study identified key features such as Visible and Near Infrared (VNIR) bands, Normalized Difference Vegetation Index (NDVI), Pigment Specific Simple Ratio (PSSR), Minimum Noise Fraction (MNF) components, and texture from specific spectral bands as crucial for species discrimination. The common technique for the analysis of dense point clouds (LiDAR or photogrammetric) in these works was Machine Learning algorithms, including RF (Fassnacht et al., 2024; Immitzer et al., 2012; Zeybek, 2021; Zhong et al., 2024), Support Vector Machine (SVM) (Sothe et al., 2019; Z. Zhang & Liu, 2013), and advanced methods such as Deep Learning (Diez et al., 2021; D. H. Kim et al., 2023; J. Liu et al., 2019; Pleşoianu et al., 2020; Y. Qi et al., 2021; N. Xu et al., 2023). In addition to being currently widely used in this type of research, (Modzelewska et al., 2020; Rana et al., 2022; Zhong et al., 2024) have shown significant potential for automated species classification by evaluating these multidimensional datasets and demonstrating noticeable improvements in classification accuracy.

In summary, to identify tree species at the individual level, it is convenient to combine spectral, textural, and spatial features from point clouds, using machine learning or deep learning algorithms, the latter being a superior performance method (Hartling et al., 2019). Some algorithms from point clouds are Point Cloud Tree Species Classification (PCTSCN), which is an intelligent classification strategy for tree species (Chen et al., 2021), PointNet and PointNet++, which are a Deep Learning network framework based on point cloud data (Fan et al., 2023; Shrestha & Mahmood, 2019), useful for partitioning the amount of data in these point clouds by spanning smaller regions. Recent studies have explored the application of these two frameworks to classify tree species using LiDAR point clouds. These models can process cluttered point clouds by automating processes and reducing manual feature extraction, which is promising in the classification of forest species in different regions of the world (B. Liu, Huang, et al., 2022).

Another useful option for classifying plant species is Class3Dp, a free software designed to classify plant species in RGB and multispectral point clouds. This software performs the machine learning-supervised classification of point clouds based on 3D and spectral information (Carbonell-Rivera, Estornell, et al., 2024).

Based on this background, in this study, we investigate the potential of RGB data and geometric features derived from UAV photogrammetric point clouds for the identification of urban tree species in the city of Cuenca (Ecuador). Using RF, we evaluated the classification performance to identify the most effective features and models to distinguish tree species based on tree crown point clouds datasets. Additionally, this analysis was expanded through PointNet and PointNet++ to determine if the use of neural networks can improve the identification of forest species from point clouds. The main contributions of this study are as follows: (i) assessing how effectively RGB data and geometric features derived from UAV-based photogrammetric point clouds can be used for urban tree species classification; and (ii) determining which classification algorithm, such as Random Forest, Point-Net, or PointNet++, achieves the highest classification accuracy when applied to point cloud representations of urban tree crowns.

3.2. Materials and methods

3.2.1. Study zone

Cuenca is in the central-southern region of Ecuador (Figure 3.1), and it lies at an average elevation of approximately 2500 meters above sea level (m.a.s.l.). In 2017, this city had around 208 public parks and green spaces within its urban zone (Pacheco & Ávila, 2017), complemented by riparian trees along its rivers. Among these green spaces, the parks with the largest surface area are Paraiso, Miraflores, and La Madre. The tree inventory of Cuenca (TIC) included data on 16,737 trees and it provides information on taxonomy, origin, crown and trunk structure, phenology, forest management, potential issues, and two photographs per tree (Pacheco & Ávila, 2017). Among these trees, 43% were introduced species, 41% native, and fewer than 16% were either endemic species or uncategorized. The most frequent species were *Salix humboldtiana Willd.*, *Tecoma stans (L.) Juss. ex Kunth, Fraxinus excelsior L.*, *Jacaranda mimosifolia D. Don*, *Prunus serotina Ehrh.*, and *Melaleuca armillaris (Sol. ex Gaertn.) Sm.* (Universidad del Azuay, 2024). Of the 171 parks inventoried in the TIC until December 2024 (Pacheco-Prado et al., 2023) according to the website https://gis.uazuay.edu.ec/iforestal/ (accessed on 12 April 2025), this study focused on 54 parks where UAV flights were conducted between 2015 and 2022.

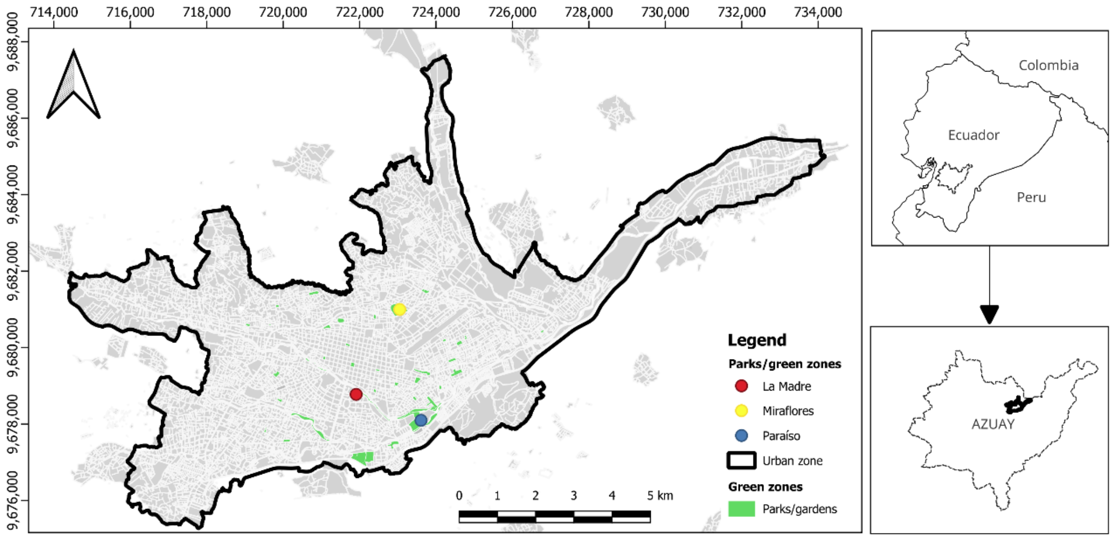

Figure 3.1. Location of parks and green areas of the study zone.

3.2.2. Workflow description

The methodology (Figure 3.2) was implemented in the following four stages: (1) Data preparation, which involved exploring the TIC database to select the target classes and their green zones. Subsequently, the point clouds corresponding to the parks that contain these tree species were prepared for processing. (2) In the Tree Segmentation stage, individual trees were delineated (automatically or manually) from the point clouds and assigned to their respective class. Furthermore, geometric attributes and spectral characteristics were obtained from RGB point clouds. (3) In the tree classification stage, we used Recursive Feature Elimination (RFE) to reduce the number of features and trained the model using Random Forest (RF) and neural network algorithms to classify the point cloud of each tree. (4) Finally, in the metrics evaluation stage, the model's performance was evaluated using metrics such as global accuracy and the Kappa index. Classification reports were generated, including class-specific metrics such as precision, recall, and F1-Score, to aid in selecting the final model and identifying the classes with the highest accuracy.

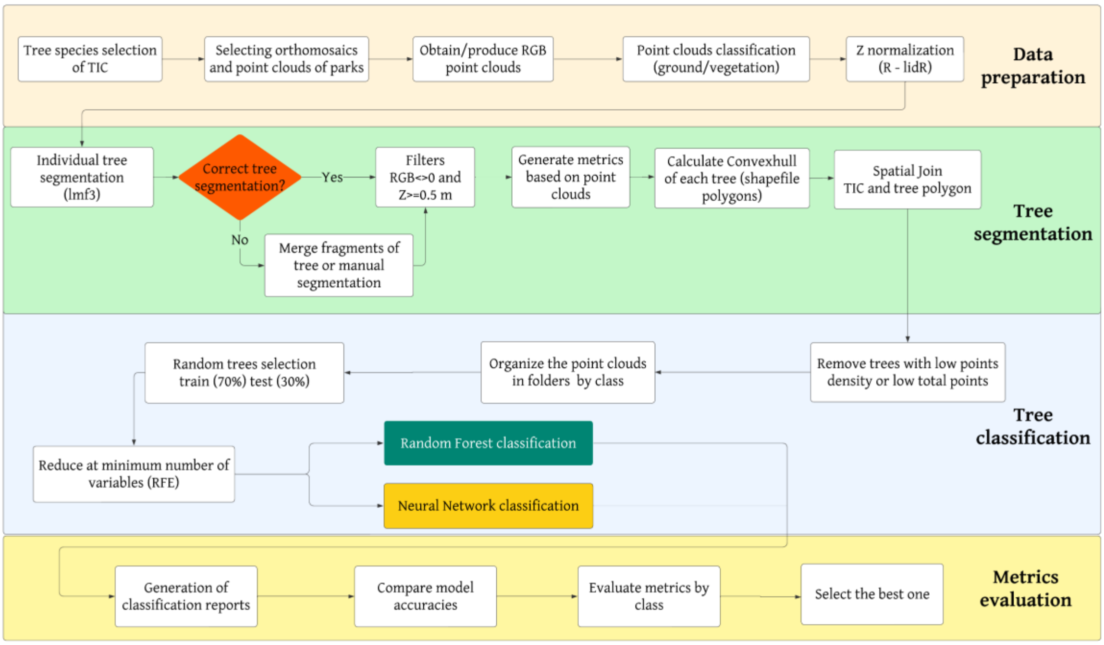

Figure 3.2. Workflow diagram.

3.2.2.1. UAV data collection

The TIC was evaluated to identify and select the classes with the highest occurrence, as described on the website https://gis.uazuay.edu.ec/herramientas/iforestal-dashboard/ (accessed on 12 April 2025). The most common species included *Salix humboldtiana Willd*., *Tecoma stans (L.) Juss. ex Kunth*, *Prunus serotina Ehrh*., *Fraxinus excelsior L*., *Jacaranda mimosifolia D. Don*, *Melaleuca armillaris (Sol. ex Gaertn.) Sm*., *Alnus acuminata Kunth*, *Schinus molle L*., *Acacia dealbata Link*, and *Callistemon lanceolatus (Sm.) Sweet*. Based on these data, 54 parks and green zones where these species are present were identified. UAV flights over these zones were conducted using various sensors (Table 3.1), all of them with Red, Green, and Blue (RGB) channels. The flights were operated between 2015 and 2022, from 7:00 AM to 5:00 PM, with altitudes ranging from 30 to 150 meters above ground level.

Table 3.1. Sensors RGB used.

Sensor Model	Focal Length (mm)	Maximum opening
DJI FC300X	4	2
Parrot Anafi	4	-
DJI FC6510	9	2.97
DJI FC6310	9	2.97
DJI FC6310S	9	2.97
Double 4k /Sony Exmor R IMX377	5.4	-

The aerial photographs captured during these flights were processed using Metashape software version 1.7.0 (Educational License) and higher. The principal outputs included orthomosaics and point clouds. In the case of the point clouds, automatic point classification was performed. The classification codes in LAS files, defined by the American Society for Photogrammetry and Remote Sensing

(ASPRS), are stored in the classification attribute of each point cloud. These codes assign values such as ground (value 2), low vegetation (value 3), medium vegetation (value 4), and high vegetation (value 5). The ground class was used to normalize tree height (Z coordinate) using the spatial interpolation of the k-nearest neighbor (KNN) approach with an inverse-distance weighting (IDW), while the vegetation classes enabled the extraction of points corresponding to a tree. This process was performed using the lidR package (version 4.1.2) in R (version 4.4.2).

3.2.2.2. Tree segmentation and feature extraction

The identification of individual trees was performed in two stages. Initially, the tree segmentation algorithm (LMF3) from the rLidar package was employed to rasterize the canopy, detect individual trees, and assign a unique treeID to all UAV points associated with each tree. Subsequently, the segmented trees were subject to manual evaluation to correct fragmentation, merging segments into a single tree where necessary. In cases where automated segmentation was insufficient, individual trees were manually delineated using CloudCompare software (version 2.13.2). For each tree, the duplicated points, non-vegetation, and vegetation-classified points with an RGB value of 0 (shadows) were removed. Each point cloud of a tree was transformed into a 2D polygon (convexhull) and linked to a TIC tree. The resulting dataset was further refined by selecting classes that could be linked to the point cloud (Table 3.2) and excluding trees with low point density or insufficient point counts. Some of the majority classes of the TIC, such as *Prunus serotina Ehrh*, had to be excluded from this process because they could not be matched with an adequate number of segmented trees.

From the tree point clouds and the RGB channels, 74 variables were produced, 36 spectral (Table 3.3) and 38 geometric (Table 3.4), based on works such as (Carbonell-Rivera et al., 2020; Shrestha & Mahmood, 2019). Variables potentially influenced by flight conditions or photogrammetric factors—such as image overlap, flight altitude, illumination, and camera angle— including point density, color channels, and spectral indices, were normalized using Z-score standardization. Finally, the mean, minimum, maximum, and standard deviation of RGB features and indexes were obtained at tree level.

Table 3.2. Examples of individual tree RGB photographs of some classes and point clouds from zenithal and front views (RGB channels). DBH is the diameter at breast height.

Class	TIC photography	Zenithal view	Front view
Acacia dealbata Link Code: 089ADE0002 Date: 2019-10-14 Crown Diameter: 8 m Height: 10 m Fuste height: 1.5 m DBH: 35 cm Origin: Introduced			
Populus alba L. Code: 033PAL0001 Date: 2017-10-01 Crown Diameter: 5 m Height: 6 m Fuste height: 3.3 m DBH: 30 cm Origin: Introduced		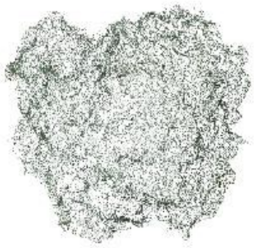	
Melaleuca armillaris (Sol. ex Gaertn.) Sm. Code: 065CPI0004 Date: 2018-12-19 Crown Diameter: 3 m Height: 4 m Fuste height: 1.8 m DBH: 17 cm Origin: Introduced			
Tecoma stans (L.) Juss. ex Kunth Code: 087TST0002 Date: 2019-05-02 Crown Diameter: 5 m Height: 5 m Fuste height: 1.7 m DBH: 10 cm Origin: Native		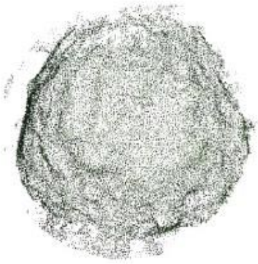	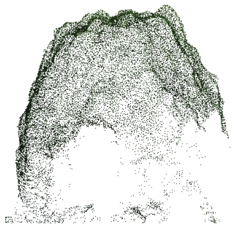
Jacaranda mimosifolia D. Don Code: 123JMI0003 Date: 2022-04-13 Crown Diameter: 5 m Height: 5 m Fuste height: 2 m DBH: 24 cm Origin: Introduced			

Schinus molle L. Code: 065SMO0001 Date: 2018-12-19 Crown Diameter: 6 m Height: 4.5 m Fuste height: 1.3 m DBH: 38 cm Origin: Introduced			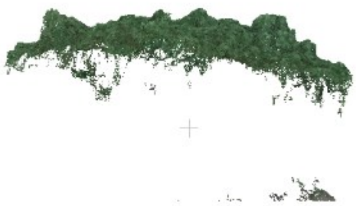
Salix humboldtiana Willd. Code: 055SHU0001 Date: 2018-09-21 Crown Diameter: 7 m Height: 12.6 m Fuste height: 2.2 m DBH: 66 cm Origin: Native		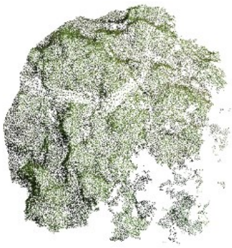	
Fraxinus excelsior L. Code: 065FEX0014 Date: 2018-12-20 Crown Diameter: 12 m Height: 12 m Fuste height: 3 m DBH: 38 cm Origin: Introduced			

Table 3.3. List of spectral features obtained from the point clouds by tree.

Index	Name	Description / Equation	N
RGB	Red/Green/Blue	Red, Green and Blue channels (normalized 0-1)	12
Intensity	Calculated from RGB colors	0.21 Red + 0.72 Green + 0.07 Blue	4
NRBDI	Normalized Red- Blue Difference Index (Carbonell-Rivera et al., 2022; Song et al., 2022)	(Red − Blue) / (Red + blue)	4
NGRDI	Normal Green–Red Difference Index (Mesas-Carrascosa et al., 2020)	(Green - Red) / (Green + Red)	4
GR	Green divided by red (Carbonell-Rivera et al., 2022)	Green / Red	4
BI	Brightness (Carbonell-Rivera et al., 2022)	Green + Red + Blue	4
GLI	Green Leaf Index (X. Zhang et al., 2019)	(2 × Green - Red - Blue) / (2 × Green + Red + Blue)	4

Table 3.4. List of geometric features obtained from the point clouds by tree.

Name	Description	N	Location
Points number	Number of points at tree level	1	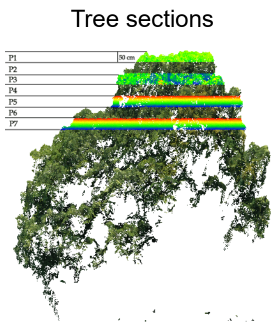
Points density	Number of points per m^2 (normalized)	1	
Height Max/ Mean	Based on Z normalized coordinate, the maximum and mean value were obtained	2	
Percentile height	The percentiles of the canopy height distribution (10th,50th,90th) in the variables zp10, zp50 y zp90 (Z. Xu et al., 2020)	3	
Area tree	Area of the polygon formed by the convex hull of the tree's point cloud.	1	
Tree Perimeter	Perimeter of the polygon formed by the convex hull of the tree's point cloud.	1	
Tree Volume	Volume of the tree estimated from its point cloud.	1	

P1-P7	The perimeter, area, volume, and shape are calculated from the polygon/object formed by the points filtered from the crown down to 0.5 meter (P1-P7). This process is repeated, lowering the filtering range incrementally, so that in the final segment, the points between 3 and 3.5 meters (P7) below the crown are included. If the tree's height does not allow for this calculation, a value of 0 is assigned.	28

N: Number of variables

A total of 809 individuals were obtained from the selected classes (Table 3.5), divided into 70% for training and 30% for testing for each class. The number of samples was highest for *Fraxinus excelsior L.*, while *Jacaranda mimosifolia D. Don* and *Schinus molle L.* had the lowest counts.

Table 3.5. Number of samples for train and test by class.

Scientific name	Code	Training	Test	Total
Acacia dealbata Link	ADE	83	35	118
Populus alba L.	PAL	60	26	86
Melaleuca armillaris (Sol. ex Gaertn.) Sm.	CPI	91	39	130
Tecoma stans (L.) Juss. ex Kunth	TST	52	22	74
Jacaranda mimosifolia D. Don	JMI	44	19	63
Schinus molle L.	SMO	46	19	65
Salix humboldtiana Willd.	SHU	89	38	127
Fraxinus excelsior L.	FEX	102	44	146
Total		567	242	809

The final tree point clouds database shows the distribution of UAV point density (points/m²) among different vegetation classes (Figure 3.3a) and the distribution of maximum tree heights (in meters) for various vegetation classes (Figure 3.3b). In the first case, point densities vary significantly between classes such as FEX. In contrast, classes such as SHU and SMO show relatively lower densities with fewer extreme values. In the second case, the maximum tree height varies considerably between classes such as ADE and SHU, which show the greatest variability and the highest outliers. In contrast, CPI and SMO demonstrate smaller maximum heights with tighter distributions, reflecting more uniform growth patterns. FEX and SHU show the highest median heights.

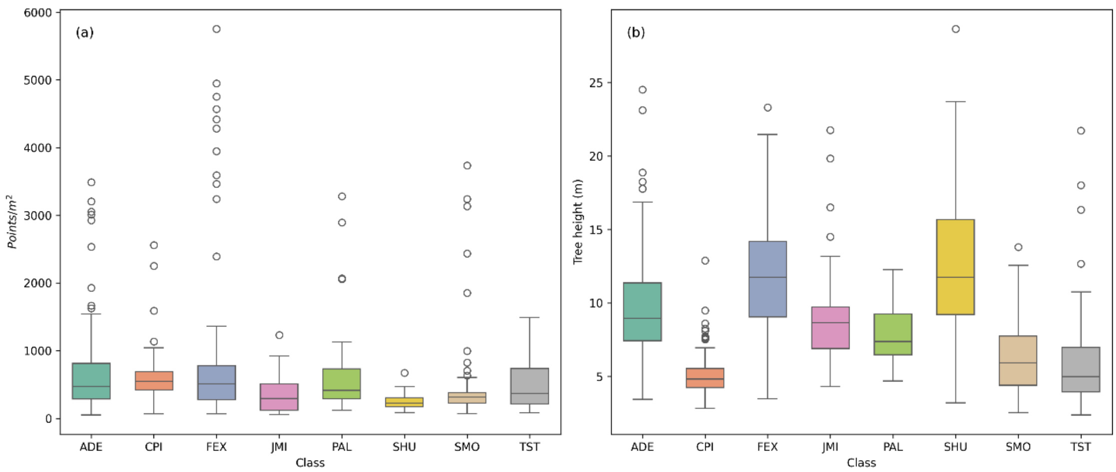

Figure 3.3. Distribution of classes by (a) Points density (points/m²) and (b) Tree height (m).

3.2.2.3. Feature selection and classification

RF was used for variable selection and point cloud classification. This algorithm is a set of decision trees, typically trained using the bagging method, where each tree is trained on a different data subset to detect errors in individual trees. Additionally, RF provides a measure of the relative importance of each variable (Gerón, 2019). To select the most relevant variables, the RFE technique was applied. In subsequent iterations, the importance measures were recomputed at each step of variable elimination to refine the selection process (D. Wang et al., 2018). For this research setting, the hyperparameters of RF were *n_estimators=500* (define the number of trees in the model) and class_weight='balanced' (adjust the weight of the classes to handle imbalances in the data).

The final model was selected based on the set of variables that achieved the highest values of accuracy (Equation 1) and Kappa (Equation 2). Additionally, this model was evaluated by class using the following metrics: Precision (Equation 3), which measures the percentage of correctly predicted positive observations out of all positive predictions made by the model; Recall (Equation 4), which represents the percentage of actual positives that were correctly identified by the model; and F1 Score (Equation 5), which is the harmonic mean of Precision and Recall (Zheng et al., 2021). These metrics can be generated using the classification_report function of the scikit-learn module, which is often applied after model predictions to assess how well the model is classifying the data into specific categories.

$$\text{Accuracy} = \frac{\text{TP} + \text{TN}}{\text{TP} + \text{TN} + \text{FP} + \text{FN}} \tag{1}$$

$$\text{Kappa} = \frac{(\text{p}_\text{o} - \text{p}_\text{e})}{(1 - \text{p}_\text{e})} \tag{2}$$

$$\text{Precision} = \frac{\text{TP}}{\text{TP} + \text{FP}} \tag{3}$$

$$\text{Recall} = \frac{\text{TP}}{\text{TP} + \text{FN}} \tag{4}$$

$$\text{F1} - \text{Score} = \frac{(2 * \text{Precision} * \text{Recall})}{\text{Recall} + \text{Precision}} \tag{5}$$

In these equations, TP represents true positives; TN denotes true negatives; FP refers to false positives; and FN indicates false negatives as defined in the confusion matrix (Zheng et al., 2021). For Cohen's Kappa, p_o is the observed agreement, representing the actual probability that both annotators assign the same label to a sample, while p_e is the expected agreement when both annotators assign the labels randomly (*Sklearn.Metrics.Cohen_kappa_score — Scikit-Learn 1.2.1 Documentation*, n.d.).

3.2.2.4. Tree identification using PointNet and PointNet++

An alternative classification was applied based on PointNet, an architecture of a neural network designed for processing and classifying 3D point clouds that operate on raw point cloud data (C. R. Qi et al., 2017), integrating them into a supervised Convolutional Neural Network architecture (García-García et al., 2016). Although the original architecture of PointNet is primarily focused on capturing the geometric shape of objects using exclusively the spatial coordinates XYZ (C. R. Qi et al., 2017). Another model evaluated is PointNet++, which features a hierarchical feature learning approach, which allows capturing the detailed geometric structure in the local environment of each point. Thanks to this, the model can extract local feature information at multiple scales within 3D objects (B. Liu, Huang, et al., 2022).

This work proposes a modification of the inputs of the deep learning models to enhance the classification. To achieve this, the PointNet architecture was adapted to process information from the normalized Z coordinates and other relevant attributes associated with each point, such as RGB color values, intensity, and spectral indices (BI and NRBDI), according to the selection of variables obtained by RFE. The experiments of this section were conducted on a High-Performance Computing (HPC) of *Corporación Ecuatoriana para el Desarrollo de la Investigación y la Academia* (CEDIA). As most of the experiments involved deep learning techniques, an NVIDIA A100-SXM4-40GB graphics card was utilized. Training the deep learning models using a GPU instead of a CPU significantly reduced the training time. We used TensorFlow-gpu (2.8.0) with 16 cores and 32 GB of memory as a computational framework, and the development package provided with Python (3.8.10).

Table 3.6 provides the parameter settings for the PointNet's model. Among these, batch size (BS) and epochs are two crucial hyperparameters that significantly impact the training process of a neural network. Batch size refers to the number of training samples processed by epoch. Smaller batch sizes provide more frequent updates, resulting in a smoother but slower training process and potentially better generalization, while larger batch sizes offer faster computation with more stable updates but may require more memory and risk poorer generalization. Epochs denote the number of times to traverse the entire training dataset during training. Increasing the number of epochs allows the model to learn better, but too many epochs can lead to overfitting, where the model learns the training data too well and fails to generalize new data (Fan et al., 2023). Choosing the right combination of batch size and epochs is essential for achieving good performance, balancing training speed, memory efficiency, and model accuracy.

Table 3.6. Hyperparameters settings evaluated for PointNet's.

Hyperparameter	**Description**	**Value**
NUM_POINT	Number of points by tree	1024,2048,3072,4096,5120
NUM_CATEGORY	Number of classes	8
BATCH SIZE	Number of batches in each epoch	32,64,96,128
EPOCHS	Number of times to the entire training dataset	20,50,100,200
OPTIMIZER	Algorithm that determines how parameters are updated.	Adam
LEARNING RATE	Step size of parameter updates in each iteration	0.001

3.3. Results

In this section, we describe the results obtained through RF and the characteristics obtained as relevant. These features were subsequently used through neural networks with the PointNet's architectures. In both cases, the classification reports of the models are presented.

3.3.1. Model accuracy and feature importance using RF

The classification model's performance was evaluated using the following eight tree species: *Acacia dealbata Link* (ADE), *Populus alba L.* (PAL), *Melaleuca armillaris (Sol. ex Gaertn.) Sm.* (CPI), *Tecoma stans (L.) Juss. ex Kunth* (TST), *Jacaranda mimosifolia D. Don* (JMI), *Schinus molle L.* (SMO), *Salix humboldtiana Willd.* (SHU), and *Fraxinus excelsior L.* (FEX). Using all variables, the accuracy and Kappa values were 0.69 and 0.63, respectively. After the RFE process, the best combination of variables (Figure 3.4) presents an accuracy of 0.70 and Kappa of 0.65. The eleven variables used were the following: nrbdi_mean, gli_mean, points_density, zp90, nrbdi_std, intensity_mean, intensity_std, height_max, zp50, zp10, and bi_std.

In Table 3.7, the rows represent the true classes (Reference), while the columns represent the predicted classes (Predicted), showing how testing samples of each class were correctly or incorrectly classified. For instance, the CPI class shows 35 correct predictions with minimal misclassifications, being the one with the highest agreement between actual data and predictions. On the other hand, the right side of the table provides evaluation metrics for each class: Precision, Recall, and the F1-score (F1), where the values summarize the model's ability to correctly classify samples for each class. For example, the PAL class achieved high performance with an F1-score of 0.82 due to high precision (0.77) and recall (0.88). In contrast, the SMO class performed poorly, with an F1-score of 0.39 due to low precision (0.50) and recall (0.32). The model's global accuracy is 0.70, with a macro average F1-score of 0.65, which indicates that the model's performance is relatively consistent, and a weighted average of 0.69, that suggests the model performs slightly better in most of the classes.

Table 3.7. Confusion matrix and classification report.

		Predicted								Report			
		ADE	PAL	CPI	TST	JMI	SMO	SHU	FEX	Precision	Recall	F1	N
Reference	ADE	25	4	2	0	1	1	0	2	0.68	0.71	0.69	35
	PAL	3	23	0	0	0	0	0	0	0.77	0.88	0.82	26
	CPI	1	0	35	2	1	0	0	0	0.73	0.90	0.80	39
	TST	1	1	0	13	0	1	4	2	0.65	0.59	0.62	22
	JMI	3	0	1	1	7	2	4	1	0.58	0.37	0.45	19
	SMO	2	1	7	1	2	6	0	0	0.50	0.32	0.39	19
	SHU	0	0	1	1	0	1	31	4	0.69	0.82	0.75	38
	FEX	2	1	2	2	1	1	6	29	0.76	0.66	0.71	44
										Acc		0.70	
										Macro Avg		0.65	
										Weighted avg		0.69	

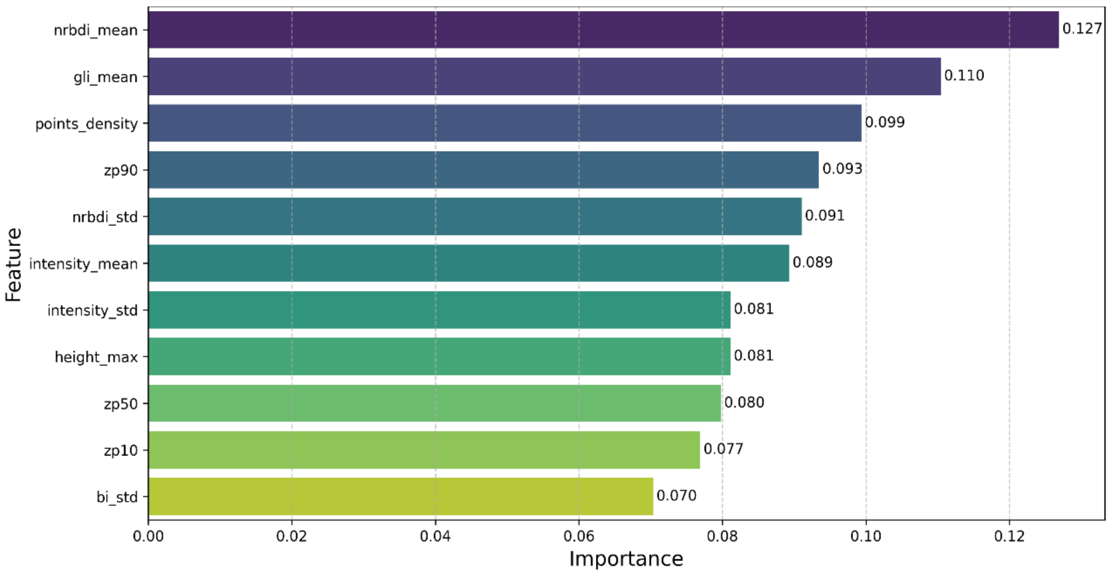

Figure 3.4. Variable importance of final RF model.

To investigate a spatial pattern of the predictions, the classification results at the species level were examined, separating correctly classified trees (Figure 3.5) from misclassified ones (Figure 3.6). A high concentration of errors (24 of the 73 misclassified trees, approximately 33 %) was located along the Tomebamba riverbank (Figure 3.7), which could be attributed to the topography of the riverbank, which alters light conditions, impacts the accuracy of the point cloud, and hinders the normalization of relative heights.

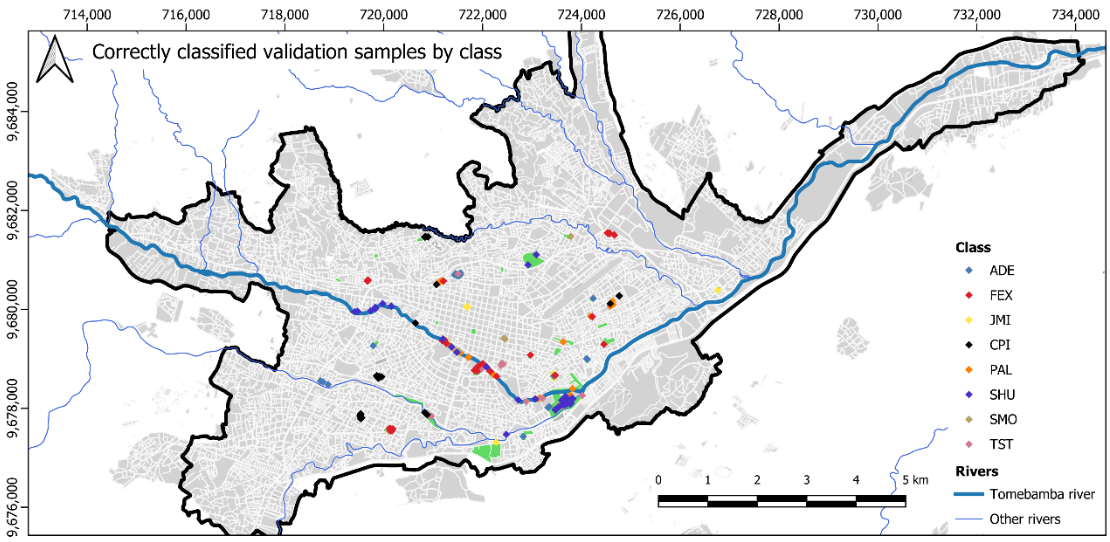

Figure 3.5. Distribution map of correctly classified tree species.

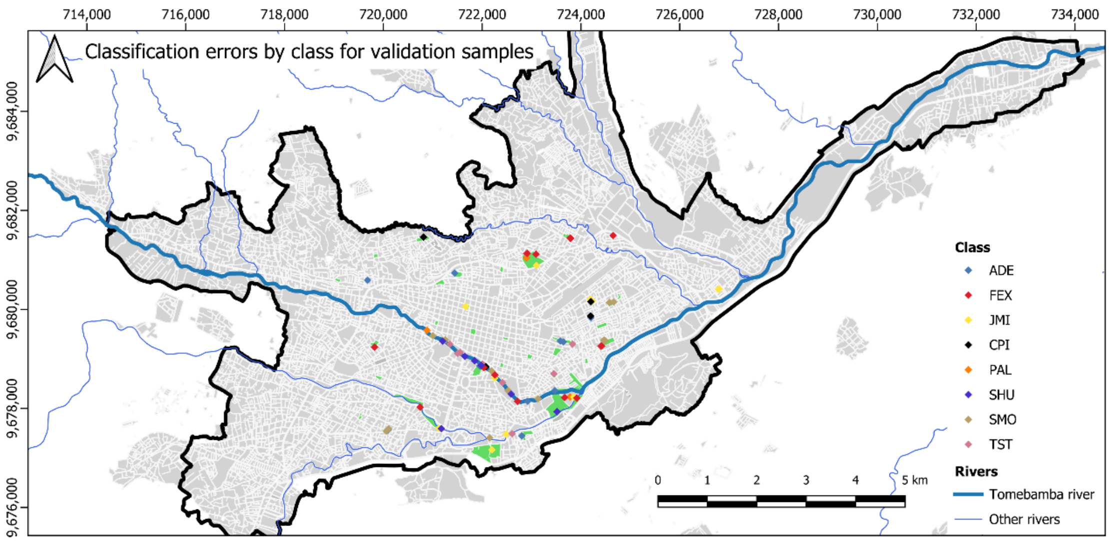

Figure 3.6. Distribution map of misclassified tree species.

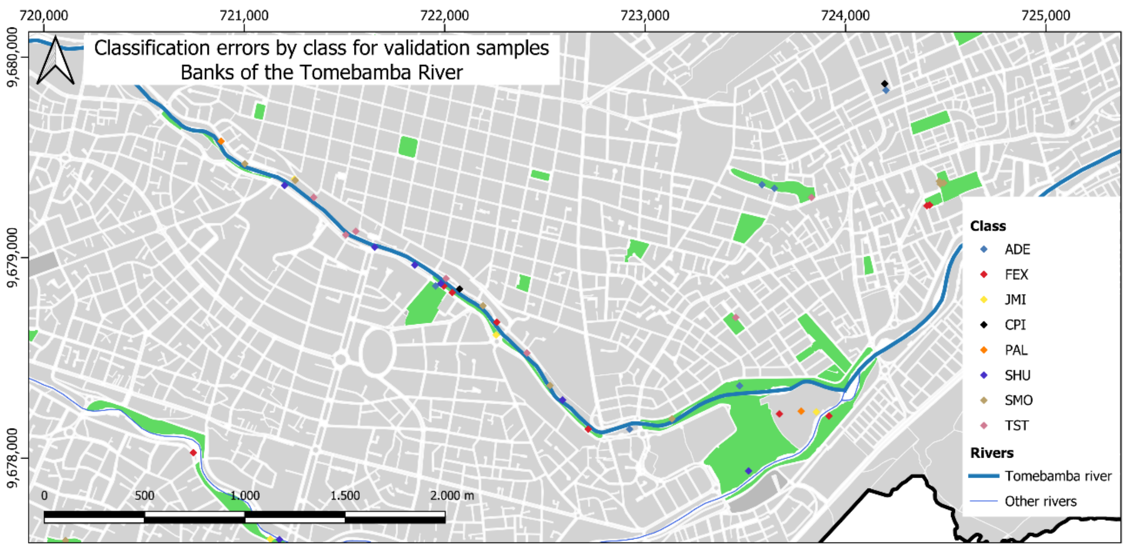

Figure 3.7. Concentration of errors along the Tomebamba Riverbank by tree species.

3.3.2. Classification probabilities using RF

Figure 3.8 shows the probability distribution for samples by class, divided into correctly identified samples ("True") and misclassified samples ("False"). The separation of the classes in the probability distributions of the correctly and incorrectly classified samples shows the model indeed assigns higher probabilities to the correct predictions. When analyzing the correct classifications (right graphic) the highest median probability is observed in some classes, including CPI (green), PAL (orange) and SHU (pink). This suggests that the selected feature set effectively captures the distinctions among these three tree species. On the other hand, wider interquartile ranges in the "False" category (left graphic) are observed in classes like ADE (blue), JMI (purple) or SMO (brown), indicating variability in the model's predictions. This would suggest that certain species are confused with others that share their traits.

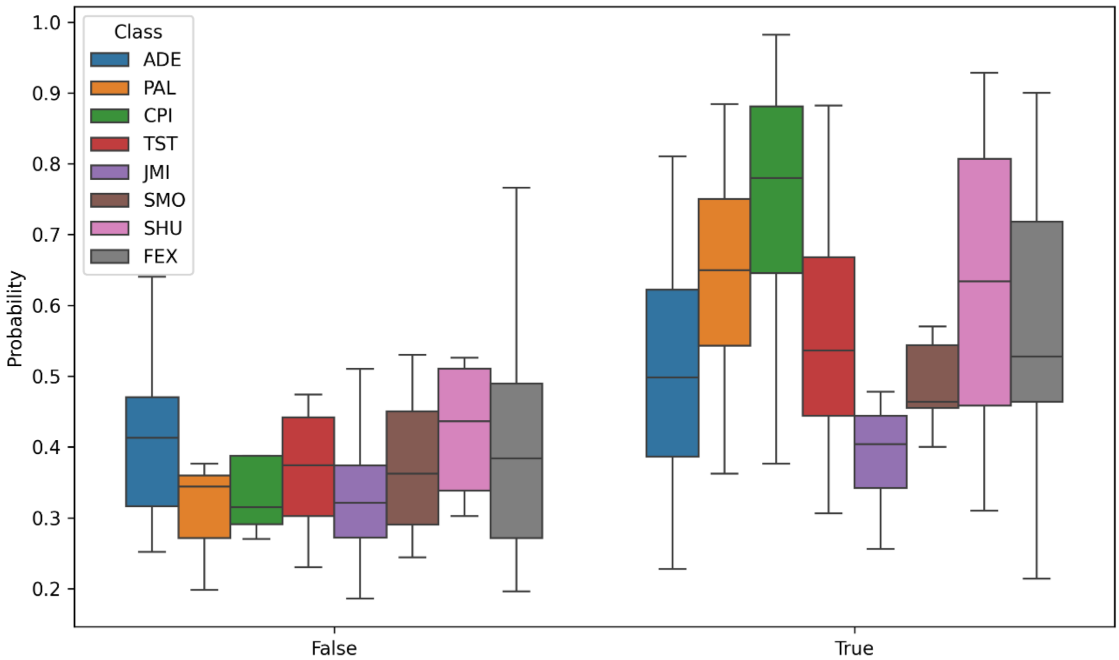

Figure 3.8. Distribution of probabilities classification assigned by RF.

3.3.3. Classification results with PointNet and PointNet++

Several models were trained using different configurations of epochs number, batch size, and the points per tree (Table 3.8). Using only the XYZ coordinates with PointNet and PointNet++, the highest accuracy achieved was 0.45. However, in this section, we evaluate these models using the variables identified as most relevant by RFE. For instance, using 4096 points and a batch size of 96 led to an accurate rise from 0.54 at 20 epochs to 0.62 at 100 epochs. Likewise, the performance was positively affected by the number of points, particularly in the range of 4096 points. The highest accuracy (0.62) was achieved with 4096 points, 100 epochs, and a batch size of 96, indicating that this configuration strikes the optimal balance between learning ability and generalization for this dataset. On the other hand, by PointNet++, the higher accuracy was obtained at 3072 points, 128 batch size, and 200 epochs, reaching a value of 0.64. Across all configurations, using 3072 and 4096 points consistently leads to a higher accuracy than smaller point sets, suggesting that PointNet++ benefits significantly from the number of points. In both cases, regarding batch sizes, high sizes (96 and 128) produce better outcomes compared to smaller (32 or 64) batch sizes in most cases, and the increasing epoch counts generally enhance the accuracy, with significant improvements seen when comparing 20 to 200 epochs.

Table 3.8. Model accuracy values categorized by training parameters: number of epochs, batch size, and number of input points.

	Epochs	**20**				**50**				**100**				**200**			
	Points/BS	**32**	**64**	**96**	**128**	**32**	**64**	**96**	**128**	**32**	**64**	**96**	**128**	**32**	**64**	**96**	**128**
PointNet	5120	0.37	0.46	0.43	0.44	0.48	0.52	0.57	0.53	0.55	0.60	0.49	0.60	0.59	0.60	0.55	0.56
	4096	0.45	0.54	0.54	0.47	0.46	0.49	0.53	0.55	0.54	0.58	0.62	0.61	0.44	0.57	0.61	0.61
	3072	0.47	0.46	0.44	0.48	0.56	0.61	0.49	0.50	0.52	0.56	0.51	0.59	0.59	0.55	0.58	0.57
	2048	0.38	0.45	0.50	0.47	0.53	0.54	0.49	0.53	0.45	0.57	0.56	0.51	0.46	0.59	0.59	0.56
	1024	0.45	0.50	0.45	0.52	0.43	0.57	0.50	0.57	0.48	0.51	0.54	0.55	0.54	0.54	0.57	0.51
PointNet++	5120	0.41	0.49	0.41	0.41	0.49	0.50	0.49	0.52	0.47	0.55	0.53	0.53	0.58	0.58	0.55	0.59
	4096	0.26	0.42	0.45	0.42	0.47	0.50	0.55	0.48	0.54	0.53	0.57	0.52	0.62	0.59	0.63	0.61
	3072	0.47	0.47	0.41	0.50	0.52	0.60	0.42	0.60	0.61	0.58	0.55	0.63	0.56	0.56	0.55	0.64
	2048	0.32	0.42	0.46	0.43	0.47	0.57	0.49	0.45	0.55	0.57	0.59	0.55	0.44	0.61	0.54	0.59
	1024	0.36	0.47	0.48	0.49	0.49	0.51	0.53	0.47	0.50	0.53	0.52	0.55	0.54	0.59	0.56	0.53

Evaluating the learning curves of the PointNet model (Figure 3.9a) shows the highest accuracy (Epochs:100, BS:96, Points:4096). The model learns quite well during training, but the learning is more irregular in validation data.

The validation accuracy improves, though not to the same level of the training data. Similarly, the validation loss decreases at first but then fluctuates and remains slightly above the training loss. This suggests that the model is slightly overfitting the training data, limiting its ability to generalize the classification to new data, although the overfitting is not drastic. In relation to the PointNet++, the model with the highest accuracy (Epochs:200, BS:128, Points:3072), Figure 3.9b shows the learning curves, achieving similarly high training accuracy but with noticeably better validation accuracy. The validation loss is more stable compared to PointNet, although some fluctuation persists. These patterns suggest that PointNet++ generalizes better, likely due to its hierarchical structure that captures local features more effectively, resulting in reduced overfitting and improved validation performance.

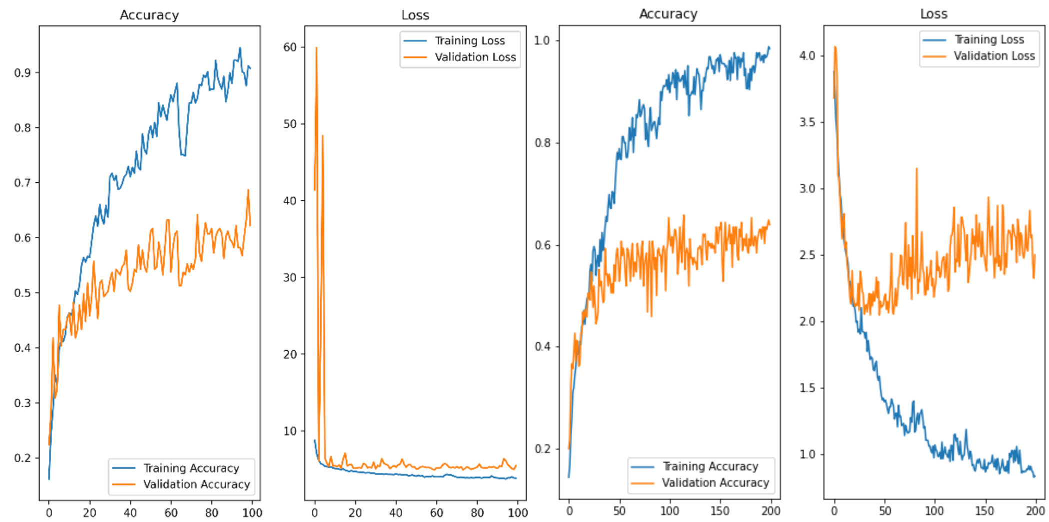

(a) (b)

Figure 3.9. Learning curves of model (a) PointNet with 4096 points, 100 epochs and batch size of 96. (b) PointNet++ with 3,072 points, 200 epochs, and batch size of 128.

The main results (Table 3.9) show that the reliability of the PointNet model has a variable performance among classes, with a global accuracy of 0.62, macro average of 0.60, and weighted average of 0.63. On the other hand, the PointNet++ model registers a global accuracy of 0.64, macro average of 0.60, and weighted average of 0.64. Classes PAL and CPI have the best performance in two models, while the JMI class has the worst. The comparison between PointNet and PointNet++ shows that PointNet++ provides better classification results in most classes. This model shows a more balanced performance between precision and recall, resulting in higher F1 scores in six of the eight species evaluated. For example, ADE improves from an F1 of 0.57 in PointNet to 0.65 in PointNet++. In contrast, the classes CPI and SMO show higher F1-Scores using PointNet. Although PointNet performs similarly in certain categories, PointNet++ presents stronger results overall, although at a higher computational cost.

Table 3.9. Confusion matrix and report of PointNet and PointNet++ model. N represents the test number

			Predicted							Report			
		ADE	PAL	CPI	TST	JMI	SMO	SHU	FEX	Precision	Recall	F1	N
Reference	PointNet												
	ADE	13	5	0	2	4	1	1	2	0.72	0.46	0.57	28
	PAL	1	19	2	0	1	1	0	0	0.68	0.79	0.73	24
	CPI	1	0	28	0	3	0	2	0	0.85	0.82	0.84	34
	TST	0	0	1	6	4	0	2	2	0.43	0.40	0.41	15
	JMI	0	1	1	2	7	0	1	0	0.23	0.58	0.33	12
	SMO	1	1	0	1	1	8	1	1	0.73	0.57	0.64	14
	SHU	0	1	0	1	6	0	25	2	0.62	0.71	0.67	35
	FEX	2	1	1	2	5	1	8	19	0.73	0.49	0.58	39
	PointNet++												
	ADE	21	3	0	1	1	2	3	1	0.64	0.66	0.65	32
	PAL	1	22	0	1	0	1	0	0	0.81	0.88	0.85	25
	CPI	1	1	27	2	0	2	0	3	0.75	0.75	0.75	36
	TST	2	0	1	8	1	0	2	1	0.38	0.53	0.44	15
	JMI	3	0	1	2	5	0	2	1	0.42	0.36	0.38	14
	SMO	2	0	3	1	3	6	1	0	0.46	0.38	0.41	16
	SHU	0	0	2	4	0	0	26	5	0.65	0.70	0.68	37
	FEX	3	1	2	2	2	2	6	23	0.68	0.56	0.61	41

3.4. Discussion

This study evaluated the potential of RGB point clouds obtained through UAVs for the identification of tree species, comparing traditional machine learning methods such as Random Forest with a deep learning approach based on PointNet. The following discussion is organized around four main topics, as follows: (1) the limitations of the dataset, (2) opportunities in the Ecuadorian context, (3) model comparison based on global accuracy and class-level performance, and (4) feature importance obtained from RF was used to select the input features for PointNet and PointNet++.

Limitations

One of the main limitations of UAV digital photogrammetric point clouds with respect to the UAV LiDAR is the lack of penetration through dense vegetation (Q. Hong et al., 2024), which restricts the acquisition of information from the ground and the internal structure of the canopy. However, at the level of trees the extraction of individual tree crown width and height using photogrammetric and LiDAR data are comparable (Man et al., 2025).

Likewise, canopy height metrics, such as the 90th (ZP90) and 50th (ZP50) height percentiles, had positive effects in RF, such as (Z. Xu et al., 2020). These metrics are particularly relevant for species with distinct height profiles, reflecting the importance of UAV structural data, to differentiate species based on vertical stratification. However, the absence of ground control points (GCPs) with GPS in UAV flights introduces potential errors in height profiles derived from photogrammetric data. In addition, this work does not analyze in depth the problem of tree segmentation since the trees had considerable spacing within the selected parks.

Although PointNet and PointNet++ are deep models specifically designed to process 3D data without the need for prior transformations, the performance may be limited when used with datasets that do not contain sufficient spatial features or when the network architecture does not adequately fit the problem.

Opportunities

Based on costs, in Ecuador, acquiring specialized equipment such as multispectral cameras or LiDAR sensors can be challenging. However, RGB UAVs offer an affordable alternative.

In the context of dimensions, works such as Man et al. (2025) focus on the radiometric aspects in 2D, whereas our approach leverages the 3D dimension information derived from the point cloud by analyzing the distribution of the Z coordinate. The use of UAV RGB point clouds enables the capture of vegetation's three-dimensional structure with a level of detail that surpasses traditional approaches, such as those based on multispectral data in some tree species (Pacheco-Prado et al., 2025).

Another main topic in this study is the use of Random Forest (RF), PointNet++ and PointNet, particularly in the context of spectral and geometric data for tree classification. Traditional Machine Learning (ML) methods, such as RF, are often based on mathematical relationships or clear rules that allow humans to understand how decisions are made. In contrast, Deep Learning (PointNet and PointNet++) operate as “black boxes” due to their high complexity and the large number of parameters (Chen et al., 2024; L. Pu et al., 2021). This means that for an analysis using ML an expert in forest areas should be available to analyze and interpret the variables selected by the model.

Although PointNet has great potential for 3D point cloud processing, traditional models such as Random Forest (RF) remain robust, particularly for classification tasks involving heterogeneous data. This is due to RF's simplicity and computational efficiency, which make it a more practical choice in many scenarios.

At the level of the tree species, the strengths of this study lie in identifying native species and understanding their key characteristics such as ecological adaptation, medicinal benefits or, in some cases, their potential negative impact on health and ecosystems. Among the notable native species are the *Tecoma stans (L.) Juss. ex Kunth* (TST), which exhibits remarkable drought tolerance, and the *Salix humboldtiana* (SHU), which thrives in humid soils and is valued for its importance in medicine and its ability to restore contaminated soils. On the other hand, some introduced species, such as the *Acacia dealbata* (ADE), can significantly affect ecosystems due to their invasive nature and ease of propagation. Similarly, the *Populus alba* (PAL) can displace native species and pose a potential health risk due to its allergenic properties (Guzmán-Salinas et al., 2023).

Models and classes performance

In this paper, the results show that the RGB channels, height distribution and the density of point clouds obtained allow them to generate high reliability in the identification of species such as *Populus alba L.* (PAL), *Melaleuca armillaris (Sol. ex Gaertn.) Sm.* (CPI), *Salix humboldtiana Willd.* (SHU), and *Fraxinus excelsior L.* (FEX) using RF. Conversely, classes such as *Schinus molle L.* (SMO) and *Jacaranda mimosifolia D. Don* (JMI) showed lower performance in this model.

In all models, species like PAL and CPI exhibit characteristics that facilitate better discrimination, with F1-scores above 0.71. In contrast, the class JMI had F1-Scores below 0.45; possibly due to the lower number of validation samples compared to other classes. However, the SMO class, which also had a limited number of samples, had moderate reliability using PointNet.

In analysis at the class level, the RF-trained model demonstrated superior performance compared to the PointNet and PointNet++ trained model for tree species classification from UAV point clouds. Using the F1 score to compare, RF had a higher reliability in classes such as ADE, TST, JMI, SHU, and FEX. On the other hand, PointNet managed to outperform RF, in the classes CPI and SMO.

Finally, using PointNet++ class PAL had a higher reliability compared to the other models.

Despite relying solely on RGB data from UAVs, this study achieved a global accuracy of 0.70 and a Kappa coefficient of 0.65, which is comparable to other works. For instance, Seidel et al. (2021) reported an accuracy of 0.86 using LiDAR scanners and key variables such as tree height, crown width, and 3D canopy structure (Seidel et al., 2021). Similarly, Sothe et al. (2019) achieved a global accuracy of 0.72 and a Kappa coefficient of 0.70 using UAV-based photogrammetric point clouds and hyperspectral data, although they classified 12 main tree species of a subtropical forest of southern Brazil. Onishi and Ise (2021), using a traditional approach based on RGB images combined with deep learning achieved up to 90% accuracy in tree species classification. However, their study was conducted in a limited geographic area. In contrast, the present study explores the potential of integrating 3D point clouds (XYZRGB) with geometric features in a more complex urban environment. This demonstrates the potential for forest identification at a lower cost compared to the more advanced technologies or traditional methods used in these studies.

Finally, the use of PointNet++ entails increased computational demands and training times, mainly due to its higher model complexity. Although PointNet++ demonstrated improved classification accuracy across most classes, it is necessary to assess whether the magnitude of this improvement justifies the additional processing time.

Feature importance

The relationship between tree crown density and UAV-derived point clouds density, using RF, is crucial for accurately assessing vertical structural attributes in remote sensing applications for classes such as ADE, CPI, TST, JMI, and SMO. Dense tree crowns typically result in higher point cloud densities due to increased surface area and canopy complexity, which enhances the photogrammetric point retrieval during UAV data acquisition. This relationship underscores the importance of optimizing UAV flight parameters, such as altitude, longitudinal, and transversal overlaps, to ensure sufficient point cloud density.

The feature importance in RF highlights the position of spectral and structural metrics in remote sensing-based forestry applications. For instance, the mean values of the Normalized Red-blue Difference Index (NRBDI_Mean) emerged as the most important variable, underscoring its strong influence on classification accuracy and the vegetation stress like apple and citrus (Glenn & Tabb, 2019). Similarly, the Green Leaf Index (GLI_Mean), the second most important feature, emphasizes the role of photosynthetic activity in species differentiation (Gitelson et al., 2022). The classes with highest accuracy in RF such as PAL, CPI, SHU and FEX are usually found in soils well supplied with water (Guzmán-Salinas et al., 2023), and their relationship with the NRBDI lies in the index's ability to provide descriptions.

Structural metrics derived from the UAV point cloud data also contributed significantly to classification performance. Point density, which represents the number of points per square meter, proved to be particularly useful for characterizing canopy heterogeneity. This finding indicates that structural information complements spectral data to distinguish species with diverse canopy structures.

3.5. Conclusion

This study compared the performance of two classification approaches for identifying eight tree species from RGB point clouds: Random Forest (RF), from a Machine Learning (ML) approach, which used spectral and geometric attributes derived from the point clouds; PointNet and PointNet++, from a Deep Learning (DL) approach, which directly processes 3D coordinates and associated attributes.

The results indicate that the Random Forest model achieved superior overall performance, with an accuracy of 0.70, compared to 0.62 obtained by PointNet and 0.64 by PointNet++. In addition, class-level analysis determined that RF outperformed PointNet's for most species, especially *Acacia dealbata Link* (ADE), *Tecoma stans (L.) Juss. ex Kunth* (TST), *Jacaranda mimosifolia D. Don* (JMI), *Fraxinus excelsior L.* (FEX), and *Salix humboldtiana Willd.* (SHU). However, PointNet demonstrated better performance on *Melaleuca armillaris (Sol. ex Gaertn.) Sm.* (CPI), and *Populus alba L.* (PAL) in PointNet++, indicating that its ability to capture three-dimensional geometry may be particularly useful for these species.

Analysis of the importance of variables in RF revealed that spectral indices such as mean Normalized Red-Blue Difference Index (nrbdi_mean) and mean Green Leaf Index (gli_mean) were the most relevant attributes for classification, followed by geometric characteristics such as maximum height, Z percentiles (zp10, zp50, zp90), normalized point density, Intensity (mean and standard deviation) and Brightness standard deviation. This suggests that the combination of RGB information together with structural variables can be used to differentiate forest species evaluated from a 3D perspective.

Finally, it is recommended that future research should first focus on balancing the number of samples in the database, so that the comparison between RF and PointNet's models is more effective. In addition, the use of multispectral attributes, in in combination with RGB data, could be evaluated. From the DL approach, other neural network architectures will be explored and mechanisms such as transfer learning or data augmentation will be implemented to improve the generalization of the PointNet-based model. Our results open the door to the more efficient monitoring and management of urban forests, particularly in areas like Ecuador where the diversity of species is high and the development and update of urban tree inventories is more challenging.

Chapter 4

Identification of Tree Species at a Close-Range Scale Using RGB Images from Smartphones

Edited version of:

Pacheco-Prado, D.; Bravo-López, E.; Ruiz, L.Á. Tree Species Identification in Urban Environments Using TensorFlow Lite and a Transfer Learning Approach. Forests 2023, 14, 1050. https://doi.org/10.3390/f14051050

Populus alba L.
Alamo blanco

Melaleuca armillaris (Sol. ex Gaertn.) Sm.
Cepillo blanco

Schinus molle L.
Ramo de novia

Salix humboldtiana
Sauce

4. IDENTIFICATION OF TREE SPECIES AT A CLOSE-RANGE SCALE USING RGB IMAGES FROM SMARTPHONES

In this chapter, RGB images obtained from the Tree Inventory of Cuenca, captured using smartphones, are used to train computer vision models to identify fourteen tree species. A Transfer Learning approach is applied using Convolutional Neural Networks, and the Data Augmentation technique was used to balance the number of samples by class.

4.1. Introduction

Urban trees benefit citizens, improving their quality of life (Pacheco & Ávila, 2017; Salam, 2020; Solomou et al., 2019); therefore, their conservation is essential for city administrators (Salam, 2020). Urban Tree Inventories (UTIs) provide information about species and location and photography of each tree (Solomou et al., 2019), which allow sustainable forest management and monitoring of urban trees and gardens (Pacheco, 2017). Nevertheless, the costs of carrying out these inventories are usually high, impeding their creation (Das et al., 2022) or updating (Branson et al., 2018), and requiring specialists to identify tree species (Wäldchen & Mäder, 2018). Participatory projects such as Tree Inventory on Portland's streets (*Tree Inventory Project | Portland.Gov*, n.d.) or New York City (*Volunteers Count Every Street Tree in New York City | US Forest Service*, n.d.); or private projects such as Cuenca-Ecuador (Ávila Pozo, 2017) with smartphones (Ávila Pozo, 2017; Nielsen et al., 2014; Pacheco & Ávila, 2017) have allowed the collection of these datasets.

In recent years, identifying plant species (Azlah et al., 2019; Goyal et al., 2022; Kaya et al., 2019; Rodríguez-Puerta et al., 2022; Wäldchen & Mäder, 2018), flowers (Xia et al., 2017), medicinal plants (Leena Rani et al., 2022), and trees (Carpentier et al., 2018) has been achieved using photographs. Examples of this are some mobile applications available in the android market, such as LeafSnap, PictureThis, PlantNet, Blossom, Seek, and others (Wäldchen & Mäder, 2018). Plant identification approaches are usually based on analyzing a single leaf followed by a flower (Wäldchen & Mäder, 2018). For these image analysis systems that apply Artificial Vision and Deep Learning methods, it is possible to customize models of local flora (Muñoz Villalobos & Bolt, 2022), to assess the health status of trees and plants (Adedoja et al., 2019; Rodríguez-Puerta et al., 2022) and aid in leaf recognition and classification (Vilasini & Ramamoorthy, 2020; R. Zhang et al., 2022) using artificial neural networks.

Several studies have analyzed the application of Deep Learning for forest analysis from different approaches. In Y. Wang et al. (2021), Deep Learning algorithms were analyzed for forest resource inventory and tree species identification, implementing neural networks of different architectures. In Cetin & Yastikli (2022), the use of Machine Learning (ML) algorithms (Random Forest, Support Vector Machines, and ANN Multilayer Perceptron) was analyzed for tree species classification in urban environments through the use and processing of LiDAR data. Although the focus of these studies is different from the one proposed in the present research, it is important to show that the use of quantitative methods based on ML algorithms contributes to the optimization of management, planning, and maintenance of tree inventories in urban areas with complex structures. On the other hand, there are also studies in which Deep Learning was applied explicitly for forest species identification. In Lasseck (2017), plant species mostly coming from western Europe and North America were identified based on images from the online collaborative Encyclopedia of Life https://eol.org/ (accessed on 20 February 2023), using Deep Convolutional Neural Network (DCNN) architectures, such as GoogleNet, ResNet, and ResNeXT. In Carpentier et al. (2018), tree species were also identified using Convolutional Neural Networks (CNNs) but based on images of the bark. The images used were obtained under different conditions and cameras to ensure a diversification of the data. The accuracy obtained was higher than 93%, demonstrating the effectiveness of the application of this methodology. In J. Liu et al. (2019), they used Deep Learning, implementing the UNET architecture (a variant of CNN), to classify tree species using forest images, considering additional important attributes for the stands and parcels from which the images were obtained, such as elevation, aspect, slope, and canopy density, and obtained accuracy results above 80% based on different validation metrics such as accuracy, Precision, and Recall. In Gajjar et al. (2022), a more specific analysis was performed, detecting and identifying plant diseases in real-time using a CNN-based architecture on an integrated platform by analyzing the leaves. The accuracy of the results obtained was higher than 96%. All these investigations demonstrate that methodologies focused on Machine Learning and Deep Learning, such as CNNs, can be used to identify forest species from different perspectives and datasets with high accuracy.

CNN is nowadays the most used Neural Network for image classification. It consists of a stack of layers encompassing an input image, performing a mathematical operation, and predicting the class or label probabilities in the output (Gogul & Kumar, 2017). This can be implemented in the TensorFlow framework (Kattenborn et al., 2021), the most stable and complete library for the Python language (Pang et al., 2020).

Image classification models using CNNs can have millions of parameters, which means that training them from the beginning requires a large amount of labeled input data (Carpentier et al., 2018; Figueroa-Mata & Mata-Montero, 2020; T. K. Kim et al., 2021) and high computing power (Paper, 2021). Another problem is that a limited number of samples can generate overfitting problems in CNN models, which consist of the poor generalization capacity of the models to new information (T. K. Kim et al., 2021). This can be reduced through two techniques: Transfer Learning (TL) and Data Augmentation (DA). TL is a process that allows the creation of new learning models by adjusting once-trained neural networks (*Creador de Modelos TensorFlow Lite*, n.d.; Paper, 2021). DA generates synthetic samples from existing data using transformations, such as image rotation, color degradation, and others, although it can cause overfitting in minority classes (Shorten & Khoshgoftaar, 2019). TensorFlow Hub offers a pre-trained and ready-to-use model for TL (*TensorFlow Hub*, n.d.) that simplifies training models using a custom dataset (*TensorFlow Lite Model Maker*, n.d.). Additionally, the TensorFlow Lite Model Maker function allows these models to be deployed for mobile devices.

The trained models can run inference on the client's devices when using TFLite files for our Java-developed Android application. AgroAId is an example; it was built to identify combinations from a plant leaf image input, recognizing 39 species and disease classes on devices with limited computing and memory resources (Reda et al., 2022). Finally, the relevant pixels for the decision to classify the image by CNN can be visualized through the GRAD-CAM (Gradient-weighted Class Activation Mapping) method, which highlights the areas of the image in the form of heat maps (T. K. Kim et al., 2021; A. Kumar et al., 2022; Selvaraju et al., 2016).

If we consider that most of the mobile applications available require an Internet connection to perform the identification of plants or forest species (Wäldchen & Mäder, 2018), that means that the inference is performed in a medium external to the mobile device and it limits its use in disconnected environments; thus our main contribution is to evaluate a methodology that trains a model that can be used offline and is based on Transfer Learning methodology due to the limited number of samples available compared to other free datasets. On the other hand, currently available mobile applications for plant identification focus on leaves or fruits because these elements are the most easily recognizable and distinctive parts of a plant. In the case of trees, the reviewed works evaluate photographs of the trunk or images with environmental noise. Nevertheless, our work analyzed trees based on their general appearance to identify those whose characteristics can be easily evaluated by a CNN, thus allowing for their identification.

This research applies and evaluates a Transfer Learning for automated identification of the most common tree species in the urban area of Cuenca (Ecuador), using computer vision techniques based on smartphone images of the local flora from the Tree Inventory of Cuenca (TIC), and can be deployed using Android smartphones.

4.2. Materials and methods

4.2.1. Study zone

Cuenca is located in Ecuador's central/southern area (Figure 4.1) at a mean elevation of 2500 m above sea level (m.a.s.l.). According to information from the Municipal Cleaning Company of Cuenca (EMAC-EP), in 2017 there were around 208 parks (public green areas) within the urban perimeter of the city (Pacheco, 2017), with the largest and the most important green areas in El Paraíso, Miraflores, and La Madre.

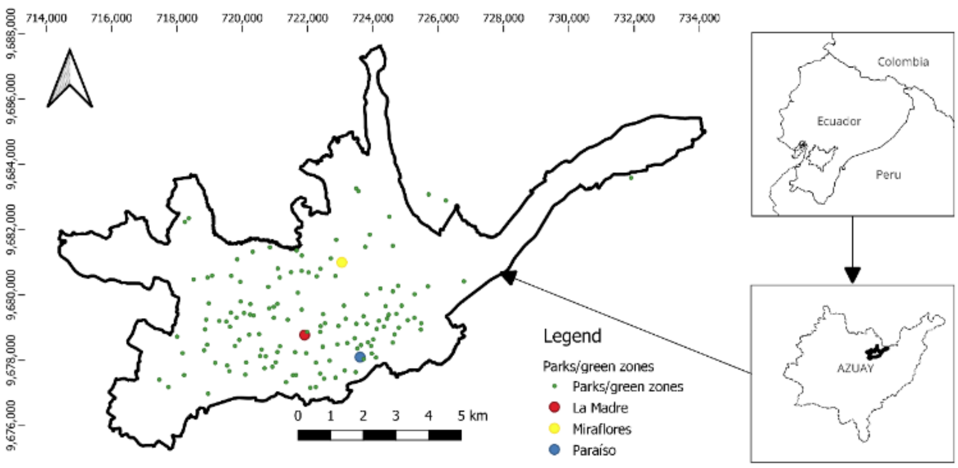

Figure 4.1. Location of the city of Cuenca and its public parks and green zones.

In Cuenca (Ecuador), the University of Azuay, through the Institute for Sectional Regime Studies of Ecuador - IERSE https://ierse.uazuay.edu.ec (accessed on 5 February 2023) and the Azuay Herbarium https://herbario.uazuay.edu.ec/ (accessed on 5 February 2023), built the Tree Inventory of Cuenca and published the results at the official website https://gis.uazuay.edu.ec/iforestal/ (accessed on 1 March 2023)(Ávila Pozo, 2017). Until June 2022, it contained 12,688 trees with information about taxonomy, origin, crown and trunk structure, phenology, forest management, potential problems and two photographs of each tree. The 52.1% corresponded to introduced species, 47.7% are native, and less than 1% are endemic species. The most frequent species are *Tecoma stans (L.) Juss. ex Kunth* (Fresno o Cholan), *Salix humboldtiana Willd.* (Sauce), *Fraxinus excelsior L.* (Urapan), *Jacaranda mimosifolia D. Don* (Jacaranda), *Prunus serotina Ehrh.* (Capuli), and *Melaleuca armillaris (Sol. ex Gaertn.) Sm.* (Cepillo Blanco).

4.2.2. Methodology

The methodology was implemented in four phases (Figure 4.2): (1) assessment of existing classes in the TIC and selection of those with the largest number of images, with trees over two meters height. (2) Image selection by activation maps and balancing of the number of images per class using an image rotation operation to reach the minimum image number. (3) Training the models with the selected images, evaluation, and producing classification reports. (4) Deployment of the top-ranked TFLite model on Android devices.

4.2.2.1. Class selection

Only those trees or shrubs over 2 m in height were selected from the TIC database. The Cucarda, Guaylo, and Tilo_or_sauco_blanco classes can be considered as shrubs (Minga & Verdugo, 2016). A total of fourteen species were finally chosen (Table 4.1) based on the availability of at least 160 samples, with the highest number of inventoried trees of native (N) or introduced (I) origin.

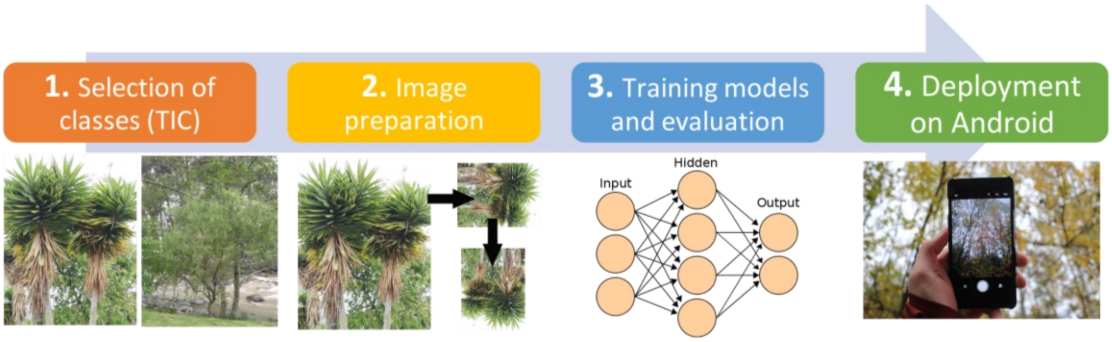

Figure 4.2. Overlay workflow of the methodology followed to create image classification model and deployment on Android devices.

Table 4.1. Tree species/class selected from the Cuenca TIC database. (N) Native and (I) introduced species.

Class Name	Code	Description	Origin	
Alamo blanco *Populus alba* L.	PAL	Tree that reaches up to 15 m in height, with straight trunks and greenish white outer bark that cracks over the years (*Populus Alba in Flora of China @ Efloras.Org*, n.d.).	I	
Capuli *Prunus serotina* Ehrh.	PSE	Tree that reaches from 8 to 15 m in height and 30 to 50 cm in diameter at breast height (DBH). It has fissured outer bark, alternate branching, and a globose crown (Minga & Verdugo, 2016).	N	
Cepillo *Callistemon lanceolatus* (Sm.) Sweet	CLA	Tree from 2 to 7 m in height with dark brown fissured outer bark. It has elongated leaves with a linear shape that are pubescent when young (Minga & Verdugo, 2016).	I	
Cepillo blanco *Melaleuca armillaris* (Sol. ex Gaertn.) Sm.	CPI	Tree from 2 to 6 m in height with straight trunk and grayish brown fibrous outer bark. It has very thin leaves of linear shape with an acute apex (Sánchez, 2016).	I	
Cipres *Cupressus macrocarpa* Hartw.	CMA	They can reach 20 m in height with an approximate diameter of about 60 cm. They have a straight trunk and thin bark with longitudinal fissures. Their leaves are very small, scale-like, and aligned in opposite pairs (Minga & Verdugo, 2016).	I	
Cucarda *Hibiscus rosa-sinensis* L.	HRO	Shrub with branched stems from 2 to 5 m in height. It has simple leaves that are rounded at the base and elongated towards the apex. Its flowers can be presented in various colors, most commonly red or pink (Minga & Verdugo, 2016).	I	
Eucalipto *Eucaliptus globulus* Labill.	EGL	They can reach more than 60 m in height. In some specimens, the outer bark is light brown with a skin-like appearance, and it peels off in strips leaving gray or brownish spots on the inner bark (Minga & Verdugo, 2016).	I	

Guabisay *Podocarpus sprucei* Parl	PSP	Tree that grows up to 15 m in height in natural environments. It has a straight trunk and grayish brown fissured outer bark. It has simple, alternate, linear leaves with a hard-textured pointed apex (Minga & Verdugo, 2016).	N	
Guaylo *Delostoma integrifolium* D. Don	DIN	Tree that reaches up to 6 m in height with a cylindrical trunk and smooth bark. It has simple, opposite elliptic to oblong elliptic leaves with entire margin and terminal inflorescence with a few clustered flowers (Minga & Verdugo, 2016).	N	
Huesito *Pittosporum undulatum* Vent.	PUN	Tree from 3 to 5 m in height with grayish brown granular outer bark texture. It has a dense or semi-dense crown of globose or ellipsoidal shape that is light green in color (de Cundinamarca - CAR Barrero Barrero Delfín Camelo Salamanca, 2012).	I	
Ramo de novia *Yucca gigantea* Lem.	YGU	Tree from 3 to 6 m in height; when mature, it usually develops several stems. Its trunk has bulges at the base that taper towards the middle part with grayish brown rough outer bark (Guillot & Van der Meer, 2009).	I	
Sauce *Salix humboldtiana*	SHU	Tree that reaches between 5 and 12 m in height and 50 cm in diameter. It has a tortuous trunk with cracked outer bark and a wide irregular crown with alternate branching (Minga & Verdugo, 2016).	I	
Tilo o Sauco blanco *Sambucus canadensis L.*	SME	Deciduous shrub that reaches up to 3 m or more in height. Its leaves are arranged in opposite pairs (*Tilo (Sambucus Canadensis) · INaturalist Ecuador*, n.d.).	I	
Urapan *Fraxinus excelsior* L.	FEX	Tree that grows up to 35 m in height with irregular crown and deciduous foliage. It has opposite, pinnate compound leaves and the leaflets are finely serrated (*Fresno (Fraxinus Uhdei) · INaturalist Ecuador*, n.d.).	I	

4.2.2.2. Image selection and preparation

From the existing species in the TIC, the fourteen with the greatest number of individuals were selected. Of these, Cipres had the least number of images, so the selection process was performed based on the number of images of this class (426), 20% of which (86 images) were reserved for validation. From this set of images, a selection process was performed through activation maps (Figure 4.3) to use only the images where the relevant pixels (red color in Figure 4.3) belonged to the actual trees and not to the context (buildings, cars, and others). For each selected image, a corresponding activation map (new image) was generated using the EfficientNetB0 base model from TensorFlow Hub and the Grad-CAM library in Python version 3.9.12. Each generated activation map was visually inspected to determine which images to eliminate based on the more relevant pixels of the tree image.

Figure 4.3. Examples of selected and unselected images from their activation maps using Grad-CAM and Inception V3.

Therefore, the number of images for training was reduced, and it was necessary to complete them through synthetic samples obtained by rotation at 90, 180, and 270 degrees (Table 4.2). This is Data augmentation (DA) which is a technique used to increase the size of the training data set by creating new images from existing ones [30]. Finally, the image size was homogenized through a Python script that performed framing from the center and resized the sample images into 224 × 224 pixel images.

Table 4.2. Number of images by class and new rotated images.

Class	Code	Original Images	Rotation 90°	Rotation 180°	Rotation 270°	Rotated Images	% Images Rotated
Alamo blanco	PAL	295	15	15	15	45	13%
Capuli	PSE	340	0	0	0	0	0%
Cepillo	CLA	340	0	0	0	0	0%
Cepillo blanco	CPI	340	0	0	0	0	0%
Cipres	CMA	271	23	23	23	69	20%
Cucarda	HRO	322	18	6	6	6	5%
Eucalipto	EGL	249	31	30	30	91	27%
Guabisay	PSP	340	0	0	0	0	0%
Guaylo	DIN	289	17	17	17	51	15%
Huesito	PUN	208	44	44	44	132	39%
Ramo de novia	YGU	172	56	56	56	168	49%
Sauce	SHU	340	0	0	0	0	0%
Tilo o sauco blanco	SME	340	0	0	0	0	0%
Urapan	FEX	340	0	0	0	0	0%
		4186	202	187	185	574	

The final photographs of the selected classes were taken between 2017 and 2019 between 07:00 and 18:00, with a higher frequency between 9:00 and 12:00. Approximately 98% of the photographs were acquired with Huawei and Samsung branded smartphones, and the remaining 2% with Apple and Sony phones.

4.2.2.3. Training and testing models

Once the training and testing images were defined, the process of model training was performed by TL, for which two base architectures with a standard input size of 224 × 224 pixels and 3 bands were selected: RestNet V2 with 101 layers, trained on ImageNet (ILSVRC-2012-CLS) (*ResNet V2 101 | TensorFlow Hub*, n.d.), and EfficientNet-Lite, with several versions with different parameters and optimized for edge devices (Ab Wahab et al., 2021). The two models were implemented under the TensorFlow Lite model maker library with 20 epochs, which represents the number of times that all training images are fed through the neural network (Mezgec & Seljak, 2017). In the training, we defined the URL of the base model used from TensorFlow Hub and the address of the folder with the validation images. Finally, we fine-tuned the whole model instead of just training the head layer (*Object Detection with TensorFlow Lite Model Maker*, n.d.).

Two approaches were used to compare the performance of the models with the evaluation dataset: the confusion matrix and the classification reports from the Scikit-learn library (Python). First, the accuracy and Cohen's Kappa metrics allowed us to assess the global reliability of the model (*Sklearn.Metrics.Cohen_kappa_score — Scikit-Learn 1.2.1 Documentation*, n.d.). In the second tool, the Precision, Recall, and F1-score (harmonic mean between Precision and Recall) (Zheng et al., 2021) were used to evaluate the performance of each class individually. The equations of these metrics are shown in Equations (1)–(5).

$$Accuracy = \frac{TP + TN}{TP + TN + FP + FN} \tag{1}$$

$$Kappa = \frac{(p_o - p_e)}{(1 - p_e)} \tag{2}$$

$$\text{Precision} = \frac{TP}{TP + FP} \tag{3}$$

$$Recall = \frac{TP}{TP + FN} \tag{4}$$

$$F1 - score = \frac{(2 * Precision * Recall)}{Recall + Precision} \tag{5}$$

where *TP* is true positive, *TN* is true negative, *FP* is false positive, and *FN* is false negative in the confusion matrix (Zheng et al., 2021). For Cohen's Kappa, is the empirical probability of agreement on the label assigned to any sample (the observed agreement ratio) and is the expected agreement when both annotators assign the labels randomly (*Sklearn.Metrics.Cohen_kappa_score — Scikit-Learn 1.2.1 Documentation*, n.d.).

4.2.2.4. Deployment of the Model in Android Application

The Tensorflow Lite model maker library was chosen for its ease of use in generating models for mobile devices and its integration with the templates proposed in the TensorFlow website (*Recognize Flowers with TensorFlow Lite on Android*, n.d.). This library saves the trained model in TFLite (TensorFlow lite) format. This format is lightweight, efficient, optimized for mobile devices, and can be used to package trained TensorFlow models for deployment (Shah & Sajnani, 2020).

The mobile devices require an interpreter to execute these models and uses a combination of hardware acceleration and software optimization to perform the inference based on input data (Reda et al., 2022; *TensorFlow Lite Inference*, n.d.).

4.3. Results

4.3.1. Learning Curves of the models

The performance of the proposed models, EfficientNet-Lite and ResNet V2 101, for forest species recognition was tested with Transfer Learning. Figure 4.4 shows the accuracy and loss learning curves of the EfficientNet-Lite model during training and validation. The training accuracy gradually increased (Figure 4.4a) and the training and validation loss decreased slowly across all epochs (Figure 4.4b); in both cases, the accuracy showed fluctuations between epochs 4 and 14 and later stabilized. Figure 4.5 shows the accuracy and loss of the ResNet-V2-101-based model from epoch three onwards, where the accuracy of the validation data reached a score of 0.9; after which the model did not learn anymore.

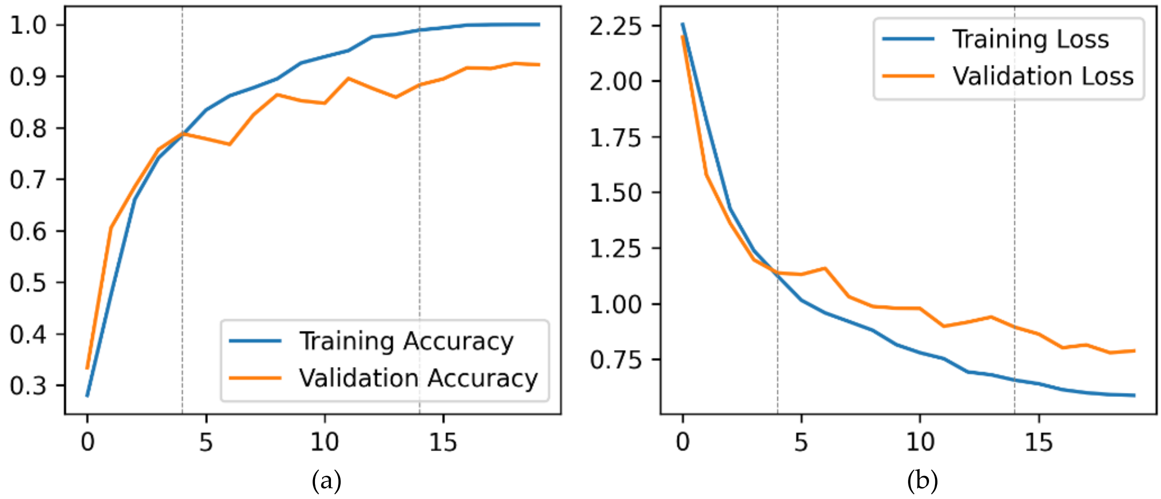

Figure 4.4. Learning curves of the EfficientNet-Lite model using Transfer Learning: (a) accuracy learning curves; (b) loss learning curves.

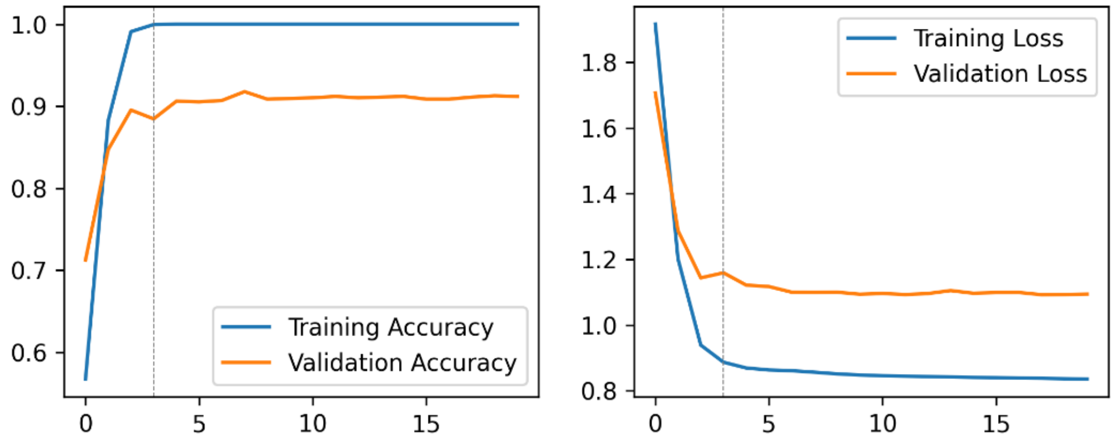

Figure 4.5. Learning curves of the ResNet V2 101 model using Transfer Learning: (a) accuracy learning curves; (b) loss learning curves.

Analyzing the accuracy and Cohen's kappa and the Accuracy (Acc) obtained from the validation dataset, the EfficientNet-Lite model performed better than the ResNet V2 101 model (Table 4.3). We evaluated the model and interpreter statistics in two ways. The first method, called Full Training, involved training the entire model, including layers and weights, which consumed a significant number of computational resources and time. The second method, called Top Layer Training, only retrained the top layers of the model, and utilized the previously learned weights and features for the other layers.

We assessed the predictions made by the TensorFlow Lite Interpreter, and we found that ResNet V2 101 was the best choice, even though its reliability decreased compared to the original model.

Table 4.3. Accuracy and kappa of model and interpreter.

	Full Training				Top Layer Training			
	Model		Interpreter		Model		Interpreter	
Base Model Name	**Acc**	**Kappa**	**Acc**	**Kappa**	**Acc**	**Kappa**	**Acc**	**Kappa**
ResNet V2 101	0.912	0.905	0.801	0.785	0.750	0.731	0.678	0.653
EfficientNet-Lite	0.922	0.916	0.770	0.752	0.780	0.763	0.648	0.621

We assessed the predictions made by the TensorFlow Lite Interpreter, and we found that ResNet V2 101 was the best choice, even though its reliability decreased compared to the original model.

4.3.2. Class Accuracy with the best model

Attending to the F1-score of the model based on ResNet V2 101, there were four highly reliable classes: Ramo de novia (YGU), Cipres (CMA), Cepillo blanco (CPI), and Sauce (SHU) (Figure 4.6). The loss of F1-score between the model and the interpreter was not homogeneous across all classes. Note that it was higher for the Cepillo (CLA) and Urapan (FEX) classes compared to the others.

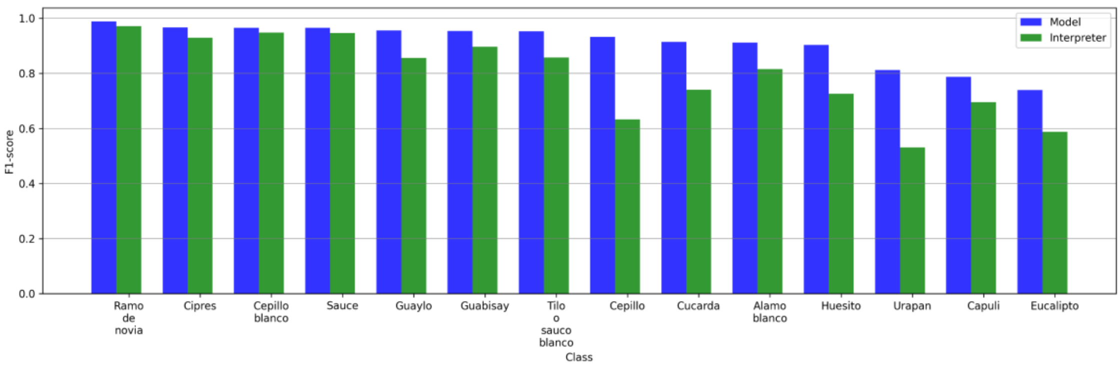

Figure 4.6. F1-scores for all classes considered using ResNet V2 101 model base.

Using the full report of the classification model (Table 4.4) and the interpreter (Table 4.5), a total of eight classes exceeded an F1-score of 0.8. The classes Eucalipto (EGL), Capuli (PSE), and Urapan (FEX) were the most difficult to classify. The confusion matrices (model and interpreter) with the greatest confusion occurred between the Eucalipto (EGL) and Capuli (PSE) classes. In the case of the interpreter, in addition to the previous one, other cases also occurred, such as the confusion of Urapan (FEX) with Eucalipto (EGL), and Cepillo (CLA) with Cucarda (HRO).

Table 4.4. Confusion matrix and classification report using ResNet V2 101 base model.

		Prediction																
		1	**2**	**3**	**4**	**5**	**6**	**7**	**8**	**9**	**10**	**11**	**12**	**13**	**14**	**Precision**	**Recall**	**F1-Score**
Real	1	82	0	0	0	1	0	0	0	1	0	0	1	0	1	0.87	0.95	0.91
	2	3	74	0	0	0	0	1	1	1	3	0	0	1	2	0.73	0.86	0.79
	3	0	2	76	2	1	4	0	1	0	0	0	0	0	0	0.99	0.88	0.93
	4	0	0	0	84	0	0	0	1	0	0	0	1	0	0	0.95	0.98	0.97
	5	0	0	0	0	86	0	0	0	0	0	0	0	0	0	0.93	1.00	0.97
	6	0	1	0	0	0	80	0	0	3	0	0	0	0	2	0.90	0.93	0.91
	7	8	19	0	0	0	0	54	0	0	0	1	0	0	4	0.90	0.63	0.74
	8	0	0	0	0	0	0	1	83	0	1	0	1	0	0	0.94	0.97	0.95
	9	0	0	0	0	0	0	0	0	86	0	0	0	0	0	0.91	1.00	0.96
	10	0	1	1	0	0	0	0	1	2	75	0	0	1	5	0.94	0.87	0.90
	11	0	0	0	1	0	0	0	0	0	0	85	0	0	0	0.99	0.99	0.99
	12	0	1	0	0	0	0	1	0	0	0	0	84	0	0	0.95	0.98	0.97
	13	0	3	0	0	0	1	0	1	0	0	0	0	80	1	0.98	0.93	0.95
	14	1	1	0	1	4	4	3	0	1	1	0	1	0	69	0.82	0.80	0.81

(1) PAL: Alamo Blanco, (2) PSE: Capuli, (3) CLA: Cepillo, (4) CPI: Cepillo blanco, (5) CMA: Cipres, (6) HRO: Cucarda, (7) EGL: Eucalipto, (8) PSP: Guabisay, (9) DIN: Guaylo, (10) PUN: Huesito, (11) YGU: Ramo de novia, (12) SHU: Sauce, (13) SME: Tilo o sauco blanco, (14) FEX: Urapan.

Evaluating the classification probabilities assigned to each of the 86 images per class (Figure 4.7), the classes with the best F1-score ranking also presented a high probability of correctness. The least favorable probabilities were for Eucalipto, which tended to be con-fused with the Capuli class. For the Urapan class, the probability of success was lower.

Table 4.5. Confusion matrix and classification report using ResNet V2 101 interpreter.

		Prediction																
		1	**2**	**3**	**4**	**5**	**6**	**7**	**8**	**9**	**10**	**11**	**12**	**13**	**14**	**Precision**	**Recall**	**F1-Score**
Real	1	84	0	0	0	1	0	0	0	0	0	0	0	0	1	0.70	0.98	0.82
	2	6	64	0	0	0	1	11	1	3	0	0	0	0	0	0.65	0.74	0.70
	3	4	5	43	4	2	13	4	4	2	0	2	0	0	3	0.86	0.50	0.63
	4	0	0	0	83	0	0	0	1	0	0	0	1	1	0	0.93	0.97	0.95
	5	1	0	0	0	85	0	0	0	0	0	0	0	0	0	0.88	0.99	0.93
	6	2	1	0	0	0	77	1	0	5	0	0	0	0	0	0.63	0.90	0.74
	7	8	17	1	0	2	1	52	0	0	0	1	0	1	3	0.57	0.60	0.59
	8	2	0	0	0	0	1	1	78	0	0	0	1	0	3	0.89	0.91	0.90
	9	5	0	0	0	0	1	0	0	80	0	0	0	0	0	0.79	0.93	0.86
	10	2	2	0	0	1	11	3	1	9	49	1	0	0	7	1.00	0.57	0.73
	11	0	0	0	1	0	0	0	0	0	0	85	0	0	0	0.96	0.99	0.97
	12	0	1	0	0	0	0	0	2	0	0	0	79	0	4	0.98	0.92	0.95
	13	2	7	1	0	0	7	1	1	0	0	0	0	66	1	0.97	0.77	0.86
	14	4	1	5	1	6	10	18	0	2	0	0	0	0	39	0.64	0.45	0.53

(1) PAL: Alamo Blanco, (2) PSE: Capuli, (3) CLA: Cepillo, (4) CPI: Cepillo blanco, (5) CMA: Cipres, (6) HRO: Cucarda, (7) EGL: Eucalipto, (8) PSP: Guabisay, (9) DIN: Guaylo, (10) PUN: Huesito, (11) YGU: Ramo de novia, (12) SHU: Sauce, (13) SME: Tilo o sauco blanco, (14) FEX: Urapan.

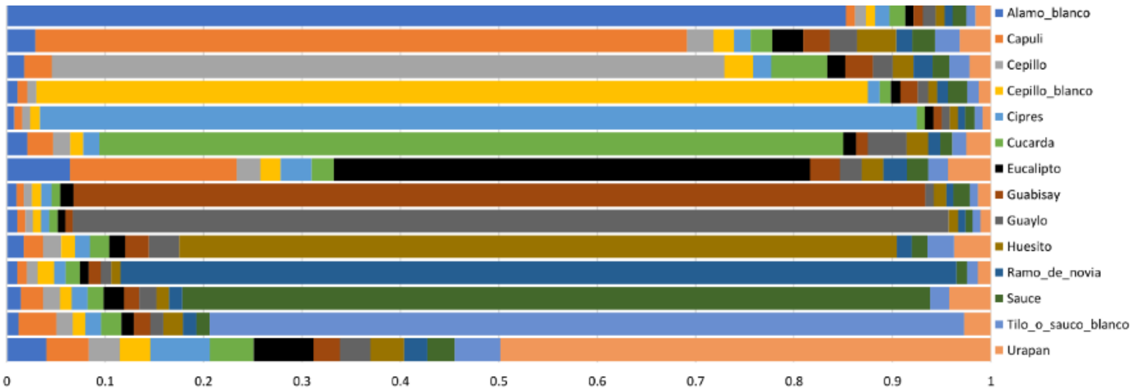

Figure 4.7. Sum of probabilities by classes of the 86 testing images per class.

4.3.3. Model deployment in Android Devices

The mobile application installer and model in mobile format (TFLite) can be downloaded from the website https://gis.uazuay.edu.ec/ (accessed on 15 March 2023). When performing the real-time prediction, the tree characteristics vary due to wind and light effects; the four highest-ranking possibilities are presented in the screen. When similar values exist, the tree cannot be classified correctly at that moment, and a change of the camera position is needed. When there is a significant difference between the first and second predictions, then there is more certainty in the result. Additionally, the proximity of the camera sensor to the object influences the prediction, as in the example shown in Figure 4.8, where the probability of the prediction varied from 51.2% to 89.5%.

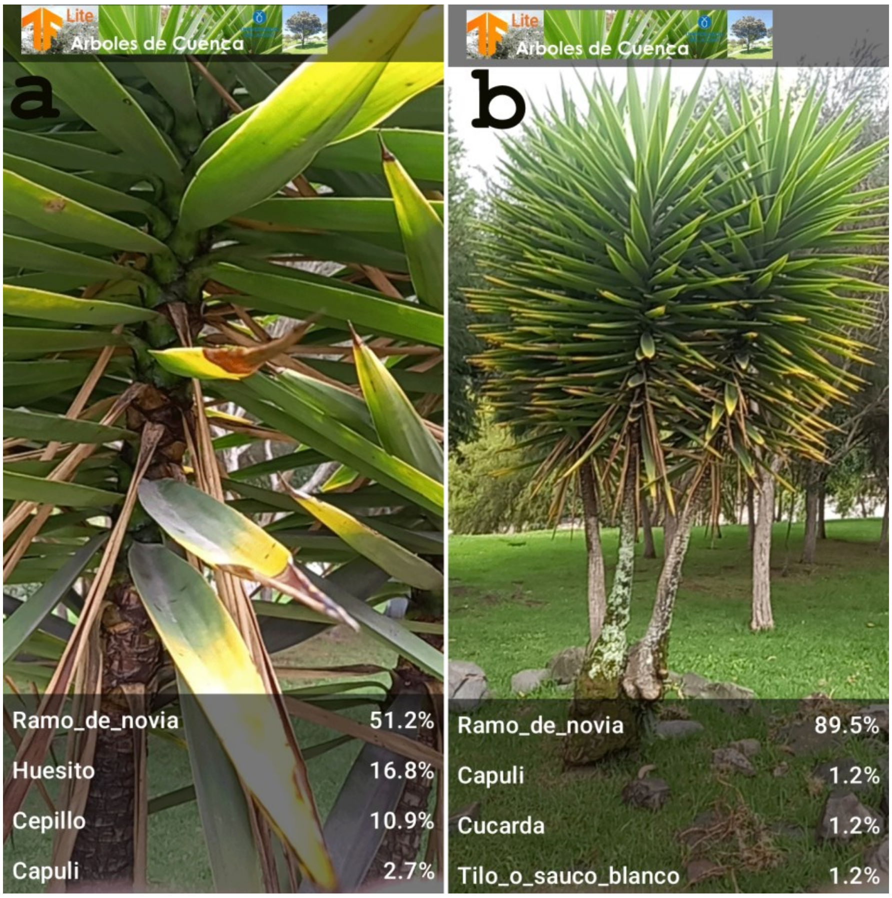

Figure 4.8. Real-time example classification of the Ramo de Novia class. (**a**) At a distance of approximately one meter, and (**b**) at a distance of approximately five meters.

4.4. Discussion

In this work, two different types of results were obtained, from a model and interpreter (using smartphones). In the first, the best accuracy and kappa metrics were obtained using EfficientNet-Lite as the base model (Transfer Learning approach), with values of 0.922 and 0.916 in the model. In the second case the best accuracy and kappa was obtained using ResNet V2 101 with values of 0.801 and 0.785, respectively. This accuracy is similar to those obtained in works such as (Homan & du Preez, 2021; Reda et al., 2022; Zheng et al., 2021). The TensorFlow Lite format, used in the interpreter, decreased the number of operations and affected the accuracy of the interpreter model.

The main difference between this work and others is that the images of TIC were taken entirely with smartphones, generally of the whole tree or shrub, and under different circumstances that add a high variability such as shadows, amount of light, distance to the object, and time of day, among others. For example, in Reda et al. (2022), the images of leaves were taken using a Sony DSC—Rx100/13 and used for the identification of plant diseases. These images were at a resolution of 20.2 megapixels. On the other hand, the images in (Homan & du Preez, 2021) focused on specific characteristics such as leaves and bark from different species.

In Transfer Learning (Gajjar et al., 2022; Reda et al., 2022), it was concluded that our dataset's best-performing model for Transfer Learning was ResNet V2 101 that was fully retrained (Natesan et al., 2019) (not only the classification layer on top). ResNet is an architecture that was previously used in similar applications such as (Reda et al., 2022) with 50 layers, while the one used in this work was 101 layers deep. From existing ResNet architectures, ResNet V2 101 had high reliability in other works with small datasets for the classification of plant leaf diseases (R. Zhang et al., 2022) or in works using drone images, such as (Dixit & Nain Chi, 2021; Natesan et al., 2019; C. Zhang et al., 2021). However, the ResNet V2 101 model has many more parameters than simpler models (L. Chen et al., 2021), which significantly increases the memory and processing requirements needed to train the model. In this work, controlling the number of images used for training was necessary due to computational constraints such as limited memory, CPU usage, and non-GPU availability, as well as processor capacity. To limit the number of images used, we chose to use only the image rotation data augmentation technique, used in other works such as (Figueroa-Mata & Mata-Montero, 2020; Reda et al., 2022).

Using the F1-score as a reference, from the fourteen classes evaluated in the model, ten exceeded a value of 0.9 and four in the interpreter. In the model, the classes with the highest value of F1-score were Guaylo (DIN), Cepillo blanco (CPI), Cipres (CMA), Sauce (SHU), and Ramo de Novia (YGU). For the interpreter, the best classes were Cipres (CMA), Cepillo blanco (CPI), Sauce (SHU), and Ramo de Novia (YGU).

The morphological characteristics of the Ramo de Novia class differentiated it from the other evaluated species, making this the most reliable class. The classes with the lowest reliability were Eucalipto (EGL) and Capuli (PSE) in the model, and Urapan (FEX) and Eucalipto (EGL) in the interpreter. As a test, the Capuli class was re-evaluated with another set of training and validation photographs to determine if this factor affected its reliability, obtaining similar results to the original classification. The morphological characteristics of this tree make it susceptible to confusion with other species. For this class, we propose to specifically evaluate the leaves (Barrientos, 2018), which are the organ most used in the identification of plants, or fruits for their identification. Other options to explore are the use of images of flowers (Wäldchen & Mäder, 2018) or bark (Carpentier et al., 2018).

These highest and lowest accuracy classes will be analyzed in future work using feature extraction such as color, texture, shape (Suwais et al., 2022), which are commonly used for leaf feature extraction, to describe the characteristics that make them identifiable to a CNN. In addition, other data augmentation techniques may be included such as Laplacian sharpening, Gaussian blur augmentation, contrast enhancement, shifting, cropping, and zooming (Mikołajczyk & Grochowski, 2018; Shaji & Hemalatha, 2022).

Even though the model's reliability was greater than that of the interpreter, we believe that further work should be able to improve the interpreter model, for example, using TensorFlow Model Optimization Toolkit (TensorFlow, 2021). This would be desirable in those circumstances where tree identification must be carried out in real time and the mobile device does not have Internet connection.

4.5. Conclusions

This paper presented an evaluation of two base models, ResNet V2 and EfficientNet-Lite, in a TensorFlow Lite model maker library for the recognition of fourteen classes of trees using the images of the TIC dataset. The performance of model with ResNet V2 101 was superior to that obtained with EfficientNet-Lite and the species Cepillo blanco (CPI), Cipres (CMA), Sauce (SHU), Guabisay (PSP), and Ramo de novia (YGU) presented the highest values of accuracy, Kappa, and F1-score in the classification. The final model had an accuracy of 0.912 and Kappa of 0.905, and with the TensorFlow Lite interpreter having an accuracy of 0.801 and Kappa of 0.785.

In the future, new tree species will be tested so they can be added to the application, generating a new classification model. It is expected that the mobile application will help non-expert users in the identification of tree species through smartphones, and it is considered a starting point for the creation of support for tree's inventories generation and maintenance in urban environments.

Chapter 5

General Discussion of Results and Conclusions

5.1 GENERAL DISCUSSION

This study evaluated the following hypotheses: *(1)"The spectral, spatial, and topographic characteristics derived from satellite imagery at regional scales enable the identification of forest species within the Andean Forest of Ecuador"; (2)"The high-resolution spatial and geometric features captured by UAV imagery at local scales enable the identification of tree species in urban areas of the Ecuadorian Andes"; and (3)"The photographs obtained from close-range smartphone imagery allow the identification of individual tree species within urban areas of the Ecuadorian Andes".* The results support this hypothesis, demonstrating that multi-scale forest analysis, combined with machine learning (ML) and deep learning (DL) techniques, can better identify between forest species, particularly when appropriate data sources and methods are selected for each scale.

Species identification at multiple spatial scales, from individual trees to entire landscapes, enhances our understanding of forest ecosystem functions, services, and processes (J. Chen et al., 2024). This identification can be performed at different scales depending on the sensor used for data collection. However, remote sensing studies for forest/tree species identification in Ecuador are limited. Considering the three scales proposed in this study, most research at the regional scale has focused on topics such as the detection of invasive plant species (Walsh et al., 2008), classification of forest types (Haro-Carrión & Southworth, 2018), *Polylepis reticulata* identification (Contreras, 2019), tree species richness (Haro-Carrión et al., 2021; Sesnie et al., 2023), assessment of changes in the páramo (Pazmiño et al., 2021), land cover classification (Castelo-Cabay et al., 2022; Velastegui-Montoya et al., 2022), forest fire monitoring (Morante-Carballo et al., 2022), land use change analysis (Muñoz Marcillo et al., 2023), Mangrove ecosystem mapping and monitoring (Caiza-Morales et al., 2024), and monitoring high wetlands (Huaraca et al., 2025).

Among these, only one study (Contreras, 2019) was focused on species identification. *Polylepis reticulata* identification was done using UAV orthophotography and Sentinel-2 spectral indices such as NDVI, SAVI5, and SAVI15 with a binary target (*Polylepis*/No *Polylepis*). In this study, satellite images that do not have areas of great size or are considered important did not adequately identify the species under study in Reserva de Producción de Fauna Chimborazo. In contrast, in the Cuenca case study, spatial resolution did not have significant impact on the identification of *Polylepis*. Instead, incorporating topographic variables was necessary to improve model performance. Additionally, better results were obtained using a multi-class approach rather than a binary one.

In Peru, two projects were carried out in the Andes region and focused on identifying forest rather than a specific species or genus: (a) Vega Isuhuaylas et al. (2018) reported an AUC of 0.81 for forest class identification using Landsat 8 OLI data with 10-fold cross-validation. (b) Pizarro et al. (2022) register a kappa of 0.81 classifying vegetation land cover. In the Cuenca case study (Chapter 2), the identification of the *Polylepis* genus achieved an accuracy of 0.90 and a Kappa coefficient of 0.89, using a combination of spectral bands and topography indices, just like Pizarro et al. (2022). However, Sentinel-2's spatial resolution in this work allows for better delineation of these stands (spatial resolution of 10 m), and better discrimination against other native species and shrub vegetation.

At the local scale, UAV data represents one of the most effective means for identifying individual tree species. The use of UAVs for tree species identification has become a widely studied topic globally. For instance, Nevalainen et al. (2017) analyzed 347 spectral and geometrical pixel features derived from UAV-based photogrammetry and hyperspectral imaging in the Vesijako research forest (southern Finland) to train various machine learning models, obtaining 95% of overall accuracy with RF and MLP. Similarly, Carbonell-Rivera et al. (2020) reported a cross-validation mean score of 0.8, evaluating RGB point clouds in the Palancia river region (Spain) using geometric (Normalized height) and spectral (R, G, B, NGRDI, NGBDI, NRBDI) metrics to classify vegetation and ground cover across five classes. Pradipkumar & Alagu Raja (2022) employed the Histogram of Oriented Gradient (HOG) descriptor to identify five tree species based on UAV images effectively. Man et al. (2025) evaluated 15 dominant tree species in the Changqing Campus of Shandong Normal University, Jinan (China), where a hyperspectral-LiDAR data fusion approach achieved an individual tree classification accuracy of 95.98% using point cloud.

In contrast, research in Ecuador remains limited. Ferreira et al. (2020) classified Amazonian palm species at the individual tree crown (ITC) level using UAV RGB images, reporting producer's accuracy of 78.6 ± 5.5% for *A. butyracea*, 98.6 ± 1.4% for *E. precatoria*, and 96.6 ± 3.4% for *I. deltoidea*. In Cuenca's case study in urban zone (Chapter 3), 809 tree crowns representing eight species were evaluated, despite the absence of prior reference species identification via remote sensing in Ecuador. This study employed spectral and geometric indices such as (Carbonell-Rivera et al., 2020). However, our work compares RF, PointNet, and PointNet++ algorithms. The RF model achieved an accuracy of 0.70 and a Kappa index of 0.65. In comparison, the PointNet model achieved an overall accuracy of 0.62, and PointNet++ reached 0.64. Although the overall results are lower than those reported in previous studies, such as Nevalainen et al. (2017), Ferreira et al. (2020), Carbonell-Rivera et al. (2020), and Man et al. (2025), particular species exhibited high identification performance. For instance, *Populus alba* L achieved F1-scores of 0.82 with RF and 0.85 with PointNet++, while *Melaleuca armillaris* (Sol. ex Gaertn.) Sm. achieved F1-scores of 0.80 with RF and 0.84 with PointNet. In the case of *Populus alba,* the result is comparable with the work of (H. Zhang et al., 2025), although their study utilized LiDAR data, our approach relies on photogrammetry.

Finally, at the close-range scale, in Ecuador no prior studies related to this scale were identified. While there are existing applications for plant identification based on leaves and fruits such as LeafSnap, PictureThis, PlantNet, Blossom, Seek, these tools do not focus on identifying the complete tree. Similarities with other works include data collection using smartphones, as in (Sun & Shi, 2023). The results of this work are comparable with (Malik et al., 2022), in controlled conditions using EfficientNet Lite model, in a transfer learning approach. In the urban zone of Cuenca (Chapter 4), the use of transfer learning and data augmentation was necessary to improve the reliability of the model, given the limited number of samples per species.

5.2 FINAL CONCLUSIONS

The general objective of this thesis was to "Identify forest and tree species in the Andean forests of Ecuador using a multi-scale approach, remote sensing data, and machine learning and deep learning methods". New geographic information technologies have enabled the generation of data at different scales, which has not yet been exploited for species identification in Ecuadorian Andean ecosystems and has been limited primarily to the classification of general categories such as native forest.

For this purpose, Machine Learning (ML) and Deep Learning (DL) were key tools that enabled the analysis in a multi-scale approach. At the regional scale (**Objectives 1 and 2**), ML was able to determine which features were most relevant for identification, depending on the forest species. In the local scale (**Objectives 3 and 4**), when analyzed using ML and DL through point clouds of each tree, it was found that ML, using Random Forest (RF), was more reliable for forest identification, mainly because RF was more effective at handling unbalanced datasets. Finally, at the close-range scale (**Objectives 5 and 6**), DL based on transfer learning and data augmentation was more effective than generating a new neural network.

Reference data on the ground is a fundamental building block for the success of ML and DL approaches. In ML, where algorithms rely heavily on selected features and training labels, it allows models to learn meaningful patterns and make reliable predictions. In DL, although feature extraction is automated, deep architecture's performance and generalization capability still depend heavily on the amount of training data, diversity, and accuracy. Therefore, it is necessary to invest a large amount of resources (human and monetary) in the careful collection, validation, and maintenance of benchmark data.

Each scale's model performance varies significantly among forest species, suggesting the need for adaptive approaches and balanced datasets to improve the classification of difficult species. In this work, the regional scale is used to identify *Polylepis* stands. On a local scale, the datasets of the tree point cloud of the UAV are imbalanced. Finally, the number of photographs was balanced on a close-range scale using the Data Augmentation technique.

The main conclusions for each of the specific objectives enumerated in section 1.7 are as follows:

Objective 1: *Compare classification scenarios using different spatial resolutions and evaluate how the spatial resolution of the input data affects the efficiency of Polylepis stand detection.*

The study demonstrated that Sentinel-2 imagery with a 10-meter spatial resolution yielded more accurate classification results than PlanetScope imagery at 5-meter resolution. This result demonstrates the importance of spectral data over spatial resolution in identifying *Polylepis* forests. Moreover, in the context of the Andes, incorporating of topographic variables was necessary to improve the model's reliability. Classification scenarios employing a multi-class objective consistently outperformed those using a binary classification framework in terms of reliability. This advantage is due to the ability of the multi-class approach to capture the complexity and heterogeneity of land cover types in the study zone. Additionally, it allows classification errors through the analysis of confusion among specific categories.

Objective 2: *Identify the optimal combination of optical, radar, and topographic variables for the identification of Polylepis stands using a pixel-based approach.*

The study demonstrated that employing a variable selection technique, such as Recursive Feature Elimination based on Random Forest, was important to improve the reliability of the models, particularly when handling regional and local scales. Reducing the number of variables facilitates interpreting these characteristics of forest species. For instance, topographic factors are necessary to study *Polylepis*, which are usually found at high altitudes (above 3300 m), on moderately steep slopes, and in specific orientations that influence microclimatic conditions.

Objective 3: *Assess the potential of spectral and geometric features derived from UAV-based photogrammetric point clouds for the identification of urban tree species.*

The findings revealed that multispectral features from the NIR and RedEdge channels of the point cloud did not have the expected impact on the tree species identification; instead, the structural variables and the vertical characterization were determining factors in identifying the tree species. Combining vegetation indices from the RGB channels with geometric variables was decisive in identifying species such as *Populus alba* L., *Melaleuca armillaris* (Sol. ex Gaertn.) Sm., and *Salix humboldtiana* Willd. Capturing three-dimensional geometry using the high-resolution of the UAVs enabled the individual modeling of each tree, which made it possible to diversify the characteristics to be evaluated, such as tree height percentiles, perimeter, area, and volume, among others of the point clouds. In this context, the main challenge to be solved is the individual tree segmentation, especially on riverbanks, where the location of the trees causes the crowns to overlap.

Objective 4: *Compare machine learning and deep learning classification algorithms to identify the most effective features and models for tree species identification based on tree crown UAV photogrammetric point clouds.*

The research introduced the integration of remote sensing and machine learning techniques that allow accurate identification of forest species at multiple scales. In local scales, species identification was optimized using UAV point clouds. Class-level analysis determining that RF (ML) outperformed PointNet's (DL) for most species, especially *Acacia dealbata* Link, *Tecoma stans* (L.) Juss. ex Kunth, *Jacaranda mimosifolia* D. Don, *Fraxinus excelsior* L., and *Salix humboldtiana* Willd. On the other hand, PointNet demonstrated a better performance on *Melaleuca armillaris* (Sol. ex Gaertn.) Sm., and *Populus alba* L. in PointNet++. Moreover, analysis of the importance of variables using RFE demonstrated that the highest reliability was obtained by combining normalized red–blue difference index, Green Leaf Index, Intensity, and Brightness with geometric characteristics based on the tree height.

Objective 5: *Evaluate the identification of individual tree species in urban environments using smartphone imagery and deep learning methods.*

The study demonstrated that using transfer learning with a data augmentation approach, in a TensorFlow Lite model maker library, produces the highest reliability when evaluating fourteen classes of trees using smartphone images. This approach was selected principally by the number of samples per class. The model's performance based on ResNet V2 101 was superior to that obtained with EfficientNet-Lite by the species *Melaleuca armillaris* (Sol. ex Gaertn.) Sm., *Cupressus macrocarpa* Hartw, *Salix humboldtiana*, *Podocarpus sprucei* Parl, and *Yucca gigantea* Lem presented the classification's highest accuracy, Kappa, and F1-score. However, the identification rules were not clearly defined; only the activation maps, which highlight the areas of the image in the form of heat maps, were generated.

Objective 6: *Explore the use of transfer learning and data augmentation techniques to enhance the efficiency of tree species identification in urban enviroments.*

The investigation concluded that our dataset's best-performing model for Transfer Learning was ResNet V2 101, which was fully retrained, not only the classification layer on top. For that purpose, controlling the number of images used for training was necessary due to computational constraints such as limited memory, CPU usage, non-GPU availability, and processor capacity. We used only the image rotation data augmentation technique to limit the number of images to train the model.

Advances in Machine Learning and Deep Learning techniques have opened up new possibilities for forest species identification in both rural (natural) and urban (anthropogenic) environments. The application of these methods at multiple scales, from regional satellite images to close observations using drones and smartphones, allows addressing the diversity of existing species, where altitudinal gradients, heterogeneous land use, and the presence of species introduced by humans coexist. This multi-scale integration improves accuracy in species detection and can strengthen monitoring, planning, and conservation of Andean forests.

A

Ab Wahab, M. N., Nazir, A., Ren, A. T. Z., Noor, M. H. M., Akbar, M. F., & Mohamed, A. S. A. (2021). Efficientnet-Lite and Hybrid CNN-KNN Implementation for Facial Expression Recognition on Raspberry Pi. *IEEE Access*, *9*, 134065–134080. https://doi.org/10.1109/ACCESS.2021.3113337

Adedoja, A., Owolawi, P. A., & Mapayi, T. (2019). Deep learning based on NASNet for plant disease recognition using leave images. *IcABCD 2019 - 2nd International Conference on Advances in Big Data, Computing and Data Communication Systems*. https://doi.org/10.1109/ICABCD.2019.8851029

Aguirre, Z., Valencia, E., Veintimilla, D., Pardo, S., & Jaramillo, N. (2024). Floristic diversity, structure, and endemism of the woody component in the lower montane evergreen forest of Valladolid parish, Zamora Chinchipe, Ecuador. *Revista Ciencia y Tecnología*, *20*(4), 121–134. https://doi.org/10.17268/rev.cyt.2024.04.09

Ai, J., Zhang, C., Chen, L., & Li, D. (2020). Mapping annual land use and land cover changes in the Yangtze Estuary Region using an object-based classification framework and landsat time series data. *Sustainability (Switzerland)*, *12*(2). https://doi.org/10.3390/su12020659

Akbari, V., Solberg, S., & Puliti, S. (2021). Multitemporal Sentinel-1 and Sentinel-2 Images for Characterization and Discrimination of Young Forest Stands under Regeneration in Norway. *IEEE Journal of Selected Topics in Applied Earth Observations and Remote Sensing*, *14*. https://doi.org/10.1109/JSTARS.2021.3073101

Alonzo, M., Andersen, H. E., Morton, D. C., & Cook, B. D. (2018). Quantifying boreal forest structure and composition using UAV structure from motion. *Forests*, *9*(3). https://doi.org/10.3390/f9030119

Arekhi, M., Goksel, C., Sanli, F. B., & Senel, G. (2019). Comparative evaluation of the spectral and spatial consistency of Sentinel-2 and Landsat-8 OLI data for Igneada longos forest. *ISPRS International Journal of Geo-Information*, *8*(2). https://doi.org/10.3390/ijgi8020056

Armenteras, D., Rodríguez, N., Retana, J., & Morales, M. (2011). Understanding deforestation in montane and lowland forests of the Colombian Andes.

Regional Environmental Change, *11*(3), 693–705. https://doi.org/10.1007/s10113-010-0200-y

Astudillo, P. X., Tinoco, B. A., & Siddons, D. C. (2015). The avifauna of Cajas National Park and Mazán Reserve, southern Ecuador, with notes on new records. *Cotinga*, *37*(February 2014), 1–11.

Atkins, J. W., Bhatt, P., Carrasco, L., Francis, E., Garabedian, J. E., Hakkenberg, C. R., Hardiman, B. S., Jung, J., Koirala, A., LaRue, E. A., Oh, S., Shao, G., Shao, G., Shugart, H. H., Spiers, A., Stovall, A. E. L., Surasinghe, T. D., Tai, X., Zhai, L., … Krause, K. (2023). Integrating forest structural diversity measurement into ecological research. *Ecosphere*, *14*(9). https://doi.org/10.1002/ecs2.4633

Ávila Pozo, L. A. (2017). Implementación de un de sistema de inventario forestal de parques urbanos en la ciudad de Cuenca. *Universidad-Verdad*, *73*, 79–89. https://doi.org/10.33324/uv.v1i73.39

Azlah, M. A. F., Chua, L. S., Rahmad, F. R., Abdullah, F. I., & Alwi, S. R. W. (2019). Review on techniques for plant leaf classification and recognition. *Computers*, *8*(4). https://doi.org/10.3390/computers8040077

B

Balha, A., Mallick, J., Pandey, S., Gupta, S., & Singh, C. K. (2021). A comparative analysis of different pixel and object-based classification algorithms using multi-source high spatial resolution satellite data for LULC mapping. *Earth Science Informatics*, *14*(4), 2231–2247. https://doi.org/10.1007/s12145-021-00685-4

Balipa, M., & Castalino, A. (2022). Alstonia Tree Detection using CNN and Inception V3 Algorithms. *3rd IEEE 2022 International Conference on Computing, Communication, and Intelligent Systems, ICCCIS 2022*, 318–321. https://doi.org/10.1109/ICCCIS56430.2022.10037697

Balthazar, V., Vanacker, V., Molina, A., & Lambin, E. F. (2015). Impacts of forest cover change on ecosystem services in high Andean mountains. *Ecological Indicators*, *48*, 63–75. https://doi.org/10.1016/j.ecolind.2014.07.043

Barrientos, J. L. (2018). Leaf Recognition with Deep Learning and Keras using GPU computing. *TFG in Computer Engineering,Engineering School,UAB University*, *February*.

Bjerreskov, K. S., Nord-Larsen, T., & Fensholt, R. (2021). Classification of nemoral forests with fusion of multi-temporal sentinel-1 and 2 data. *Remote Sensing*, *13*(5). https://doi.org/10.3390/rs13050950

Blundo, C., Malizia, L. R., Blake, J. G., & Brown, A. D. (2012). Tree species distribution in Andean forests: influence of regional and local factors. *Journal of Tropical Ecology*, *28*(1), 83–95. https://doi.org/10.1017/S0266467411000617

Bolyn, C., Michez, A., Gaucher, P., Lejeune, P., & Bonnet, S. (2018). Forest mapping and species composition using supervised per pixel classification of Sentinel-2 imagery. *Biotechnol. Agron. Soc. Environ. 2018*, *22*(3), 172–187.

Branson, S., Wegner, J. D., Hall, D., Lang, N., Schindler, K., & Perona, P. (2018). From Google Maps to a fine-grained catalog of street trees. *ISPRS Journal of Photogrammetry and Remote Sensing*, *135*, 13–30. https://doi.org/10.1016/j.isprsjprs.2017.11.008

Briechle, S., Krzystek, P., & Vosselman, G. (2020). Classification of tree species and standing dead trees by fusing UAV-based LiDAR data and multispectral imagery in the 3D deep neural network Pointnet++. *ISPRS Annals of the Photogrammetry, Remote Sensing and Spatial Information Sciences*, *V-2–2020*, 203–210. https://doi.org/10.5194/isprs-annals-V-2-2020-203-2020

Burt, A., Disney, M., & Calders, K. (2019). Extracting individual trees from lidar point clouds using treeseg. *Methods in Ecology and Evolution*, *10*(3). https://doi.org/10.1111/2041-210X.13121

Buxton, R. T., Mckenna, M. F., Mennitt, D., Fristrup, K., Crooks, K., Angeloni, L., & Wittemyer, G. (2000). *Deforestation in Continental Ecuador with a Focus on Protected Areas*. 1–19. papers3://publication/uuid/FB750DBC-0865-4EE5-BD7E-EDCFB1FE35EF

C

Caballero-Villalobos, L., Fajardo-Gutiérrez, F., Calbi, M., & Silva-Arias, G. A. (2021). Climate Change Can Drive a Significant Loss of Suitable Habitat for Polylepis quadrijuga, a Treeline Species in the Sky Islands of the Northern Andes. *Frontiers in Ecology and Evolution*, *9*. https://doi.org/10.3389/fevo.2021.661550

Caiza-Morales, L., Gómez, C., Torres, R., Nicolau, A. P., & Olano, J. M. (2024). MANGLEE: A Tool for Mapping and Monitoring MANgrove Ecosystem on Google Earth Engine—A Case Study in Ecuador. *Journal of Geovisualization and Spatial Analysis*, *8*(1), 17. https://doi.org/10.1007/s41651-024-00175-3

Calva, J., Ortíz, N., Calapucha, J., Chango, G., & Pallo, C. (2020). *Los Bosques de Ecuador. Los bosques, su importancia y sus limitaciones*. https://es.scribd.com/document/477024333/Los-Bosques-de-Ecuador

Carbonell-Rivera, J. P., Estornell, J., Ruiz, L. Á., Crespo-Peremarch, P., Almonacid-Caballer, J., & Torralba, J. (2024). Class3Dp: A supervised classifier of vegetation species from point clouds. *Environmental Modelling and Software*, *171*. https://doi.org/10.1016/j.envsoft.2023.105859

Carbonell-Rivera, J. P., Estornell, J., Ruiz, L. A., Torralba, J., & Crespo-Peremarch, P. (2020). Classification of UAV-based photogrammetric point clouds of riverine species using machine learning algorithms: a case study in the Palancia river, Spain. *The International Archives of the Photogrammetry, Remote Sensing and Spatial Information Sciences*, *XLIII-B2-2020*, 659–666. https://doi.org/10.5194/isprs-archives-XLIII-B2-2020-659-2020

Carbonell-Rivera, J. P., Ruiz, L. Á., Estornel, J., Simó-Martí, M., Quille-Mamani, J., & Torralba, J. (2024). Comparación de biomasa estimada a partir de mediciones clásicas y nubes de puntos UAV clasificadas mediante Class3Dp. *XX Congreso de La Asociación Española de Teledetección. Teledetección y Cambio Global: Retos y Oportunidades Para Un Crecimiento Azul*, 219–222. https://www.researchgate.net/publication/381322826

Carbonell-Rivera, J. P., Torralba, J., Estornell, J., Ruiz, L. Á., & Crespo-Peremarch, P. (2022). Classification of Mediterranean Shrub Species from UAV Point Clouds. *Remote Sensing*, *14*(1), 199. https://doi.org/10.3390/rs14010199

Carpentier, M., Giguere, P., & Gaudreault, J. (2018). Tree Species Identification from Bark Images Using Convolutional Neural Networks. *IEEE International Conference on Intelligent Robots and Systems*, 1075–1081. https://doi.org/10.1109/IROS.2018.8593514

Carrasco Espinoza, M., Pineda López, R., Miguel, R., & Munguía, P. (2010). Calidad del habitat en los ríos Tomebamba y Yanuncay en Ecuador. *Cienca@UAQ*, *3*(2), 13–26.

Castelo-Cabay, M., Piedra-Fernandez, J. A., & Ayala, R. (2022). Deep learning for land use and land cover classification from the Ecuadorian Paramo. *International Journal of Digital Earth*, *15*(1), 1001–1017. https://doi.org/10.1080/17538947.2022.2088872

Castillo, D. D., Carrasco, J. C., Quevedo, L. A., Ricaurte, C. B., Gavilanes, A. V, & Borz, S. A. (2017). Diversity, Composition and Structure of Andean High Forest in Ecuador, South America. *Bulletin of the Transilvania University of Braşov*, *10*(2), 16.

Castillo, D. D., Jara, C. A., Ricaurte, C. B., Vaca, B. E., & Quevedo, L. A. (2018). Photosynthetic activity and Canopy Height Model determined by Uav Rgb and IR close-range remote-sensing in the high andean polylepis relict forest, Ecuador. *Bulletin of the Transilvania University of Brasov, Series II: Forestry, Wood Industry, Agricultural Food Engineering*, *11*(60), 1–16.

Castillo Vizuete, D. D., Gavilanes Montoya, A. V., Chávez Velásquez, C. R., & Borz, S. A. (2023). A Critical Review on the Perspectives of the Forestry Sector in Ecuador. *Land*, *12*(1), 258. https://doi.org/10.3390/land12010258

Cetin, Z., & Yastikli, N. (2022). The Use of Machine Learning Algorithms in Urban Tree Species Classification. *ISPRS International Journal of Geo-Information*, *11*(4). https://doi.org/10.3390/ijgi11040226

Chen, J., Chen, Y., & Liu, Z. (2021). Classification of typical tree species in laser point cloud based on deep learning. *Remote Sensing*, *13*(23). https://doi.org/10.3390/rs13234750

Chen, J., Liang, X., Liu, Z., Gong, W., Chen, Y., Hyyppä, J., Kukko, A., & Wang, Y. (2024). Tree species recognition from close-range sensing: A review. *Remote Sensing of Environment*, *313*. https://doi.org/10.1016/j.rse.2024.114337

Chen, L., Li, S., Bai, Q., Yang, J., Jiang, S., & Miao, Y. (2021). Review of image classification algorithms based on convolutional neural networks. *Remote Sensing*, *13*(22), 1–51. https://doi.org/10.3390/rs13224712

Chraibi, E., Arnold, H., Luque, S., Deacon, A., Magurran, A. E., & Féret, J. B. (2021). A remote sensing approach to understanding patterns of secondary succession in tropical forest. *Remote Sensing*, *13*(11). https://doi.org/10.3390/rs13112148

Clark, M. L., Roberts, D. A., & Clark, D. B. (2005). Hyperspectral discrimination of tropical rain forest tree species at leaf to crown scales. *Remote Sensing of Environment*, *96*(3–4), 375–398. https://doi.org/10.1016/j.rse.2005.03.009

Contreras, O. (2019). *Identificación de la especie Polylepis Reticulata mediante teledetección en las zonas alto andinas del Ecuador* [Escuela Superior Politécnica de Chimborazo]. http://dspace.espoch.edu.ec/handle/123456789/10749

Creador de modelos TensorFlow Lite. (n.d.). Retrieved August 4, 2022, from https://www.tensorflow.org/lite/models/modify/model_maker

Cuenca. (2015). *Plan de desarrollo y ordenamiento territorial del cantón Cuenca*.

Cuenca, G. M. (2016). *Atlas Cartográfico del Plan de Desarrollo y Ordenamiento Territorial* (p. 105).

Cuesta, F., Peralvo, M., Merino-Viteri, A., Bustamante, M., Baquero, F., Freile, J. F., Muriel, P., & Torres-Carvajal, O. (2017). Priority areas for biodiversity conservation in mainland Ecuador. *Neotropical Biodiversity*, *3*(1), 93–106. https://doi.org/10.1080/23766808.2017.1295705

Curatola Fernández, G., Obermeier, W., Gerique, A., López Sandoval, M., Lehnert, L., Thies, B., & Bendix, J. (2015). Land Cover Change in the Andes of Southern Ecuador—Patterns and Drivers. *Remote Sensing*, *7*(3), 2509–2542. https://doi.org/10.3390/rs70302509

Cuyckens, G. A. E., & Renison, D. (2018). Ecología y conservación de los bosques montanos de Polylepis: Una introducción al número especial. *Ecología Austral*, *28*(1bis), 157–162. https://doi.org/10.25260/EA.18.28.1.1.766

D

Das, S., Sun, Q. (Chayn), & Zhou, H. (2022). GeoAI to implement an individual tree inventory: Framework and application of heat mitigation. *Urban Forestry and Urban Greening*, *74*, 127634. https://doi.org/10.1016/j.ufug.2022.127634

Dash, J. P., Pearse, G. D., & Watt, M. S. (2018). UAV multispectral imagery can complement satellite data for monitoring forest health. *Remote Sensing*, *10*(8), 1–22. https://doi.org/10.3390/rs10081216

de Cundinamarca - CAR Barrero Barrero Delfín Camelo Salamanca, D. O. E. A. R. F. A. M. V. G. E. (2012). *Vegetación del territorio CAR: 450 especies de sus llanuras y montañas*.

De Luca, G., Silva, J. M. N., Cerasoli, S., Araújo, J., Campos, J., Di Fazio, S., & Modica, G. (2019). Object-based land cover classification of cork oak woodlands using UAV imagery and Orfeo Toolbox. *Remote Sensing*, *11*(10). https://doi.org/10.3390/rs11101238

Diez, Y., Kentsch, S., Fukuda, M., López Cáceres, M. L., Moritake, K., & Cabezas, M. (2021). Deep Learning in Forestry using UAV-acquired RGB data: A practical review. In *Remote Sensing* (Vol. 13, Issue 14). MDPI AG. https://doi.org/10.3390/rs13142837

Dixit, A., & Nain Chi, Y. (2021). Classification and Recognition of Urban Tree Defects in a Small Dataset using Convolutional Neural Network, Resnet-50 Architecture, and Data Augmentation. *Journal of Forests*, *8*(1), 61–70. https://doi.org/10.18488/journal.101.2021.81.61.70

Dostálová, A., Hollaus, M., Milenković, M., & Wagner, W. (2016). Forest Area Derivation From Sentinel-1 Data. *ISPRS Annals of Photogrammetry, Remote*

Sensing and Spatial Information Sciences, *III–7*(July), 227–233. https://doi.org/10.5194/isprsannals-iii-7-227-2016

Dufour, S., Bernez, I., Betbeder, J., Corgne, S., Hubert-Moy, L., Nabucet, J., Rapinel, S., Sawtschuk, J., & Trollé, C. (2013). Monitoring restored riparian vegetation: how can recent developments in remote sensing sciences help? *Knowledge and Management of Aquatic Ecosystems*, *410*, 10. https://doi.org/10.1051/kmae/2013068

Duque, A., Peña, M. A., Cuesta, F., González-Caro, S., Kennedy, P., Phillips, O. L., Calderón-Loor, M., Blundo, C., Carilla, J., Cayola, L., Farfán-Ríos, W., Fuentes, A., Grau, R., Homeier, J., Loza-Rivera, M. I., Malhi, Y., Malizia, A., Malizia, L., Martínez-Villa, J. A., … Feeley, K. J. (2021). Mature Andean forests as globally important carbon sinks and future carbon refuges. *Nature Communications*, *12*(1). https://doi.org/10.1038/s41467-021-22459-8

E

Ecke, S., Stehr, F., Frey, J., Tiede, D., Dempewolf, J., Klemmt, H. J., Endres, E., & Seifert, T. (2024). Towards operational UAV-based forest health monitoring: Species identification and crown condition assessment by means of deep learning. *Computers and Electronics in Agriculture*, *219*. https://doi.org/10.1016/j.compag.2024.108785

Eltner, A., & Sofia, G. (2020). Structure from motion photogrammetric technique. In *Developments in Earth Surface Processes* (Vol. 23, pp. 1–24). https://doi.org/10.1016/B978-0-444-64177-9.00001-1

F

Fan, Z., Wei, J., Zhang, R., & Zhang, W. (2023). Tree Species Classification Based on PointNet++ and Airborne Laser Survey Point Cloud Data Enhancement. *Forests*, *14*(6). https://doi.org/10.3390/f14061246

FAO. (2020). *Global Forest Resources Assessment 2020*. FAO. https://doi.org/10.4060/ca8753en

FAO, & UNEP. (2020). El estado de los bosques del mundo 2020. In *The State of the World's Forests 2020*. FAO and UNEP. https://doi.org/10.4060/ca8642es

Fassnacht, F. E., White, J. C., Wulder, M. A., & Næsset, E. (2024). Remote sensing in forestry: current challenges, considerations and directions. *Forestry: An International Journal of Forest Research*, *97*(1), 11–37. https://doi.org/10.1093/forestry/cpad024

Favorskaya, M., Tkacheva, A., Danilin, I. M., & Medvedev, E. M. (2015). Fusion of airborne LiDAR and digital photography data for tree crowns segmentation and measurement. *Smart Innovation, Systems and Technologies*, *40*. https://doi.org/10.1007/978-3-319-19830-9_18

Feng, X., & Li, P. (2019). A Tree Species Mapping Method from UAV Images over Urban Area Using Similarity in Tree-Crown Object Histograms. *Remote Sensing*, *11*(17), 1982. https://doi.org/10.3390/rs11171982

Ferreira, M. P., Almeida, D. R. A. de, Papa, D. de A., Minervino, J. B. S., Veras, H. F. P., Formighieri, A., Santos, C. A. N., Ferreira, M. A. D., Figueiredo, E. O., & Ferreira, E. J. L. (2020). Individual tree detection and species classification of Amazonian palms using UAV images and deep learning. *Forest Ecology and Management*, *475*, 118397. https://doi.org/10.1016/j.foreco.2020.118397

Figueroa-Mata, G., & Mata-Montero, E. (2020). Using a convolutional siamese network for image-based plant species identification with small datasets. *Biomimetics*, *5*(1). https://doi.org/10.3390/biomimetics5010008

Fresno (Fraxinus uhdei) · iNaturalist Ecuador. (n.d.). Retrieved January 4, 2023, from https://ecuador.inaturalist.org/taxa/134212-Fraxinus-uhdei

G

Gajjar, R., Gajjar, N., Thakor, V. J., Patel, N. P., & Ruparelia, S. (2022). Real-time detection and identification of plant leaf diseases using convolutional neural networks on an embedded platform. *Visual Computer*, *38*(8). https://doi.org/10.1007/s00371-021-02164-9

García-García, A., Gómez-Donoso, F., García-Rodríguez, J., Orts-Escolano, S., Cazorla, M., & Azorin-López, J. (2016). Pointnet: A 3d convolutional neural network for real-time object class recognition. *2016 International Joint Conference on Neural Networks (IJCNN)*, 1578–1584.

Georganos, S., Grippa, T., Vanhuysse, S., Lennert, M., Shimoni, M., & Wolff, E. (2018). Very High Resolution Object-Based Land Use-Land Cover Urban Classification Using Extreme Gradient Boosting. *IEEE Geoscience and Remote Sensing Letters*, *15*(4), 607–611. https://doi.org/10.1109/LGRS.2018.2803259

Georgieva, M., Georgiev, G., Ivanov, M., Tyufekchiev, K., Belilov, S., Dodev, Y., Glogov, P., Georgieva, M. L., Popov, G., & Madzhov, S. (2022). Integrated approach for health status assessment of urban forests in the municipalities of Etropole and Pravets, Bulgaria. *Silva Balcanica*, *23*(1). https://doi.org/10.3897/silvabalcanica.23.e91220

Gerón, A. (2019). *Hands-on Machine Learning with Scikit-Learn, Keras & Tensorflow* (Second). O'Reilly Media.

Gitelson, A., Viña, A., Inoue, Y., Arkebauer, T., Schlemmer, M., & Schepers, J. (2022). Uncertainty in the evaluation of photosynthetic canopy traits using the green leaf area index. *Agricultural and Forest Meteorology*, *320*, 108955. https://doi.org/10.1016/j.agrformet.2022.108955

Glenn, D. M., & Tabb, A. (2019). Evaluation of Five Methods to Measure Normalized Difference Vegetation Index (NDVI) in Apple and Citrus. *International Journal of Fruit Science*, *19*(2), 191–210. https://doi.org/10.1080/15538362.2018.1502720

Gobierno Provincial del Azuay. (2015). *Plan de desarrollo y ordenamiento territorial del Azuay actualizado 2015 - 2030*. http://app.sni.gob.ec/visorseguimiento/DescargaGAD/data/sigadplusdiagnostico/0160000190001_DIAGNÓSTICO FINAL_17-08-2015_09-23-05.pdf

Gogul, I., & Kumar, V. S. (2017). Flower species recognition system using convolution neural networks and transfer learning. *2017 4th International Conference on Signal Processing, Communication and Networking, ICSCN 2017*, 1–6. https://doi.org/10.1109/ICSCN.2017.8085675

Gorelick, N., Hancher, M., Dixon, M., Ilyushchenko, S., Thau, D., & Moore, R. (2017). Google Earth Engine: Planetary-scale geospatial analysis for everyone. *Remote Sensing of Environment*. https://doi.org/10.1016/j.rse.2017.06.031

Goyal, N., Kumar, N., & Gupta, K. (2022). Lower-dimensional intrinsic structural representation of leaf images and plant recognition. *Signal, Image and Video Processing*, *16*(1), 203–210. https://doi.org/10.1007/s11760-021-01983-6

Grabska, E., Hostert, P., Pflugmacher, D., & Ostapowicz, K. (2019). Forest stand species mapping using the sentinel-2 time series. *Remote Sensing*, *11*(10). https://doi.org/10.3390/rs11101197

Greco, R., Barca, E., Raumonen, P., Persia, M., & Tartarino, P. (2023). Methodology for measuring dendrometric parameters in a mediterranean forest with UAVs flying inside forest. *International Journal of Applied Earth Observation and Geoinformation*, *122*. https://doi.org/10.1016/j.jag.2023.103426

Guillot, D., & Van der Meer, P. (2009). El género Yucca L en España. In *España. Monografías de la revista Bouteloua* (Vol. 2).

Guimarães, N., Pádua, L., Marques, P., Silva, N., Peres, E., & Sousa, J. J. (2020). Forestry remote sensing from unmanned aerial vehicles: A review focusing on the data, processing and potentialities. In *Remote Sensing* (Vol. 12, Issue 6). MDPI AG. https://doi.org/10.3390/rs12061046

Guzmán-Salinas, N., Jiménez-Pesántez, M., Minga-Ochoa, D., Delgado-Inga, O., & Martínez, E. (2023). *Árboles urbanos de Cuenca*. Casa Editora de la Universidad del Azuay. https://doi.org/10.33324/ceuazuay.296

H

Hamedianfar, A., Mohamedou, C., Kangas, A., & Vauhkonen, J. (2022). Deep learning for forest inventory and planning: a critical review on the remote sensing approaches so far and prospects for further applications. *Forestry: An International Journal of Forest Research*, *95*(4), 451–465. https://doi.org/10.1093/forestry/cpac002

Haq, M. A., Rahaman, G., Baral, P., & Ghosh, A. (2021). Deep Learning Based Supervised Image Classification Using UAV Images for Forest Areas Classification. *Journal of the Indian Society of Remote Sensing*, *49*(3). https://doi.org/10.1007/s12524-020-01231-3

Haro-Carrión, X., Loiselle, B., & Putz, F. E. (2021). Tree Species Diversity, Composition and Aboveground Biomass Across Dry Forest Land-Cover Types in Coastal Ecuador. *Tropical Conservation Science*, *14*. https://doi.org/10.1177/1940082921995415

Haro-Carrión, X., & Southworth, J. (2018). Understanding Land Cover Change in a Fragmented Forest Landscape in a Biodiversity Hotspot of Coastal Ecuador. *Remote Sensing*, *10*(12), 1980. https://doi.org/10.3390/rs10121980

Hartling, S., Sagan, V., & Maimaitijiang, M. (2021). Urban tree species classification using UAV-based multi-sensor data fusion and machine learning. *GIScience & Remote Sensing*, *58*(8), 1250–1275. https://doi.org/10.1080/15481603.2021.1974275

Hartling, S., Sagan, V., Sidike, P., Maimaitijiang, M., & Carron, J. (2019). Urban tree species classification using a worldview-2/3 and liDAR data fusion approach and deep learning. *Sensors (Switzerland)*, *19*(6). https://doi.org/10.3390/s19061284

Herzog, S. K., Martinez, R., Jorgensen, P. M., & Tienssen, H. (2012). *Cambio Climático y Biodiversidad en los Andes Tropicales*.

Homan, D., & du Preez, J. A. (2021). Automated feature-specific tree species identification from natural images using deep semi-supervised learning. *Ecological Informatics*, *66*(October), 101475. https://doi.org/10.1016/j.ecoinf.2021.101475

Hong, Q., Ge, Z., Wang, X., Li, Y., Xia, X., & Chen, Y. (2024). Measuring canopy morphology of saltmarsh plant patches using UAV-based LiDAR data. *Frontiers in Marine Science*, *11*. https://doi.org/10.3389/fmars.2024.1378687

Hong, Y., Xu, J., Wu, C., Pang, Y., Zhang, S., Chen, D., & Yang, B. (2023). Combining Multisource Data and Machine Learning Approaches for Multiscale Estimation of Forest Biomass. *Forests*, *14*(11). https://doi.org/10.3390/f14112248

Hościło, A., & Lewandowska, A. (2019). Mapping Forest Type and Tree Species on a Regional Scale Using Multi-Temporal Sentinel-2 Data. *Remote Sensing*, *11*(8), 929. https://doi.org/10.3390/rs11080929

Hou, J., Zhou, H., Hu, J., Yu, H., & Hu, H. (2023). A Multi-Scale Convolution and Multi-Layer Fusion Network for Remote Sensing Forest Tree Species Recognition. *Remote Sensing*, *15*(19). https://doi.org/10.3390/rs15194732

Huang, X., Wu, W., Shen, T., Xie, L., Qin, Y., Peng, S., Zhou, X., Fu, X., Li, J., Zhang, Z., Zhang, M., Liu, Y., Jiang, J., Ou, P., Huangfu, W., & Zhang, Y. (2021). Estimating forest canopy cover by multiscale remote sensing in northeast Jiangxi, China. *Land*, *10*(4). https://doi.org/10.3390/land10040433

Huaraca, L., Bourrel, L., Zapata-Ríos, X., Páez-Bimos, S., Lahuatte, B., Galeas, R., Fuentes, P., & Frappart, F. (2025). Multitemporal Monitoring of Ecuadorian Andean High Wetlands Using Radar and Multispectral Remote Sensing. *Water*, *17*(11), 1637. https://doi.org/10.3390/w17111637

I

IDB - Index DataBase. (n.d.). Retrieved May 7, 2024, from https://www.indexdatabase.de/

Iglhaut, J., Cabo, C., Puliti, S., Piermattei, L., O'Connor, J., & Rosette, J. (2019). Structure from Motion Photogrammetry in Forestry: a Review. In *Current Forestry Reports* (Vol. 5, Issue 3). https://doi.org/10.1007/s40725-019-00094-3

Immitzer, M., Atzberger, C., & Koukal, T. (2012). Tree species classification with Random forest using very high spatial resolution 8-band worldView-2 satellite data. *Remote Sensing*, *4*(9). https://doi.org/10.3390/rs4092661

J

Jadán, O., Donoso, D. A., Cedillo, H., Bermúdez, F., & Cabrera, O. (2021). Floristic groups, and changes in diversity and structure of trees, in tropical montane forests in the southern andes of Ecuador. *Diversity*, *13*(9). https://doi.org/10.3390/d13090400

Jarvis, A., Reuter, H. I., Nelson, A., Guevara, E., & others. (2008). *Hole-filled SRTM for the globe Version 4, available from the CGIAR-CSI SRTM 90m Database*.

K

Kapari, M., Sibanda, M., Magidi, J., Mabhaudhi, T., Nhamo, L., & Mpandeli, S. (2024). Comparing Machine Learning Algorithms for Estimating the Maize Crop Water Stress Index (CWSI) Using UAV-Acquired Remotely Sensed Data in Smallholder Croplands. *Drones*, *8*(2). https://doi.org/10.3390/drones8020061

Kattenborn, T., Leitloff, J., Schiefer, F., & Hinz, S. (2021). Review on Convolutional Neural Networks (CNN) in vegetation remote sensing. *ISPRS Journal of Photogrammetry and Remote Sensing*, *173*, 24–49. https://doi.org/https://doi.org/10.1016/j.isprsjprs.2020.12.010

Kaya, A., Keceli, A. S., Catal, C., Yalic, H. Y., Temucin, H., & Tekinerdogan, B. (2019). Analysis of transfer learning for deep neural network based plant classification models. *Computers and Electronics in Agriculture*, *158*(January), 20–29. https://doi.org/10.1016/j.compag.2019.01.041

Ke, Y., & Quackenbush, L. J. (2011). A review of methods for automatic individual tree-crown detection and delineation from passive remote sensing. In *International Journal of Remote Sensing* (Vol. 32, Issue 17). https://doi.org/10.1080/01431161.2010.494184

Kim, D. H., Ko, C. U., Kim, D. G., Kang, J. T., Park, J. M., & Cho, H. J. (2023). Automated Segmentation of Individual Tree Structures Using Deep Learning over LiDAR Point Cloud Data. *Forests*, *14*(6). https://doi.org/10.3390/f14061159

Kim, T. K., Kim, S., Won, M., Lim, J. H., Yoon, S., Jang, K., Lee, K. H., Park, Y. D., & Kim, H. S. (2021). Utilizing machine learning for detecting flowering in mid - range digital repeat photography. *Ecological Modelling*, *440*(July 2020), 109419. https://doi.org/10.1016/j.ecolmodel.2020.109419

Kivinen, S., Koivisto, E., Keski-Saari, S., Poikolainen, L., Tanhuanpää, T., Kuzmin, A., Viinikka, A., Heikkinen, R. K., Pykälä, J., Virkkala, R., Vihervaara, P., & Kumpula, T. (2020). A keystone species, European aspen (Populus tremula L.), in boreal forests: Ecological role, knowledge needs and mapping using remote sensing. *Forest Ecology and Management*, *462*, 118008. https://doi.org/10.1016/j.foreco.2020.118008

Kleemann, J., Zamora, C., Villacis-Chiluisa, A. B., Cuenca, P., Koo, H., Noh, J. K., Fürst, C., & Thiel, M. (2022). Deforestation in Continental Ecuador with a Focus on Protected Areas. *Land*, *11*(2), 268. https://doi.org/10.3390/land11020268

Kovanič, Ľ., Topitzer, B., Peťovský, P., Blišťan, P., Gergeľová, M. B., & Blišťanová, M. (2023). Review of Photogrammetric and LiDAR Applications of UAV. In *Applied Sciences (Switzerland)* (Vol. 13, Issue 11). MDPI. https://doi.org/10.3390/app13116732

Kumar, A., Singh, S. B., Satapathy, S. C., & Rout, M. (2022). MOSQUITO-NET: A deep learning based <scp>CADx</scp> system for malaria diagnosis along with model interpretation using <scp>GradCam</scp> and class activation maps. *Expert Systems*, *39*(7), 1–10. https://doi.org/10.1111/exsy.12695

Kumar, L., & Mutanga, O. (2018). Google Earth Engine applications since inception: Usage, trends, and potential. *Remote Sensing*, *10*(10), 1–15. https://doi.org/10.3390/rs10101509

L

Lasseck, M. (2017). Image-based plant species identification with deep Convolutional Neural Networks. *CEUR Workshop Proceedings*, *1866*.

Lechner, A. M., Foody, G. M., & Boyd, D. S. (2020). Applications in Remote Sensing to Forest Ecology and Management. *One Earth*, *2*(5), 405–412. https://doi.org/10.1016/j.oneear.2020.05.001

Leena Rani, A., Devika, G., Vinutha H., R., Karegowda, A. G., Vidya, S., & Bhat, S. (2022). Identification of Medicinal Leaves Using State of Art Deep Learning Techniques. *IEEE International Conference on Distributed Computing and Electrical Circuits and Electronics, ICDCECE 2022*, 11–15. https://doi.org/10.1109/ICDCECE53908.2022.9792712

Li, X., Zheng, Z., Xu, C., Zhao, P., Chen, J., Wu, J., Zhao, X., Mu, X., Zhao, D., & Zeng, Y. (2023). Individual tree-based forest species diversity estimation by classification and clustering methods using UAV data. *Frontiers in Ecology and Evolution*, *11*. https://doi.org/10.3389/fevo.2023.1139458

Lian, X., Zhang, H., Xiao, W., Lei, Y., Ge, L., Qin, K., He, Y., Dong, Q., Li, L., Han, Y., Fan, H., Li, Y., Shi, L., & Chang, J. (2022). Biomass Calculations of Individual Trees Based on Unmanned Aerial Vehicle Multispectral Imagery and Laser Scanning Combined with Terrestrial Laser Scanning in Complex Stands. *Remote Sensing*, *14*(19). https://doi.org/10.3390/rs14194715

Ligono, L. K., & Okolie, C. J. (2022). Integrated analysis of Mangrove changes using the Mangrove Vegetation Index and Random Forest classification in the Gambia. *The International Archives of the Photogrammetry, Remote Sensing and Spatial Information Sciences*, *XLVI-M-2–2022*(M-2–2022), 153–157. https://doi.org/10.5194/isprs-archives-XLVI-M-2-2022-153-2022

Lindberg, E., & Holmgren, J. (2017). Individual Tree Crown Methods for 3D Data from Remote Sensing. *Current Forestry Reports*, *3*(1), 19–31. https://doi.org/10.1007/s40725-017-0051-6

Lines, E. R., Fischer, F. J., Owen, H. J. F., & Jucker, T. (2022). The shape of trees: Reimagining forest ecology in three dimensions with remote sensing. *Journal of Ecology*, *110*(8). https://doi.org/10.1111/1365-2745.13944

Liu, B., Chen, S., Huang, H., & Tian, X. (2022). Tree Species Classification of Backpack Laser Scanning Data Using the PointNet++ Point Cloud Deep Learning Method. *Remote Sensing*, *14*(15). https://doi.org/10.3390/rs14153809

Liu, B., Huang, H., Su, Y., Chen, S., Li, Z., Chen, E., & Tian, X. (2022). Tree Species Classification Using Ground-Based LiDAR Data by Various Point Cloud Deep Learning Methods. *Remote Sensing*, *14*(22). https://doi.org/10.3390/rs14225733

Liu, J., Wang, X., & Wang, T. (2019). Classification of tree species and stock volume estimation in ground forest images using Deep Learning. *Computers and Electronics in Agriculture*, *166*. https://doi.org/10.1016/j.compag.2019.105012

Liu, Y., Gong, W., Hu, X., & Gong, J. (2018). Forest type identification with random forest using Sentinel-1A, Sentinel-2A, multi-temporal Landsat-8 and DEM data. *Remote Sensing*, *10*(6). https://doi.org/10.3390/rs10060946

López, V. L., Huertas Herrera, A., Rosas, Y. M., & Cellini, J. M. (2022). Optimal environmental drivers of high-mountains forest: Polylepis tarapacana cover evaluation in their southernmost distribution range of the Andes. *Trees, Forests and People*, *9*. https://doi.org/10.1016/j.tfp.2022.100321

Lou, P., Fu, B., He, H., Chen, J., Wu, T., Lin, X., Liu, L., Fan, D., & Deng, T. (2021). An Effective Method for Canopy Chlorophyll Content Estimation of Marsh Vegetation Based on Multiscale Remote Sensing Data. *IEEE Journal of Selected Topics in Applied Earth Observations and Remote Sensing*, *14*, 5311–5325. https://doi.org/10.1109/JSTARS.2021.3081565

Luber, A., Ramachandran, V., Jaafar, W. S. W. M., Bajaj, S., De-Miguel, S., Cardil, A., Doaemo, W., & Mohan, M. (2023). UAVs for monitoring responses of regenerating forests under increasing climate change-driven droughts - A review. *IOP Conference Series: Earth and Environmental Science*, *1167*(1). https://doi.org/10.1088/1755-1315/1167/1/012030

M

Ma, M., Liu, J., Liu, M., Zeng, J., & Li, Y. (2021). Tree species classification based on sentinel-2 imagery and random forest classifier in the eastern regions of the qilian mountains. *Forests*, *12*(12). https://doi.org/10.3390/f12121736

Ma, W., Yang, H., Wu, Y., Xiong, Y., Hu, T., Jiao, L., & Hou, B. (2019). Change detection based on multi-grained cascade forest and multi-scale fusion for SAR images. *Remote Sensing*, *11*(2), 1–25. https://doi.org/10.3390/rs11020142

Ma, Z., Dong, Y., Zi, J., Xu, F., & Chen, F. (2023). Forest-PointNet: A Deep Learning Model for Vertical Structure Segmentation in Complex Forest Scenes. *Remote Sensing*, *15*(19). https://doi.org/10.3390/rs15194793

Ma, Z., Pang, Y., Wang, D., Liang, X., Chen, B., Lu, H., Weinacker, H., & Koch, B. (2020). Individual tree crown segmentation of a larch plantation using airborne laser scanning data based on region growing and canopy morphology features. *Remote Sensing*, *12*(7). https://doi.org/10.3390/rs12071078

MAE. (2017). *Deforestación Del Ecuador Continental Periodo 2014-2016*. *1*(1), 1–8.

MAE, & FAO. (2015). *Especies forestales leñosas arbóreas y arbustivas de los bosques montanos del Ecuador*.

Malik, O. A., Ismail, N., Hussein, B. R., & Yahya, U. (2022). Automated Real-Time Identification of Medicinal Plants Species in Natural Environment Using Deep Learning Models—A Case Study from Borneo Region. *Plants*, *11*(15), 1952. https://doi.org/10.3390/plants11151952

Man, Q., Yang, X., Liu, H., Zhang, B., Dong, P., Wu, J., Liu, C., Han, C., Zhou, C., Tan, Z., & Yu, Q. (2025). Comparison of UAV-Based LiDAR and

Photogrammetric Point Cloud for Individual Tree Species Classification of Urban Areas. *Remote Sensing*, *17*(7), 1212. https://doi.org/10.3390/rs17071212

Mesas-Carrascosa, F.-J., de Castro, A. I., Torres-Sánchez, J., Triviño-Tarradas, P., Jiménez-Brenes, F. M., García-Ferrer, A., & López-Granados, F. (2020). Classification of 3D Point Clouds Using Color Vegetation Indices for Precision Viticulture and Digitizing Applications. *Remote Sensing*, *12*(2), 317. https://doi.org/10.3390/rs12020317

Mezgec, S., & Seljak, B. K. (2017). Nutrinet: A deep learning food and drink image recognition system for dietary assessment. *Nutrients*, *9*(7), 1–19. https://doi.org/10.3390/nu9070657

Michałowska, M., & Rapiński, J. (2021). A Review of Tree Species Classification Based on Airborne LiDAR Data and Applied Classifiers. *Remote Sensing*, *13*(3), 353. https://doi.org/10.3390/rs13030353

Mikołajczyk, A., & Grochowski, M. (2018). Data augmentation for improving deep learning in image classification problem. *2018 International Interdisciplinary PhD Workshop, IIPhDW 2018*, 117–122. https://doi.org/10.1109/IIPHDW.2018.8388338

Minga, D., & Verdugo, A. (2016). Árboles y Arbustos de los ríos de Cuenca. In *Serie Textos Apoyo a la Docencia Universidad del Azuay*.

Minga-Ochoa, D., Ansaloni, R., Verdugo-Navas, A., & Ulloa-Ulloa, C. (2019). *Flora del páramo del Cajas, Ecuador*. Casa Editora Universidad del Azuay. https://doi.org/10.33324/ceuazuay.42

Mishra, A. P., Rai, I. D., Pangtey, D., & Padalia, H. (2021). Vegetation Characterization at Community Level Using Sentinel-2 Satellite Data and Random Forest Classifier in Western Himalayan Foothills, Uttarakhand. *Journal of the Indian Society of Remote Sensing*, *49*(4), 759–771. https://doi.org/10.1007/s12524-020-01253-x

Mngadi, M., Odindi, J., Peerbhay, K., & Mutanga, O. (2021). Examining the effectiveness of Sentinel-1 and 2 imagery for commercial forest species mapping. *Geocarto International*, *36*(1), 1–12. https://doi.org/10.1080/10106049.2019.1585483

Modzelewska, A., Fassnacht, F. E., & Stereńczak, K. (2020). Tree species identification within an extensive forest area with diverse management regimes using airborne hyperspectral data. *International Journal of Applied Earth Observation and Geoinformation*, *84*. https://doi.org/10.1016/j.jag.2019.101960

Morante-Carballo, F., Bravo-Montero, Lady, Carrión-Mero, P., Velastegui-Montoya, A., & Berrezueta, E. (2022). Forest Fire Assessment Using Remote Sensing to Support the Development of an Action Plan Proposal in Ecuador. *Remote Sensing*, *14*(8), 1783. https://doi.org/10.3390/rs14081783

Mouafik, M., Chakhchar, A., Fouad, M., & El Aboudi, A. (2024). Remote Sensing Technologies for Monitoring Argane Forest Stands: A Comprehensive Review. *Geographies*, *4*(3), 441–461. https://doi.org/10.3390/geographies4030024

Muñoz Marcillo, J. L., Cabrera Sinche, B., & Toulkeridis, T. (2023). Analysis of land use change using remote sensing and GIS techniques in the Cazaderos forest, Loja province, Southern Ecuador. *Revista Geográfica de Chile Terra Australis*, *59*. https://doi.org/10.23854/07199562.2023592.munoz

Muñoz Villalobos, I. A., & Bolt, A. (2022). Diseño y desarrollo de aplicación móvil para la clasificación de flora nativa chilena utilizando redes neuronales convolucionales. *AtoZ: Novas Práticas Em Informação e Conhecimento*, *11*, 1. https://doi.org/10.5380/atoz.v11i0.81419

N

Naciones Unidas. (2018). La Agenda 2030 y los Objetivos de Desarrollo Sostenible Una oportunidad para América Latina y el Caribe. In *Publicación de las Naciones Unidas*.

Nandy, S., Srinet, R., & Padalia, H. (2021). Mapping Forest Height and Aboveground Biomass by Integrating ICESat-2, Sentinel-1 and Sentinel-2 Data Using Random Forest Algorithm in Northwest Himalayan Foothills of India. *Geophysical Research Letters*, *48*(14), 1–10. https://doi.org/10.1029/2021GL093799

Natesan, S., Armenakis, C., & Vepakomma, U. (2019). Resnet-based tree species classification using uav images. *International Archives of the Photogrammetry, Remote Sensing and Spatial Information Sciences - ISPRS Archives*, *42*(2/W13), 475–481. https://doi.org/10.5194/isprs-archives-XLII-2-W13-475-2019

Navarro, G., Molina, J. A., & Barra, N. D. la. (2005). Classification of the high-Andean Polylepis forests in Bolivia. *Plant Ecology*, *176*(1), 113–130. https://doi.org/10.1007/s11258-004-0025-1

Nevalainen, O., Honkavaara, E., Tuominen, S., Viljanen, N., Hakala, T., Yu, X., Hyyppä, J., Saari, H., Pölönen, I., Imai, N., & Tommaselli, A. (2017). Individual Tree Detection and Classification with UAV-Based

Photogrammetric Point Clouds and Hyperspectral Imaging. *Remote Sensing*, *9*(3), 185. https://doi.org/10.3390/rs9030185

Nielsen, A. B., Östberg, J., & Delshammar, T. (2014). Review of urban tree inventory methods used to collect data at single-tree level. *Arboriculture and Urban Forestry*, *40*(2), 96–111. https://doi.org/10.48044/jauf.2014.011

Noh, J. K., Echeverria, C., Gaona, G., Kleemann, J., Koo, H., Fürst, C., & Cuenca, P. (2022). Forest Ecosystem Fragmentation in Ecuador: Challenges for Sustainable Land Use in the Tropical Andean. *Land*, *11*(2). https://doi.org/10.3390/land11020287

O

Object Detection with TensorFlow Lite Model Maker. (n.d.). Retrieved February 6, 2023, from https://www.tensorflow.org/lite/models/modify/model_maker/object_detection

Onishi, M., & Ise, T. (2021). Explainable identification and mapping of trees using UAV RGB image and deep learning. *Scientific Reports*, *11*(1). https://doi.org/10.1038/s41598-020-79653-9

P

Pacheco, D. (2017). Drones en espacios urbanos: Caso de estudio en parques, jardines y patrimonio. *Estoa*, *11*, 159–168. https://doi.org/10.18537/est.v006.n011.a12

Pacheco, D., & Ávila, L. (2017). Inventario de parques y jardines de la ciudad de Cuenca con UAV y smartphones. *XVI Conferencia de Sistemas de Información Geográfica*, 173–179. https://revistas.uazuay.edu.ec/index.php/memorias/issue/view/7

Pacheco-Prado, D., Bravo-López, E., & Martínez-Urgilés, E. (2025). Tree Species Identification Using UAV RGB and Multispectral Cloud Points. In D. G. and L. P. H. V. Olmedo Cifuentes Gonzalo Fernando and Arcos Avilés (Ed.), *Emerging Research in Intelligent Systems* (pp. 66–79). Springer Nature Switzerland.

Pacheco-Prado, D., Bravo-López, E., & Ruiz, L. Á. (2023). Tree Species Identification in Urban Environments Using TensorFlow Lite and a Transfer Learning Approach. *Forests*, *14*(5). https://doi.org/10.3390/f14051050

Pacheco-Prado, D., Bravo-López, E., & Ruiz, L. Á. (2024). Mapping Polylepis Forest Using Sentinel, PlanetScope Images, and Topographical Features with Machine Learning. *Remote Sensing*, *16*(22), 4271. https://doi.org/10.3390/rs16224271

Paneque-Gálvez, J., McCall, M. K., Napoletano, B. M., Wich, S. A., & Koh, L. P. (2014). Small drones for community-based forest monitoring: An assessment of their feasibility and potential in tropical areas. *Forests*, *5*(6), 1481–1507.

Pang, B., Nijkamp, E., & Wu, Y. N. (2020). Deep Learning With TensorFlow: A Review. *Journal of Educational and Behavioral Statistics*, *45*(2), 227–248. https://doi.org/10.3102/1076998619872761

Paper, D. (2021). Simple Transfer Learning with TensorFlow Hub. In *State-of-the-Art Deep Learning Models in TensorFlow* (pp. 153–169). Apress. https://doi.org/10.1007/978-1-4842-7341-8_6

Pazmiño, Y., de Felipe, J. J., Vallbé, M., Cargua, F., & Quevedo, L. (2021). Identification of a Set of Variables for the Classification of Páramo Soils Using a Nonparametric Model, Remote Sensing, and Organic Carbon. *Sustainability*, *13*(16), 9462. https://doi.org/10.3390/su13169462

Persson, M., Lindberg, E., & Reese, H. (2018). Tree species classification with multi-temporal Sentinel-2 data. *Remote Sensing*, *10*(11). https://doi.org/10.3390/rs10111794

Phiri, D., Simwanda, M., Salekin, S., Nyirenda, V., Murayama, Y., & Ranagalage, M. (2020). Sentinel-2 Data for Land Cover/Use Mapping: A Review. *Remote Sensing*, *12*(14), 2291. https://doi.org/10.3390/rs12142291

Picos, J., Bastos, G., Míguez, D., Alonso, L., & Armesto, J. (2020). Individual tree detection in a eucalyptus plantation using unmanned aerial vehicle (UAV)-LiDAR. *Remote Sensing*, *12*(5). https://doi.org/10.3390/rs12050885

Pizarro, S. E., Pricope, N. G., Vargas-Machuca, D., Huanca, O., & Ñaupari, J. (2022). Mapping Land Cover Types for Highland Andean Ecosystems in Peru Using Google Earth Engine. *Remote Sensing*, *14*(7), 1562. https://doi.org/10.3390/rs14071562

Pleşoianu, A. I., Stupariu, M. S., Şandric, I., Pătru-Stupariu, I., & Drăguţ, L. (2020). Individual tree-crown detection and species classification in very high-resolution remote sensing imagery using a deep learning ensemble model. *Remote Sensing*, *12*(15). https://doi.org/10.3390/RS12152426

Populus alba in Flora of China @ efloras.org. (n.d.). Retrieved May 10, 2022, from http://www.efloras.org/florataxon.aspx?flora_id=2&taxon_id=200005643

Pradipkumar, V. H., & Alagu Raja, R. A. (2022). Automatic Identification of Tree Species from UAV Images Using Machine Learning Approaches. *Journal of the Indian Society of Remote Sensing*, *50*(12), 2447–2464. https://doi.org/10.1007/s12524-022-01608-6

Prado, D. P., & Ruiz, L. Á. (2019). Comparative of Machine Learning Algorithms and Datasets to Classify Natural Coverage in the Cajas National Park (Ecuador) Based on GEOBIA Approach. *Proceedings*, *19*(1). https://doi.org/10.3390/proceedings2019019020

Pratama, B. (2023). *Performing Feature Selection in Google Earth Engine (GEE) Using Recursive Feature Elimination (RFE) | by Pratama Bima | Artificial Intelligence in Plain English*. https://ai.plainenglish.io/performing-feature-selection-in-google-earth-engine-gee-using-recursive-feature-elimination-rfe-0f5ba2789c4c

Praticò, S., Solano, F., Di Fazio, S., & Modica, G. (2021). Machine learning classification of mediterranean forest habitats in google earth engine based on seasonal sentinel-2 time-series and input image composition optimisation. *Remote Sensing*, *13*(4), 1–28. https://doi.org/10.3390/rs13040586

Pu, L., Xv, J., & Deng, F. (2021). An Automatic Method for Tree Species Point Cloud Segmentation Based on Deep Learning. *Journal of the Indian Society of Remote Sensing*, *49*(9), 2163–2172. https://doi.org/10.1007/s12524-021-01358-x

Pu, R. (2014). Tree species classification. In G. Wang & Q. Weng (Eds.), *Remote Sensing of Natural Resources*. CRC Press, Taylor & Francis Group.

Pu, R. (2021). Mapping Tree Species Using Advanced Remote Sensing Technologies: A State-of-the-Art Review and Perspective. *Journal of Remote Sensing*, *2021*. https://doi.org/10.34133/2021/9812624

Puliti, S., Gobakken, T., Ørka, H. O., & Næsset, E. (2017). Assessing 3D point clouds from aerial photographs for species-specific forest inventories. *Scandinavian Journal of Forest Research*, *32*(1), 68–79. https://doi.org/10.1080/02827581.2016.1186727

Q

Qi, C. R., Su, H., Mo, K., & Guibas, L. J. (2017). *PointNet: Deep Learning on Point Sets for 3D Classification and Segmentation*.

Qi, Y., Dong, X., Chen, P., Lee, K.-H., Lan, Y., Lu, X., Jia, R., Deng, J., & Zhang, Y. (2021). Canopy Volume Extraction of Citrus reticulate Blanco cv. Shatangju Trees Using UAV Image-Based Point Cloud Deep Learning. *Remote Sensing*, *13*(17), 3437. https://doi.org/10.3390/rs13173437

R

Rana, P., St-Onge, B., Prieur, J. F., Cristina Budei, B., Tolvanen, A., & Tokola, T. (2022). Effect of feature standardization on reducing the requirements of field samples for individual tree species classification using ALS data. *ISPRS Journal of Photogrammetry and Remote Sensing*, *184*. https://doi.org/10.1016/j.isprsjprs.2022.01.003

Recognize Flowers with TensorFlow Lite on Android. (n.d.). Retrieved September 6, 2022, from https://codelabs.developers.google.com/codelabs/recognize-flowers-with-tensorflow-on-android#0

Reda, M., Suwwan, R., Alkafri, S., Rashed, Y., & Shanableh, T. (2022). AgroAId: A Mobile App System for Visual Classification of Plant Species and Diseases Using Deep Learning and TensorFlow Lite. *Informatics*, *9*(3). https://doi.org/10.3390/informatics9030055

Remondino, F., Barazzetti, L., Nex, F., Scaioni, M., & Sarazzi, D. (2011). UAV photogrammetry for mapping and 3d modeling–current status and future perspectives. *The International Archives of the Photogrammetry, Remote Sensing and Spatial Information Sciences*, *38-1/C22*(September), 25–31. https://doi.org/10.5194/isprsarchives-XXXVIII-1-C22-25-2011

ResNet V2 101 | TensorFlow Hub. (n.d.). Retrieved February 6, 2023, from https://tfhub.dev/google/imagenet/resnet_v2_101/feature_vector/5

Rieckmann, M., Adomßent, M., Härdtle, W., & Aguirre, P. (2011). Sustainable Development and Conservation of Biodiversity Hotspots in Latin America: The Case of Ecuador. In *Biodiversity Hotspots* (pp. 435–452). Springer Berlin Heidelberg. https://doi.org/10.1007/978-3-642-20992-5_22

Rivas, C. A., Guerrero-Casado, J., & Navarro-Cerrillo, R. M. (2024). Functional connectivity across dominant forest ecosystems in Ecuador: A major challenge for a country with a high deforestation rate. *Journal for Nature Conservation*, *78*, 126549. https://doi.org/10.1016/j.jnc.2023.126549

Roca, J., & Arellano, B. (2021). *Application of Conventional UAVs for the Identification and Classification of Dense Green Spaces* (pp. 364–388). https://doi.org/10.4018/978-1-7998-2249-3.ch012

Rodríguez-Puerta, F., Barrera, C., García, B., Pérez-Rodríguez, F., & García-Pedrero, A. M. (2022). Mapping Tree Canopy in Urban Environments Using Point Clouds from Airborne Laser Scanning and Street Level Imagery. *Sensors*, *22*(9), 3269. https://doi.org/10.3390/S22093269

Rojas, R., Flexas, J., & Coopman, R. E. (2022). Particularities of the highest elevation treeline in the world: Polylepis tarapacana Phil. as a model to study ecophysiological adaptations to extreme environments. *Flora: Morphology, Distribution, Functional Ecology of Plants*, *292*. https://doi.org/10.1016/j.flora.2022.152076

Romoleroux, K., Cárate-Tandalla, D., Erler, R., & Navarrete, H. (2016). Plantas vasculares de los bosques de Polylepis en los páramos de Oyacachi. In *Flora web*. https://repositorio.puce.edu.ec/handle/123456789/1185

Ruiz, L. Á., Recio, J. A., Crespo-Peremarch, P., & Sapena, M. (2016). An object-based approach for mapping forest structural types based on low-density LiDAR and multispectral imagery. *Geocarto International*, *6049*(November), 1–15. https://doi.org/10.1080/10106049.2016.1265595

S

Salam, A. (2020). Internet of Things for Sustainable Forestry. In *Internet of Things* (pp. 243–271).

Sánchez, J. (2016). *Flora ornamental española*. http://www.arbolesornamentales.es/

Schwager, P., & Berg, C. (2021). Remote sensing variables improve species distribution models for alpine plant species. *Basic and Applied Ecology*, *54*. https://doi.org/10.1016/j.baae.2021.04.002

Seidel, D., Annighöfer, P., Thielman, A., Seifert, Q. E., Thauer, J.-H., Glatthorn, J., Ehbrecht, M., Kneib, T., & Ammer, C. (2021). Predicting Tree Species From 3D Laser Scanning Point Clouds Using Deep Learning. *Frontiers in Plant Science*, *12*. https://doi.org/10.3389/fpls.2021.635440

Selvaraju, R. R., Cogswell, M., Das, A., Vedantam, R., Parikh, D., & Batra, D. (2016). Grad-cam: Why did you say that? visual explanations from deep networks via gradient-based localization. *Revista Do Hospital Das Cl??Nicas*, *17*, 331–336.

Sentinel-2 MSI: MultiSpectral Instrument, Level-2A. (n.d.). Retrieved March 30, 2021, from https://developers.google.com/earth-engine/datasets/catalog/COPERNICUS_S2_SR#description

Sesnie, S., Espinosa, C., Jara-Guerrero, A., & Tapia-Armijos, M. (2023). Ensemble Machine Learning for Mapping Tree Species Alpha-Diversity Using Multi-Source Satellite Data in an Ecuadorian Seasonally Dry Forest. *Remote Sensing*, *15*(3), 583. https://doi.org/10.3390/rs15030583

Shah, V., & Sajnani, N. (2020). Multi-Class Image Classification using CNN and Tflite. *International Journal of Research in Engineering, Science and Management*, *3*(11), 65–68. https://doi.org/10.47607/ijresm.2020.375

Shaji, A. P., & Hemalatha, S. (2022). Data augmentation for Improving Rice Leaf Disease Classification on Residual Network Architecture. *Proceedings - IEEE International Conference on Advances in Computing, Communication and Applied Informatics, ACCAI 2022*. https://doi.org/10.1109/ACCAI53970.2022.9752495

Shi, Y., Wang, T., Skidmore, A. K., & Heurich, M. (2018). Important LiDAR metrics for discriminating forest tree species in Central Europe. *ISPRS Journal of Photogrammetry and Remote Sensing*, *137*. https://doi.org/10.1016/j.isprsjprs.2018.02.002

Shorten, C., & Khoshgoftaar, T. M. (2019). A survey on Image Data Augmentation for Deep Learning. *Journal of Big Data*, *6*(1). https://doi.org/10.1186/s40537-019-0197-0

Shrestha, A., & Mahmood, A. (2019). Review of deep learning algorithms and architectures. In *IEEE Access* (Vol. 7). https://doi.org/10.1109/ACCESS.2019.2912200

Sierra, R., Calva, O., & Guevara, A. (2021). La Deforestación en el Ecuador, 1990 – 2018: Factores, Promotores y Tendencias Recientes. *Ministerio de Ambiente y Agua Del Ecuador, Ministerio de Agricultura Del Ecuador, En El Marco de La Implementación Del Programa Integral Amazónico de Conservación de Bosques y Producción Sostenible.*, 216. https://www.proamazonia.org/wp-content/uploads/2021/06/Deforestación_Ecuador_com2.pdf

Sierra, R., Campos, F., & Chamberlin, J. (2002). Assessing biodiversity conservation priorities: ecosystem risk and representativeness in continental Ecuador. *Landscape and Urban Planning*, *59*(2), 95–110. https://doi.org/10.1016/S0169-2046(02)00006-3

SIGTIERRAS. (2017). Ortofotografía del Ecuador. El país desde otra perspectiva. *Ministerio de Agricultura y Ganadería*, *1*, 88. http://www.sigtierras.gob.ec/wp-content/uploads/revista/Ortofotografia.pdf

SigTierras – Ministerio de Agricultura, Ganadería, Acuacultura y Pesca. (n.d.). Retrieved April 19, 2017, from http://www.agricultura.gob.ec/sigtierras/

sklearn.metrics.cohen_kappa_score — scikit-learn 1.2.1 documentation. (n.d.). Retrieved January 1, 2023, from https://scikit-learn.org/stable/modules/generated/sklearn.metrics.cohen_kappa_score.html

Solomou, A. D., Topalidou, E. T., Germani, R., Argiri, A., & Karetsos, G. (2019). Importance, utilization and health of urban forests: A review. *Notulae Botanicae Horti Agrobotanici Cluj-Napoca*, *47*(1), 10–16. https://doi.org/10.15835/nbha47111316

Song, X., Wu, F., Lu, X., Yang, T., Ju, C., Sun, C., & Liu, T. (2022). The Classification of Farming Progress in Rice–Wheat Rotation Fields Based on UAV RGB Images and the Regional Mean Model. *Agriculture*, *12*(2), 124. https://doi.org/10.3390/agriculture12020124

Sothe, C., Dalponte, M., de Almeida, C. M., Schimalski, M. B., Lima, C. L., Liesenberg, V., Takahashi Miyoshi, G., & Garcia Tommaselli, A. M. (2019). Tree Species Classification in a Highly Diverse Subtropical Forest Integrating UAV-Based Photogrammetric Point Cloud and Hyperspectral Data. *Remote Sensing*, *11*(11), 1338. https://doi.org/10.3390/rs11111338

Strasser, T., Riedler, B., Adamczyk, J., Lang, S., Osberger, A., & Pernkopf, L. (2014). *Multi-scale Forest Habitat Monitoring Using Remote Sensing Data*. https://doi.org/10.1553/giscience2014s49

Sun, X., & Shi, Y. (2023). The image recognition of urban greening tree species based on deep learning and CAMP-MKNet model. *Urban Forestry & Urban Greening*, *85*, 127970. https://doi.org/10.1016/j.ufug.2023.127970

Suwais, K., Alheeti, K., & Al_Dosary, D. (2022). A Review on Classification Methods for Plants Leaves Recognition. *International Journal of Advanced Computer Science and Applications*, *13*(2), 92–100. https://doi.org/10.14569/IJACSA.2022.0130211

Svoboda, J., Štych, P., Laštovička, J., Paluba, D., & Kobliuk, N. (2022). Random Forest Classification of Land Use, Land-Use Change and Forestry (LULUCF) Using Sentinel-2 Data—A Case Study of Czechia. *Remote Sensing*, *14*(5). https://doi.org/10.3390/rs14051189

T

Tao, W. (2014). Multi-view dense match for forest area. *International Archives of the Photogrammetry, Remote Sensing and Spatial Information Sciences - ISPRS Archives*, *40*(1). https://doi.org/10.5194/isprsarchives-XL-1-397-2014

Tassi, A., & Vizzari, M. (2020). Object-Oriented LULC Classification in Google Earth Engine Combining SNIC, GLCM, and Machine Learning Algorithms. *Remote Sensing*, *12*(22), 3776. https://doi.org/10.3390/rs12223776

Tejedor Garavito, N., Álvarez, E., Arango Caro, S., Araujo Murakami, A., Blundo, C., Boza Espinoza, T., La Torre Cuadros, M., Gaviria, J., Gutíerrez, N., Jørgensen, P., León, B., López Camacho, R., Malizia, L., Millán, B., Moraes, M., Pacheco, S., Rey Benayas, J., Reynel, C., & Timaná de la Flor, M. (2012). Evaluación del estado de conservación de los bosques montanos en los Andes tropicales. *Ecosistemas*, *21*(1–2), 148–166. https://www.revistaecosistemas.net/index.php/ecosistemas/article/view/34

Tejedor Garavito, N., Newton, A. C., & Oldfield, S. (2015). Regional Red List assessment of tree species in upper montane forests of the Tropical Andes. *Oryx*, *49*(3), 397–409. https://doi.org/10.1017/S0030605315000198

Tenesaca, C., Quindi, T., Delgado, G., Toledo, E., & Delgado, O. (2017). Generación del mapa de cobertura y uso del suelo de la provincia del Azuay. *Instituto de Estudios de Régimen Seccional Del Ecuador IERSE*, *73*(2), 23–37. https://doi.org/10.13140/RG.2.2.31077.50409

TensorFlow. (2021). *Model optimization | TensorFlow Lite*. https://www.tensorflow.org/lite/performance/model_optimization

TensorFlow Hub. (n.d.). Retrieved January 18, 2023, from https://www.tensorflow.org/hub

TensorFlow Lite inference. (n.d.). Retrieved February 16, 2023, from https://www.tensorflow.org/lite/guide/inference

TensorFlow Lite Model Maker. (n.d.). Retrieved January 18, 2023, from https://www.tensorflow.org/lite/models/modify/model_maker

Tilo (Sambucus canadensis) · iNaturalist Ecuador. (n.d.). Retrieved January 4, 2023, from https://ecuador.inaturalist.org/taxa/84300-Sambucus-canadensis

Tree Inventory Project | Portland.gov. (n.d.). Retrieved November 11, 2022, from https://www.portland.gov/trees/get-involved/treeinventory

Tufail, S., Riggs, H., Tariq, M., & Sarwat, A. I. (2023). Advancements and Challenges in Machine Learning: A Comprehensive Review of Models, Libraries, Applications, and Algorithms. *Electronics*, *12*(8), 1789. https://doi.org/10.3390/electronics12081789

U

Uçar, Z., Akay, A. E., & Bilici, E. (2020). Towards green smart cities: Importance of Urban forestry and urban vegetation. *International Archives of the Photogrammetry, Remote Sensing and Spatial Information Sciences - ISPRS Archives*, *44*(4/W3), 399–403. https://doi.org/10.5194/isprs-archives-XLIV-4-W3-2020-399-2020

Ulloa, C., Álvarez, S., Jørgensen, P., & Minga, D. (2008). Guía de 100 Plantas silvestres del páramo del Parque Nacional Cajas. *Guia de 100 Plantas Silvestres Del Paramodel Parque Nacional de Cajas*, 91. https://www.mobot.org/MOBOT/research/paramo/pdf/GuiaPlantas.pdf

Universidad del Azuay. (2024). *Dashboard Inventario Forestal Cuenca*. https://gis.uazuay.edu.ec/herramientas/iforestal-dashboard/

V

Vali, A., Comai, S., & Matteucci, M. (2020). Deep learning for land use and land cover classification based on hyperspectral and multispectral earth observation data: A review. *Remote Sensing*, *12*(15). https://doi.org/10.3390/RS12152495

Vallejo, S., Quingaísa, E., Ortiz, P., & Vinueza, L. (2007). El Agro y Vida Rural en Ecuador: Comportamiento 2000-2007 y Perspectivas 2008. *IICA, Quito, EC*.

Vega Isuhuaylas, L. A., Hirata, Y., Santos, L. C. V., & Torobeo, N. S. (2018). Natural forest mapping in the Andes (Peru): A comparison of the performance of machine-learning algorithms. *Remote Sensing*, *10*(5). https://doi.org/10.3390/rs10050782

Velastegui-Montoya, A., Rivera-Torres, H., Herrera-Matamoros, V., Sadeck, L., & Quevedo, R. P. (2022). Application of Google Earth Engine for land Cover Classification in Yasuni National Park, Ecuador. *IGARSS 2022 - 2022 IEEE International Geoscience and Remote Sensing Symposium*, 6376–6379. https://doi.org/10.1109/IGARSS46834.2022.9884886

Vilasini, M., & Ramamoorthy, P. (2020). CNN approaches for classification of Indian leaf species using smartphones. *Computers, Materials and Continua*, *62*(3), 1445–1472. https://doi.org/10.32604/cmc.2020.08857

Vizzari, M. (2022). PlanetScope, Sentinel-2, and Sentinel-1 Data Integration for Object-Based Land Cover Classification in Google Earth Engine. *Remote Sensing*, *14*(11). https://doi.org/10.3390/rs14112628

Volunteers Count Every Street Tree in New York City | US Forest Service. (n.d.). Retrieved November 11, 2022, from https://www.fs.usda.gov/features/volunteers-count-every-street-tree-new-york-city-0

W

Wäldchen, J., & Mäder, P. (2018). Plant Species Identification Using Computer Vision Techniques: A Systematic Literature Review. In *Archives of Computational Methods in Engineering* (Vol. 25, Issue 2). Springer Netherlands. https://doi.org/10.1007/s11831-016-9206-z

Walsh, S. J., McCleary, A. L., Mena, C. F., Shao, Y., Tuttle, J. P., González, A., & Atkinson, R. (2008). QuickBird and Hyperion data analysis of an invasive plant species in the Galapagos Islands of Ecuador: Implications for control and land use management. *Remote Sensing of Environment*, *112*(5), 1927–1941. https://doi.org/10.1016/j.rse.2007.06.028

Wang, D., Wan, B., Qiu, P., Su, Y., Guo, Q., Wang, R., Sun, F., & Wu, X. (2018). Evaluating the performance of Sentinel-2, Landsat 8 and Pléiades-1 in mapping mangrove extent and species. *Remote Sensing*, *10*(9). https://doi.org/10.3390/rs10091468

Wang, J., Yang, D., Detto, M., Nelson, B. W., Chen, M., Guan, K., Wu, S., Yan, Z., & Wu, J. (2020). Multi-scale integration of satellite remote sensing improves characterization of dry-season green-up in an Amazon tropical evergreen forest. *Remote Sensing of Environment*, *246*. https://doi.org/10.1016/j.rse.2020.111865

Wang, Y., Zhang, W., Gao, R., Jin, Z., & Wang, X. (2021). Recent advances in the application of deep learning methods to forestry. In *Wood Science and Technology* (Vol. 55, Issue 5). https://doi.org/10.1007/s00226-021-01309-2

Waser, L. T., Rüetschi, M., Psomas, A., Small, D., & Rehush, N. (2021). Mapping dominant leaf type based on combined Sentinel-1/-2 data – Challenges for mountainous countries. *ISPRS Journal of Photogrammetry and Remote Sensing*, *180*, 209–226. https://doi.org/10.1016/j.isprsjprs.2021.08.017

Westoby, M. J., Brasington, J., Glasser, N. F., Hambrey, M. J., & Reynolds, J. M. (2012). "Structure-from-Motion" photogrammetry: A low-cost, effective tool for geoscience applications. *Geomorphology*, *179*. https://doi.org/10.1016/j.geomorph.2012.08.021

X

Xi, Y., Ren, C., Tian, Q., Ren, Y., Dong, X., & Zhang, Z. (2021). Exploitation of Time Series Sentinel-2 Data and Different Machine Learning Algorithms for Detailed Tree Species Classification. *IEEE Journal of Selected Topics in Applied Earth Observations and Remote Sensing*, *14*. https://doi.org/10.1109/JSTARS.2021.3098817

Xia, X., Xu, C., & Nan, B. (2017). Inception-v3 for flower classification. *2017 2nd International Conference on Image, Vision and Computing, ICIVC 2017*, 783–787. https://doi.org/10.1109/ICIVC.2017.7984661

Xu, C., Morgenroth, J., & Manley, B. (2015). Integrating Data from Discrete Return Airborne LiDAR and Optical Sensors to Enhance the Accuracy of Forest Description: A Review. *Current Forestry Reports*, *1*(3). https://doi.org/10.1007/s40725-015-0019-3

Xu, D., Wang, H., Xu, W., Luan, Z., & Xu, X. (2021). LiDAR applications to estimate forest biomass at individual tree scale: Opportunities, challenges and future perspectives. *Forests*, *12*(5). https://doi.org/10.3390/f12050550

Xu, K., Tian, Q., Yang, Y., Yue, J., & Tang, S. (2019). How up-scaling of remote-sensing images affects land-cover classification by comparison with multiscale satellite images. *International Journal of Remote Sensing*, *40*(7), 2784–2810. https://doi.org/10.1080/01431161.2018.1533656

Xu, N., Qin, R., & Song, S. (2023). Point cloud registration for LiDAR and photogrammetric data: A critical synthesis and performance analysis on classic and deep learning algorithms. In *ISPRS Open Journal of Photogrammetry and Remote Sensing* (Vol. 8). https://doi.org/10.1016/j.ophoto.2023.100032

Xu, Z., Shen, X., Cao, L., Coops, N. C., Goodbody, T. R. H., Zhong, T., Zhao, W., Sun, Q., Ba, S., Zhang, Z., & Wu, X. (2020). Tree species classification using UAS-based digital aerial photogrammetry point clouds and multispectral imageries in subtropical natural forests. *International Journal of Applied Earth Observation and Geoinformation*, *92*, 102173. https://doi.org/10.1016/j.jag.2020.102173

Z

Zeybek, M. (2021). Classification of UAV point clouds by random forest machine learning algorithm. *Turkish Journal of Engineering*, *5*(2), 48–57. https://doi.org/10.31127/tuje.669566

Zeybek, M. (2025). Integrating advanced remote sensing technologies and machine learning in urban forestry: a comprehensive review and future outlook. *Measurement Science and Technology*, *36*(6), 062004. https://doi.org/10.1088/1361-6501/addf66

Zhang, C., Xia, K., Feng, H., Yang, Y., & Du, X. (2021). Tree species classification using deep learning and RGB optical images obtained by an unmanned aerial vehicle. *Journal of Forestry Research*, *32*(5), 1879–1888. https://doi.org/10.1007/s11676-020-01245-0

Zhang, H., Liu, B., Yang, B., Guo, J., Hu, Z., Zhang, M., Yang, Z., & Zhang, J. (2025). Efficient tree species classification using machine and deep learning algorithms based on UAV-LiDAR data in North China. *Frontiers in Forests and Global Change*, *8*. https://doi.org/10.3389/ffgc.2025.1431603

Zhang, R., Zhu, Y., Ge, Z., Mu, H., Qi, D., & Ni, H. (2022). Transfer Learning for Leaf Small Dataset Using Improved ResNet50 Network with Mixed Activation Functions. *Forests*, *13*(12). https://doi.org/10.3390/f13122072

Zhang, X., Zhang, F., Qi, Y., Deng, L., Wang, X., & Yang, S. (2019). New research methods for vegetation information extraction based on visible light remote sensing images from an unmanned aerial vehicle (UAV). *International Journal of Applied Earth Observation and Geoinformation*, *78*, 215–226. https://doi.org/10.1016/j.jag.2019.01.001

Zhang, Z., & Liu, X. (2013). Support vector machines for tree species identification using LiDAR-derived structure and intensity variables. *Geocarto International*, *28*(4). https://doi.org/10.1080/10106049.2012.710653

Zheng, H., Sherazi, S. W. A., Son, S. H., & Lee, J. Y. (2021). A deep convolutional neural network-based multi-class image classification for automatic wafer map failure recognition in semiconductor manufacturing. *Applied Sciences (Switzerland)*, *11*(20). https://doi.org/10.3390/app11209769

Zhong, H., Zhang, Z., Liu, H., Wu, J., & Lin, W. (2024). Individual Tree Species Identification for Complex Coniferous and Broad-Leaved Mixed Forests Based on Deep Learning Combined with UAV LiDAR Data and RGB Images. *Forests*, *15*(2). https://doi.org/10.3390/f15020293

Zhou, J., Chen, X., Li, S., Dong, R., Wang, X., Zhang, C., & Zhang, L. (2023). Multispecies individual tree crown extraction and classification based on BlendMask and high-resolution UAV images. *Journal of Applied Remote Sensing*, *17*(01). https://doi.org/10.1117/1.JRS.17.016503